I. INVESTIGATION OF THE EFFECTS OF SURFACE TOPOLOGY UPON COLLISION DYNAMICS IN THE HeH_2^+ AND NeH_2^+ SYSTEMS

II. AN AB INITIO STUDY OF ROTATIONALLY INELASTIC SCATTERING IN THE He - CO_2 SYSTEM

By

COURTNEY LYNN STROUD

Bachelor of Science

Oklahoma State University

1975

Submitted to the Faculty of the Graduate College
of the Oklahoma State University
in partial fulfillment of the requirements
for the Degree of
DOCTOR OF PHILOSOPHY
December, 1978

I. INVESTIGATION OF THE EFFECTS OF SURFACE TOPOLOGY UPON COLLISION DYNAMICS IN THE HeH_2^+ AND NeH_2^+ SYSTEMS

II. AN AB INITIO STUDY OF ROTATIONALLY INELASTIC SCATTERING IN THE He - CO_2 SYSTEM

Thesis Approved:

Leonel M. Raff
Thesis Adviser

J. Paul Devlin

Roger E. Kroffs

Norman N Durham
Dean of the Graduate College

ACKNOWLEDGMENTS

Truly no research effort, and especially that of the Ph.D. aspirant, is the work of one individual. Often in the first year the student has little, if any, idea of what he is doing, and it is only with the help of his adviser and much mistake-making (and correcting) that he comes to an understanding of his particular area of research. In my case, I had an exceptionally competent adviser, Dr. Lionel Raff, who willingly and knowledgeably discussed any problem that came up. I wish to thank him, not only for his guidance and help in handling the problems that arose, but more importantly for teaching me, by his own example, the scientific method.

As others who greatly helped me in my graduate career, I wish to thank all of the people in my lab for letting me discuss problems and ideas with them, but especially Dave Martin and Dr. N. Sathyamurthy. I also acknowledge the invaluable assistance of Jim Brandt and Max McKee in dealing with the university computer, and of Carl Jordan for so quickly and kindly making the many plots I requested. Finally, I extend my sincere gratitude to Dr. Russell T. Pack, who promptly and graciously shared with me many of his calculational methods and results on the He - CO_2 system, and to Aron Kuppermann for providing prior to publication a copy of his experimentally determined potential-energy surface.

I gratefully acknowledge financial support received from the Department of Chemistry through a teaching assistantship, to the National Science Foundation through a research assistantship (NSF grant CHE 75-18967 A02), from CONOCO through a CONOCO fellowship, and from the Graduate College and the Department of Chemistry through numerous fee waivers.

My thanks go to Dolores Behrens for typing the final copy of this thesis.

I give my heartfelt thanks and love to my family for providing such continuous encouragement, support, and love throughout my life and particularly these past few years. Finally, I happily dedicate this thesis to Danny, my husband and best friend, whose companionship, criticism, and love made this work truly fulfilling.

TABLE OF CONTENTS

LIST OF TABLES

LIST OF FIGURES

CHAPTER I

INTRODUCTION

For many years the lack of experimental techniques for carrying out laser, molecular beam, or chemiluminescence studies limited the development of theories of reaction dynamics. The hard sphere collision theory and the activated complex theory represented the extent of the theoretician's means for studying chemical reactions. However, the ever broadening spectrum of experimental techniques available and the evolution of the digital computer as a theoretical tool have enabled attention to be focussed upon the treatment of the individual molecular collision; consequently, theories of collision dynamics have blossomed.

The understanding of collision dynamics is of critical importance in the development and improvement of theories of chemical reactivity which are, in turn, applicable to a variety of fields. For instance, a large number of simple molecules have been discovered in dense interstellar clouds (1). The study of the history and present conditions of these clouds requires a knowledge of the types of reaction each chemical species undergoes as well as the rates at which each reaction proceeds. Similar knowledge is needed in the study of reactions important in the upper atmosphere of both the earth and other planets (2).

Collision dynamics is essential to the study of moderation effects in hot-atom reactions and of unimolecular reactions such as the tautomerization of CH_3NC to CH_3CN. The critical area of application is in the

field of lasers. The operation of the laser is based upon the excitation of a rotational-vibrational (ro-vibrational) or an electronic mode of a molecule. The excitation comes about through an energy transfer process, such as the transfer of energy from one molecule to another during the course of a collision occurring between the two. This process is clearly the most significant performance-limiting factor in chemical lasers; therefore, a detailed understanding of energy transfer processes is necessary to improve and understand the efficiency of laser systems.

The Study of Collision Dynamics

The first phase in the study of collision dynamics is the determination of the potential energy of the system being studied, i.e., finding the interaction energy of the particles which comprise the system as a function of their relative positions. The most common representation of the potential energy of a system involving more than two atoms is the potential-energy surface. Such a hypersurface is usually represented in the form of a map showing energy contours as a function of suitable bond distances and angles. Because this type of representation is used, a potential-energy surface that is a function of two independent variables is called a two-dimensional (2D) surface.

As will be seen later, the accuracy of the potential-energy surface is of paramount importance in obtaining reliable results from scattering studies. Potentially, the most accurate type of potential-energy surface is the ab initio surface, i.e., one calculated from first principles. Examples of ab initio calculational methods are the Hartree-Fock self-consistent field (HF-SCF) and the linear combination of atomic

orbitals, molecular orbital, self-consistent field (LCAO-MO-SCF) procedures, of which only the latter method is currently used for systems involving more than one atom. These methods are not the most accurate available because both ignore electron correlation effects, the tendency of the electrons in the system to shift so as to minimize their mutual repulsion. A procedure which includes these effects is called a configuration-interaction (CI) study and the most accurate surfaces available today are those computed by an ab initio method which includes CI.

One of the drawbacks to present ab initio calculations is the size of the system which can be treated. Computer storage capacities limit the number of integrals which can be calculated and stored, and prevent the handling of anything but systems involving atoms from the first three periods of the periodic table. Still, the number of ab initio surfaces has grown rapidly in recent years (3).

Also limiting the extensive use of ab initio potential-energy surfaces is the fact that the potential energy must be computed for each distinct geometry of the system and limitations of computer time restrict the number of geometries that can be considered. This necessitates the use of some type of interpolation procedure to generate the actual surface from the ab initio points. Analytic functions containing a number of adjustable parameters have been used in several cases (4) to fit the ab initio values but have been found to fit the values well in some areas and poorly in others (5). A more accurate fit is obtained with the cubic spline interpolation procedure (6) used by McLaughlin and Thompson (7) in their treatment of the $HeH^+ + H_2$ reaction dynamics. This method has been found to be quite acceptable for both quantum

mechanical (8) and classical (9) scattering methods and has the advantage of generating a surface which passes through each of the ab initio points and which is free of the bias inherent in an analytic fit.

The semiempirical potential-energy surface has enjoyed broad use in past years (10). Here a simplified expression is used to represent the potential energy, and experimental data is then either incorporated directly into the expression or fitted by adjusting parameters within the expression. One of the most firmly established of the semiempirical methods is the London-Eyring-Polanyi-Sato (LEPS) formalism (11); however, the method of diatomics-in-molecules is another semiempirical method which has recently gained in popularity.

Semiempirical surfaces have the advantage of being simple and fast to compute and can be used to describe a much wider variety of systems than ab initio surfaces presently are able to do. Semiempirical surfaces do not, however, possess the accuracy that is rapidly becoming a prerequisite for the detailed investigation of more complex systems. Because of this very inaccuracy, however, semiempirical surfaces of the diatomics-in-molecules type play a vital role in the determination of the features of the potential-energy surface which most greatly influence the outcome of scattering studies.

The second phase in the study of collision dynamics is the scattering study. This is the actual mathematical investigation of the collision occurring between the reacting species and its subsequent effects on their identity and behavior. There are two types of scattering studies that can be investigated in a system: reactive and nonreactive scattering. Reactive scattering occurs when collision of the reactants results in the chemical identity of one or more of the reactants being

altered. Nonreactive scattering also occurs as the result of a collision, but here the identity of the reactants remains intact while the distribution of energy between them changes. Elastic scattering is the type of nonreactive scattering which occurs when the collision brings about a change only in the center-of-mass translational energy of each of the reactants. Inelastic scattering results when the distribution of internal energy as well as the translational energy of the reactants is altered by their impact. In particular, inelastic scattering studies are used to investigate the excitation of the internal energy modes of a molecule upon collision with another species, i.e., the energy transfer process.

The scattering study is effected either quantum mechanically by solving the Schrödinger equation or classically by solving Hamilton's equations of motion. This determines the position of the particles in the system as a function of time, which allows the investigator to follow the motion of each of the particles in the system as the reaction time progresses and thus to determine reactivity for a system under a particular set of initial conditions. The system is evolved through time mathematically until the trend in the geometry of the system makes it clear either that the reactants will remain unchanged or that products have been formed.

The accuracy of the potential energy is crucial to the quality of the scattering results because solving the Schrödinger equation requires knowledge of the potential energy and solution of the classical equations of motion requires that the first derivative of the potential energy be known. In either case, errors in the potential-energy surface can seriously affect the outcome of a scattering study.

Quantum mechanical (QM) studies are the only exact means of looking at the scattering of a system (12). QM methods have the advantage of treating all channels of the system in one calculation and, therefore, the final result is easy to interpret. Unfortunately, computation time for a single calculation is so large as to be prohibitive and present storage capacities prevent the wide use of QM treatments while simultaneously limiting the size of the system which can be handled. Systems whose products could be formed in a wide variety of rotational quantum states, for instance, cannot be treated quantum mechanically without first making approximations which limit the number of possible product channels. This is especially true for polyatomic systems.

Classical calculations, on the other hand, are easier and much faster to perform but are inherently approximate. The most popular classical method for studying scattering is the quasiclassical trajectory (QCT) method first described by Karplus, Porter, and Sharma (13). Here classical behavior is followed throughout the calculation except at the outset where vibrational and rotational energies are quantized. The difficulty with the QCT method and all classical procedures is that energy may flow freely between any coupled energy modes. Careful statistical procedures must therefore be used to interpret the results, especially when inelastic scattering is being treated. Another difficulty lies in the fact that the classical equations of motion depend on the gradient of the potential energy. This makes classical methods very sensitive to inaccuracies in the potential-energy surface, more so than QM methods, which depend on the energy itself and not its derivative. Both methods depend heavily on the accuracy of the potential-energy surface; however, for a given potential-energy surface, the QM result will

be less affected by inaccuracies in the surface than the QCT result. Since classical methods are often the only feasible means available for handling the more complex systems, the importance of employing a highly accurate potential-energy surface is paramount.

The study of collision dynamics has lately seen the development of a statistical treatment which may be of great use in augmenting scattering results. The work of Levine and Bernstein (14) and others has recently made the application of information theory to theoretical data quite feasible. Use of the surprisal formalism--surprisal is a measure of the "unexpectedness" of a result--has brought the theory to the point where predictions of quantities such as state-to-state transition probabilities can perhaps be made within acceptable error limits. This would allow fewer actual scattering calculations to be performed and would therefore reduce computation times.

This discussion has emphasized the fact that any thorough theoretical treatment of the collision dynamics of a chemical system must involve the computation of a sufficiently accurate potential-energy surface for the system and the utilization of this surface in performing scattering calculations. These studies may be performed classically or quantum mechanically and may be supplemented with surprisal predictions. Where possible, the results of the calculations are compared with actual experimental quantities in order to assess the validity of the theoretical treatment. It seems logical, therefore, to present the research involved in this dissertation in the order mentioned above. First, each of the investigations will be summarized; the details of each study will be presented in subsequent chapters.

Calculation of Ab Initio Potential-Energy Surfaces

As was mentioned earlier, semiempirical surfaces have been used widely and are still popular for scattering studies of more complex systems; however, the trend for smaller systems is away from the semiempirical surface toward the ab initio. This potential increase in the accuracy of the surface can sometimes change even the qualitative results of reactive scattering studies, as is the case for the HeH_2^+ system described in this work. Consequently, the use of ab initio surfaces is not only preferable, but in some cases essential.

In this work two new ab initio surfaces are presented, the first of which is for the collinear NeH_2^+ ion-molecule system. Interest in the computation of the collinear NeH_2^+ surface has evolved from the study of the effects of reagent vibration and surface topology on the predicted reactivity of the HeH_2^+ system. Because the two systems have similar electronic structures and have shown similar experimental behavior, a logical extension of the HeH_2^+ study is to treat reactive scattering in the NeH_2^+ system. This requires both an ab initio and a semiempirical surface, where the semiempirical surface is of the diatomics-in-molecules type. Hayes et al (15) have computed ab initio potential energies for the collinear NeH_2^+ system and have fitted to these values a diatomics-in-molecules functional form. Although the semiempirical surface can be incorporated directly into a quasiclassical trajectory study of the reaction dynamics of this system, the ab initio values can not. The nature of the distribution of ab initio potential-energy values over the geometries of the system makes it impossible to generate the entire potential-energy surface using the accurate method of interpolation with

cubic splines (6). Furthermore, a simple augmentation of the potential energy values by additional ab initio calculations is not possible with the available computer facilities. For accurate trajectory studies to be performed on an ab initio surface for the collinear NeH_2^+ system, an entirely new potential-energy surface must be calculated--one in which the ab initio energies are computed for a distribution of geometries amenable to interpolation with the spline-fitting procedure. Such a surface is reported in this work.

The second ab initio surface that has been computed is for the He - CO_2 rigid rotor system. Since many lasers work by the excitation of ro-vibrational modes of the CO_2 molecule, knowledge of the rotational relaxation rates for each ro-vibrational transition, as well as a detailed mechanism for the relaxation process, is necessary in order to optimize the performance of CO_2 lasers. Helium is often used as a diluent in CO_2 lasers, making the He - CO_2 system an attractive system to study because of the experimental data available and the potential practical uses for theoretical results.

The first step in obtaining these objectives is again the calculation of a potential-energy surface for the system. A potential-energy function which would completely describe the He - CO_2 system must be a function of six internal coordinates; fortunately, the surface necessary to study rotational transitions in CO_2 does not have to involve this full set of six variables. The fact that rotational excitation depends chiefly on the angle and distance between the atom and the molecule allows the potential energy to be reduced to an approximate function of two variables: the distance R from helium to the CO_2 center of mass and the angle between R and the CO_2 bond axis.

Within this framework an LCAO-MO-SCF procedure has been employed to calculate ab initio potential energy values for 256 distinct He - CO_2 geometries. A two-dimensional cubic spline interpolation procedure has been used to generate the full potential-energy surface from the ab initio points.

The generation of this surface follows the calculation of a similar surface computed by Parker, Snow, and Pack (16), who used the modified electron gas model developed by Gordon and Kim (17) as their basis of calculation. Their surface also depends on the two variables mentioned above. This is very fortunate as it allows comparisons to be made between results obtained on the two surfaces, thereby allowing further insight into the accuracy of the potential-energy surface needed to obtain reliable inelastic scattering data.

Investigation of the Effects of Surface Topology Upon Collision Dynamics

The ab initio surface calculated for the collinear NeH_2^+ system is to be used in the investigation of the effects of surface topology on the outcome of reactive scattering studies involving the Ne + $H_2^+(v) \rightarrow$ NeH^+ + H reaction. Interest in the features of the potential-energy surface and their influence upon chemical reactivity has increased since Polanyi and Wong (18), Mok and Polanyi (19), and Hijazi and Laidler (20) demonstrated that dynamic effects--those effects which arise due to momentum transfer requirements (21)--are enhanced on surfaces on which the potential energy barrier lies in the exit or product channel of the surface. In particular, reagent vibration was found to enhance greatly

the reactivity of the system. A nonhypothetical system which attracted immediate attention was the HeH_2^+ ion-molecule system. There had been many experimental investigations performed on this system as well as others--photoionization (22), infrared chemiluminescence (23), electron impact (24), and crossed molecular beam (25) studies--which indicated higher reactivity for cases in which the reacting diatomic species is in an excited vibrational state, i.e., the reaction $He + H_2^+(v) \rightarrow HeH^+ + H$ occurs more readily when $v \neq 0$. The amount and definitiveness of the experimental data, as well as the fact that the HeH_2^+ system is within the capabilities of QM scattering calculations, made this a highly attractive system to study.

Theoretical work on the system took two different routes. In one case, ab initio energies computed by Brown and Hayes (26) for the collinear system were used to calibrate a diatomics-in-molecules (DIM) potential-energy surface. This is a semiempirical surface obtained by treating the potential energy of the system as the sum of the potential energy of each pair of atoms. Actually, two DIM surfaces were calculated: Kuntz (27) generated a 2D collinear surface and Kuntz and Whitton (28) generated a full 3D hypersurface. Exact QM calculations were performed on the 2D surface by Kouri and Baer, Adams, and Zuhrt et al (29), all of whom found that reagent vibration retarded the reactivity of the system. Kuntz and Whitton (28) performed quasiclassical trajectories on the 3D surface and, unlike the investigators of the 2D system, obtained results in agreement with experiment: the reactivity of the HeH_2^+ system increased with increasing H_2^+ vibrational energy.

This conflict between the QM calculations and the experimental findings was due to one or more of the following reasons:

1. The lack of CI in the computation of the ab initio values--an LCAO-MO-SCF procedure was used--caused the energies to be an inaccurate representation of the system.
2. The differences between QM and QCT procedures were sufficiently pronounced to alter the qualitative outcome of scattering studies performed using them.
3. The 2D DIM fit to the ab initio values was inadequate.

The work of Sathyamurthy et al (30) resolved this conflict. Their work represents the other route take in the investigation of the HeH_2^+ system. The ab initio values of Brown and Hayes were again used, but this time a collinear surface was generated by the two-dimensional cubic spline interpolation technique. The surface thus produced was called the spline-fitted ab initio (SAI) surface. On this surface quasiclassical trajectories were performed, and it was found that reactivity increased with reagent vibrational excitation, in agreement with both experiment and the trajectories performed by Kuntz and Whitton on the 3D DIM hypersurface. This work indicated that the ab initio values of Brown and Hayes were of sufficient accuracy to give qualitatively correct results and that a collinear potential-energy surface was an adequate representation of the HeH_2^+ system provided the ab initio values were accurately interpolated. Sathyamurthy et al went on to demonstrate that the difference was not due to the calculational procedure used: they performed trajectories on the 2D DIM potential-energy surface of Kuntz and upon a surface in which DIM values were spline-fitted to form an SDIM potential-energy surface. These calculations were in accord showing that the results obtained on the SAI surface were not an artifact of the spline-fitting procedure and that the choice of QM or QCT

method did not affect the qualitative outcome of the calculation.

Clearly, only one difference remains: the inadequacy of the DIM fit to the collinear data. A comparison of the DIM and SAI surfaces for the HeH_2^+ system shows many similarities between the two surfaces. All evidence indicates, however, that the discrepancies between the two surfaces are responsible for the conflicting results obtained. It has recently been suggested that these differences are due to the shape of the inner repulsive wall of the interaction region (31). This hypothesis can be confirmed by performing quasiclassical trajectories on the SAI surface with the inner wall replaced by that of the DIM surface. If the inner wall is indeed responsible for the inadequacy of the DIM fit, the reactivity computed in this manner should closely agree with that predicted by scattering studies on the DIM surface. Analogously, studies performed on a DIM surface with an SAI inner wall should exhibit the same behavior as those performed on the SAI surface. The results of just such a study are reported here.

The NeH_2^+ system has exhibited the same experimental behavior as the HeH_2^+ system (22b). Furthermore, the collinear potential-energy surfaces computed for this system show barriers in the product valley, indicating that collisions involving H_2^+ in an excited vibrational state should show more tendency to react with neon than H_2^+ in its ground state. Calculations similar to those performed on the HeH_2^+ system can thus be performed and an assessment made of the influence of the shape of the inner repulsive wall on the dynamical outcome of Ne - H_2^+ collisions. The results from this study are included in this work and provide further elucidation of the role played by the potential-energy

surface in reactive scattering calculations.

Quantum Mechanical Scattering Calculations in the HeH_2^+ System

The HeH_2^+ system offers the opportunity to study the differences between QM and QCT procedures performed on an accurate ab initio surface. The quasiclassical trajectories have already been performed on this surface by Sathyamurthy et al (30) and their results have been shown to give agreement with experimental findings. However, as was discussed earlier, the QCT method is a classical procedure and studies have indicated that classical values tend to overestimate the reactivity of a system when the system energies are near the threshold energy (32). An exact QM study performed on this SAI surface would allow the quantitative assessment of the usefulness of the classical approximation in treating the HeH_2^+ system and qualitative assessments to be made for similar systems.

The QM method that is used in this study is a time-dependent procedure first described and used by McCullough and Wyatt (12) in their treatment of the dynamics of the collinear $H + H_2$ reaction. Reactive scattering in the HeH_2^+ system is computed for six different distributions of translational and vibrational energies, all of which have also been computed by the QCT procedure. The results given here are the most accurate calculated for the collinear HeH_2^+ system and thus provide a firm basis for the assessment of the usefulness of the QCT procedure in treating the dynamics of the HeH_2^+ and similar systems.

Polyatomic Collision Dynamics - Rotational Excitation in the He - CO_2 System

One of the main thrusts of current studies of collision dynamics is the extension of dynamical theories to polyatomic systems. Work on the hot-atom system T* + CH_4 (33) and energy transfer studies in systems involving CO_2 represent the first movements in this direction, but studies even on these systems are far from complete due to the complexity of the scattering calculations and the restricted nature of the potential-energy surface that can be employed.

Although traditional techniques such as chemiluminescence, shock wave, ultrasonic, and molecular beam methods are responsible for much of the experimental data on energy transfer processes in existence today (34) (35), the laser is rapidly moving toward a position of prominence in the investigation and characterization of energy transfer processes (36). Because CO_2 is an integral part of many laser systems, understanding the rotational and vibrational excitations and relaxations that occur in this molecule is vital to the improvement of gain and efficiency in CO_2 lasers.

The vibrational processes occurring in CO_2 as a result of collisions with species such as H_2, CO_2, HF, He, and O have received quite extensive experimental attention. In particular, the relaxation of the CO_2 asymmetric stretching mode

$$CO_2(00^o1) + X \rightarrow CO_2(nm^l0) + X,$$

the primary mode through which lasing occurs, has been studied extensively by laser fluorescence techniques. Temperature-dependent rate

constants have been determined for many collision partners (37), including helium (38) and other rare gases (39). This experimental work on the CO_2 laser has made the theoretical treatment of CO_2-X systems feasible.

Early studies of vibrational energy transfer (40) have been somewhat restricted in scope: Thommarson et al (41) performed 2D classical studies on He - CO_2, while Bass (42) employed a hard-sphere model to treat T → V (translational to vibrational) transfer in O - NH_3 and O - CO_2. Suzukawa (43) was the first to treat T → V, T → R, and V → R transfers in rare gas-CO_2 systems by a full 3D classical treatment using a realistic semiempirical potential-energy surface. Sathyamurthy and Raff (44) studied vibrational relaxation for the bimolecular CO_2 - H_2 system using an ab initio intermolecular potential. These last two studies represent the most accurate studies into vibrational energy transfer processes yet completed.

With the vibrational studies well under way, interest has spread to rotational energy transfer processes. Guha and Saha (45) have used a semiclassical approach and a semiempirical potential-energy surface to study rotational excitation in the CO_2 - H_2 system while Raff and Sathyamurthy (46) are now performing similar studies on their ab initio surface. Interest in the study of He - CO_2 and Ar - CO_2 systems has developed with the calculation of angle- and distance-dependent potential-energy surfaces based on the electron gas model. In order to analyze the accuracy of these potentials calculated by Parker et al (16), Preston and Pack (47) have performed classical trajectory calculations of rotational transitions for Ar - CO_2 and have obtained results in excellent agreement with molecular beam studies performed on the

Ar - CO_2 systems (48). Shimoni and Kouri (49) have used the electron gas surface for He - CO_2 to investigate a statistical approximation based on the QM coupled states approach, while Goldflam et al (50) have used the same surface to extend the surprisal formulation of Levine and Bernstein (14) to the prediction of rotationally inelastic cross sections. All of the work based on the electron gas model of the He - CO_2 potential-energy surface makes it imperative that the strengths and weaknesses of this surface be fully assessed. The first step in executing this comparison is the study of rotationally inelastic scattering on an accurate ab initio surface for the He - CO_2 system, followed by a similar study on the electron gas surface. As was previously mentioned, both surfaces have been computed and can be used to carry out four-body QCT calculations for rotationally inelastic transitions in the He - CO_2 system. The results from this study can be compared with the quantum mechanical calculations of Parker and Pack (16b), and with experimental data on the system (51). In particular, Keil, Parker, and Kuppermann (51c) have determined an empirical potential-energy surface for the He - CO_2 system from a crossed molecular beam study. The results of QCT scattering calculations on all three potential-energy surfaces are presented in this work.

CHAPTER II

AB INITIO POTENTIAL-ENERGY SURFACES FOR THE $Ne + H_2^+$ SYSTEM AND THE $He - CO_2$ RIGID ROTOR SYSTEM

The $Ne + H_2^+$ System

The first step in a scattering study is the calculation of a potential-energy surface which adequately describes the system being treated. If this calculation is performed using *ab initio* methods, it often involves such a large amount of time and computation that it is treated as a separate problem from the actual dynamical study. Indeed, in the study of the HeH_2^+ system, both the *ab initio* and diatomics-in-molecules surfaces were published prior to any trajectory studies. This was also the case for the NeH_2^+ system: Hayes *et al* (15) computed *ab initio* potential energy values and fitted a diatomics-in-molecules functional form to these values for the collinear system. They did not, however, report any scattering studies. Although the diatomics-in-molecules surface could be incorporated directly into a trajectory study of NeH_2^+ reaction dyanmics, the *ab initio* values could not.

Hayes *et al* (15) calculated *ab initio* potential energy values for 47 linear geometries of the NeH_2^+ system by an LCAO-MO-SCF method using a basis set consisting of 35 grouped Cartesian gaussian functions: a (3s, 1p) set on each hydrogen atom and a (5s, 4p, 1d) set on neon. The

geometries investigated fall upon eight rays emanating from the point $(R_{NeH},R_{HH}) = (4.03,4.00)$, where R_{NeH} is the NeH internuclear distance and R_{HH} is the HH distance measured in atomic units (see Figure 1). From this pattern of geometries, it is clear that Hayes et al intended the ab initio values to be fitted to a rotated Morse curve function in order to generate the full potential-energy surface. The dependence of the Morse parameters D, β, and r_e on the swing angle θ shown in Figure 2 could be determined by fitting a Morse function to each of the eight rays. Once $D(\theta)$, $\beta(\theta)$, and $r_e(\theta)$ are known, either by interpolation methods or by assuming a simple functional form for the dependence, the entire potential-energy surface can be generated.

The above was not used in this work because it was shown in the HeH_2^+ work (28-31) that the assumption of a particular functional form for the system interaction could introduce a bias into the description of the potential-energy surface which could seriously affect the outcome of scattering studies performed on that surface. Instead, a purely numerican interpolation procedure, the cubic splinefit, was used to generate potential energy values as a function of (r,θ). Because the splinefitting procedure requires that a rectangular grid of energies be used in the interpolation, it was first necessary to obtain such a grid of energies from the ab initio values along the eight rays. This was accomplished by using a one-dimensional splinefit of the ab initio energies along each ray to obtain a rectangular grid of energies in (r,θ), where r is the distance from a point on the ray to (4.03,4.00) and θ is the swing angle of the ray (see Figure 2). The array of energies generated could have then been used directly in the quasiclassical trajectory program, but would have required substantial modifications of the

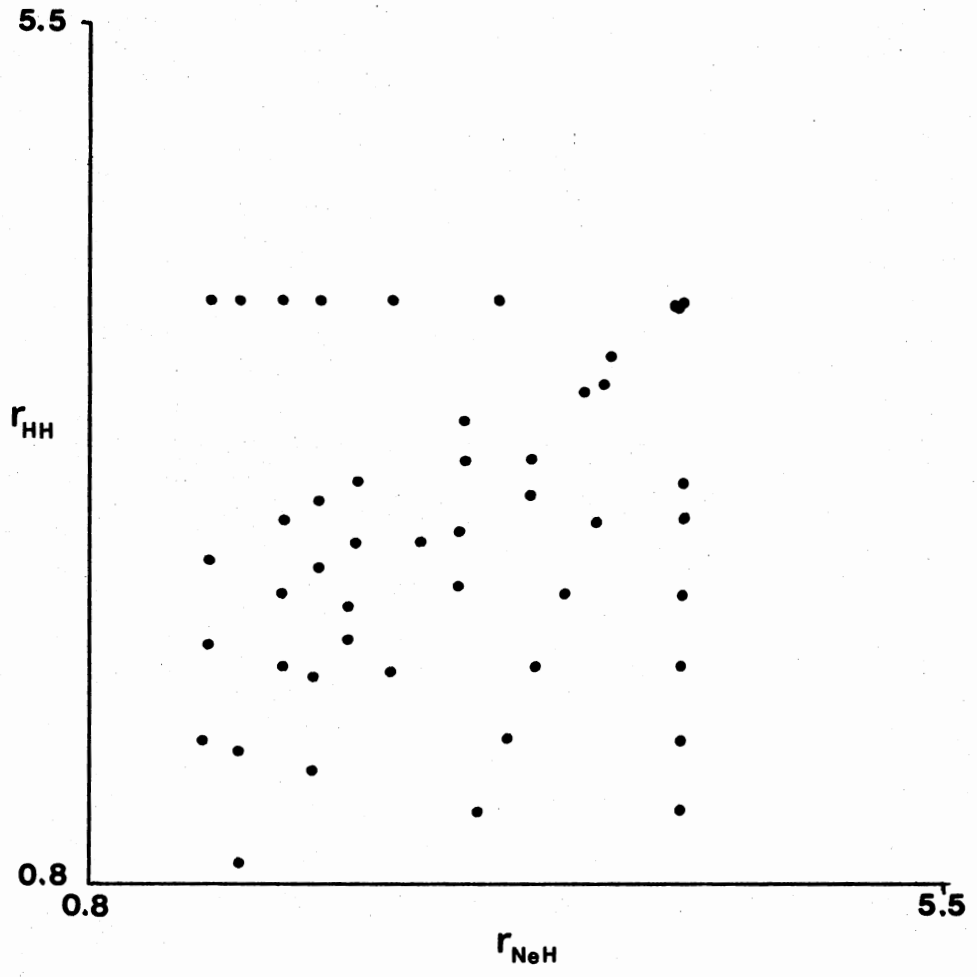

Figure 1. Geometries of the Collinear NeH_2^+ System for Which Hayes et al Calculated Ab Initio Potential Energies. Distances are given in atomic units

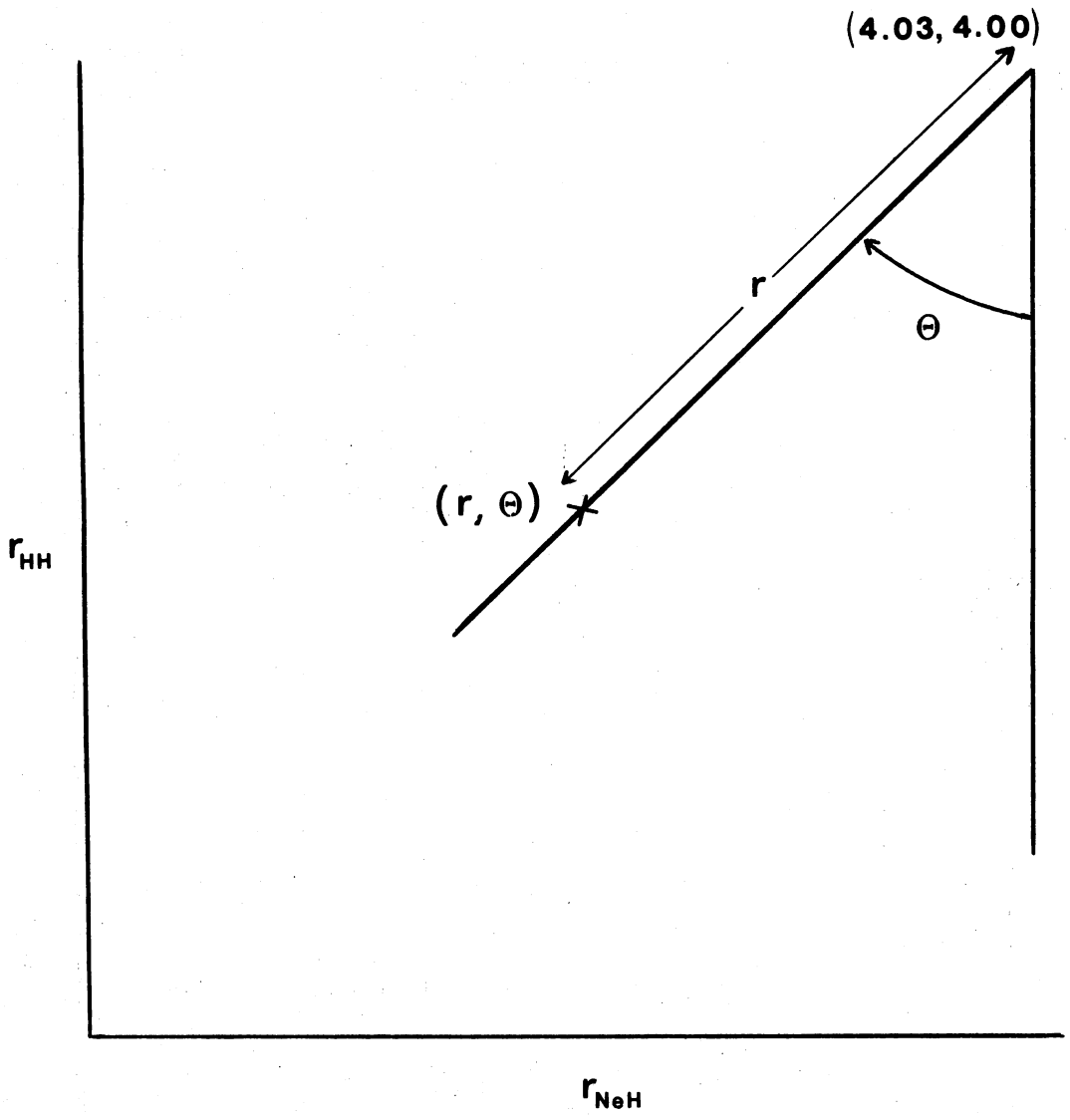

Figure 2. The Two Variables Used in the Attempt to Generate a Spline-fitted Surface From the Ab Initio Values of Hayes et al. r is the distance in atomic units from the point on the ray to (4.03,4.00). θ is the swing angle of the ray relative to the line r_{NeH} = 4.03 a.u.

existing algorithm. To avoid these difficulties, a two-dimensional splinefit of the energies of the (r,θ) grid was utilized to generate a set of energies falling on a more conventional (R_{NeH},R_{HH}) grid. This set of energies was employed in the scattering computations.

A contour plot of the resulting potential-energy surface (SAI_{Hayes}) showed it to be inadequate for making reliable calculations (see Figure 3). The contours did not exhibit the smooth behavior expected and were significantly distorted from the surface shown in the work of Hayes et al (15). In particular, the inner wall region displayed these characteristics, and it was probable, from the results of the work done by Sathyamurthy et al (31), that the qualitative outcome of our study would be affected. The defects in the surface were very likely the result of uncertainties introduced by the number of interpolations necessary to reach the desired (R_{NeH},R_{HH}) grid of energies from the values of the potential energies along the rays, as well as the fact that the density of ab initio energies in the interaction region was probably too low to give an accurate representation of the potential-energy surface in this area using the spline-fitting procedure. It was necessary, therefore, either to augment the ab initio potential energy values of Hayes et al with further ab initio calculations, or to generate an entirely new ab initio potential-energy surface. The latter alternative was chosen because the LCAO-MO-SCF procedure available could not accomodate the d orbitals used in Hayes' description of neon and thus would not produce energies on the same level of accuracy as those of Hayes et al. The new surface would be one whose potential energy values would form an (R_{NeH}, R_{HH}) grid and could be used directly in the quasiclassical trajectory procedure.

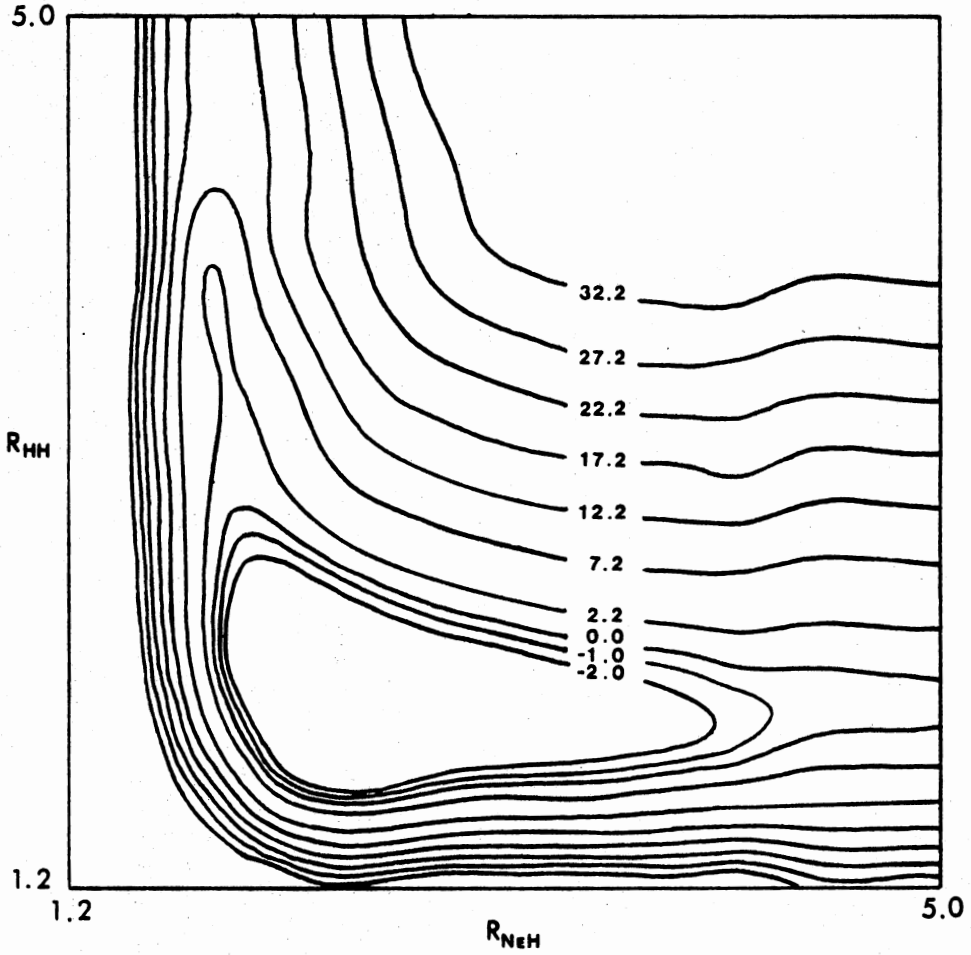

Figure 3. Contour Plot of the Potential-Energy Surface for the Collinear NeH_2^+ System Based on a Splinefit to the Ab Initio Values of Hayes et al (SAI_{Hayes}). Contours are in kcal/mole relative to an asymptotic limit of -129.13873 a.u. Distances are in atomic units

Gaussian-70 (52) was employed to calculate the ab initio energies as a function of the NeH and HH internuclear distances. The basis set used was identical to that of Hayes et al with the exception of the d orbitals on neon, i.e., a (3s,1p) set on each hydrogen atom and a (5s, 4p) basis on neon was employed (see Table I). Ab initio energies for 210 linear geometries were calculated covering the area from (R_{NeH}, R_{HH}) = 1.4 - 5.5 a.u. (see Figure 4). The potential energies at distances greater than 5.5 a.u. were obtained from graphs of potential energy vs. R_i at constant R_j (i=NeH,HH; j=NeH,HH). The asymptotic limits for these graphs were determined by adding the difference between the diatomics-in-molecules energies of Hayes et al (see Table II) at R_i = 5.5 and R_i = 10.0 a.u. to the ab initio energies at R_i = 5.5 a.u. The full set of potential energies is shown in Table III.

The potential-energy surface for the NeH_2^+ system was generated from a two-dimensional splinefit of the energies shown in Table III and was labelled the SAI_{G-70} surface. A contour map of this surface is given in Figure 5. The SAI_{G-70} surface, as expected, was found not to parallel the SAI_{Hayes} surface. Exclusion of the d orbitals on neon resulted in a well depth that was 0.17 eV shallower and which was displaced farther into the reactant channel by 0.3 a.u. However, a comparison of Figures 1 and 4 clearly shows a higher density of points both in the interaction region and in the reactant and product channels of the SAI_{G-70} surface and should allow a representation of the essential features of the NeH_2^+ system that is accurate enough to yield qualitatively correct results in the trajectory study of this system.

Figure 6 shows a map of the diatomics-in-molecules surface that is used in conjunction with the SAI_{G-70} surface in the dynamical

TABLE I

ORBITALS USED IN THE LCAO-MO-SCF CALCULATION OF POTENTIAL ENERGIES IN THE COLLINEAR Ne + H_2^+ SYSTEM. THE ORBITAL FORM IS

$$\phi_k = \sum_{i=1}^{n} f(x,y,z)\, a_{ki}\, \exp(-\alpha r^2)$$

Atom	Orbital[a]	n	i	a_{ki}	Exponent
H	s	3	1	0.025374	33.640
			2	0.189684	5.058
			3	0.852933	1.147
	s	1	1	1.000000	0.3211
	s	1	1	1.000000	0.1013
	p	1	1	1.000000	1.3202
Ne	s	6	1	0.000767	28660.000
			2	0.006068	4263.000
			3	0.032474	946.800
			4	0.131468	261.500
			5	0.397723	83.340
			6	0.542491	29.170
	s	2	1	0.269065	29.170
			2	0.764121	10.760
	s	1	1	1.000000	3.343
	s	1	1	1.000000	1.241
	s	1	1	1.000000	0.4063

TABLE I (Continued)

Atom	Orbital[a]	n	i	a_{ki}	Exponent
Ne	p	3	1	0.036154	84.840
			2	0.239503	19.710
			3	0.811934	6.219
	p	1	1	1.000000	2.211
	p	1	1	1.000000	0.7853
	p	1	1	1.000000	0.2566

[a]For s orbitals, f(x,y,z) = 1; for p orbitals, f(x,y,z) = x,y,z.

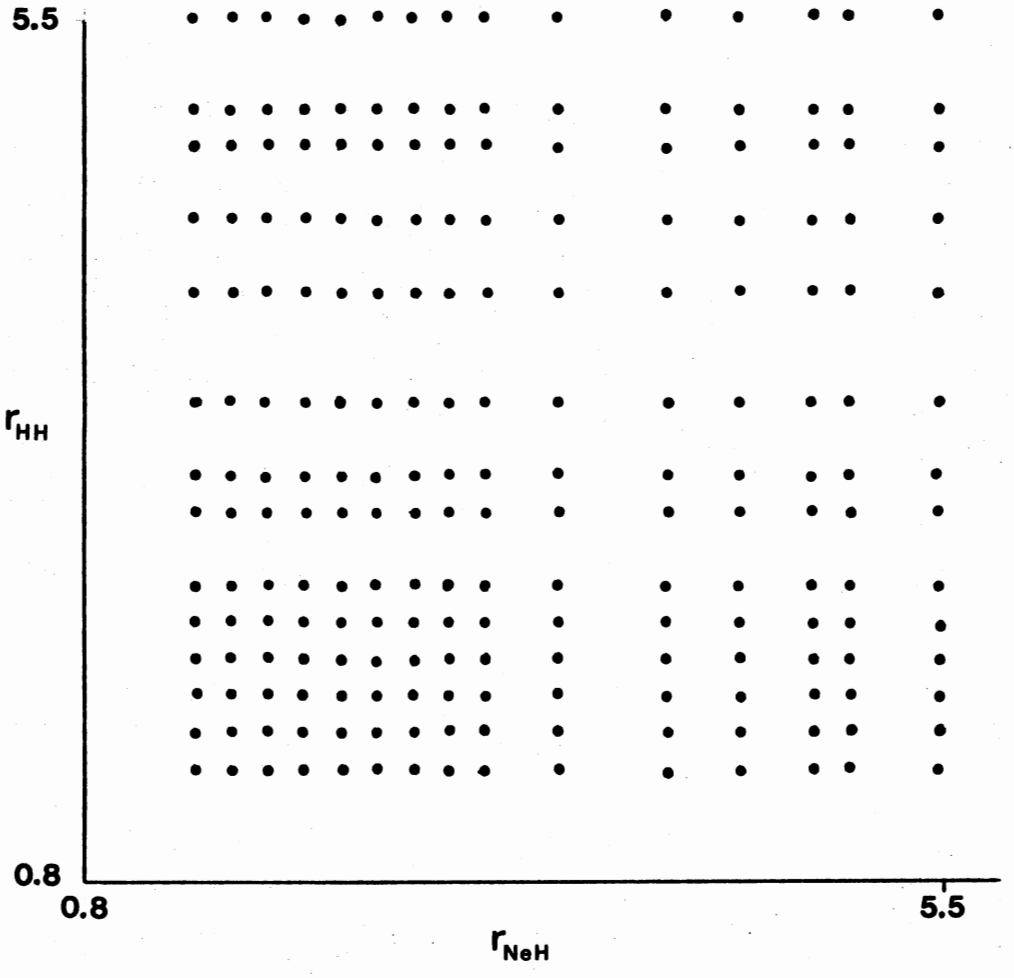

Figure 4. Geometries of the Linear NeH_2^+ System for Which Gaussian-70 Was Used to Calculate Ab Initio Potential Energies. This figure is on the same scale as Figure 1

TABLE II

MORSE PARAMETERS[a] USED BY HAYES ET AL TO GENERATE THE DIATOMICS-IN-MOLECULES SURFACE[b]

Molecule	State	r_e(a.u.)	D (eV)	β(a.u.$^{-1}$)
NeH^+	$^1\Sigma^+$	1.840	2.264831	1.436
NeH	$^2\Sigma^+$	1.700	1.6825672	1.500
H_2^+	$^2\Sigma_g^+$	2.003	2.7909801	0.6756
H_2^+	$^2\Sigma_u^+$	1.999	3.01561145	0.7455

[a]The Morse and anti-Morse interaction energies are given by

$$E = D \{\exp(-2\beta(r-r_e)) \mp 2\exp(-\beta(r-r_e))\}.$$

[b]The NeH parameters were obtained by fitting the DIM model to three of the SCF points. See reference 15.

TABLE III

ENERGIES USED TO GENERATE THE SAI_{G-70} SURFACE FOR THE COLLINEAR NeH_2^+ SYSTEM. ENERGIES ARE IN eV AND DISTANCES IN ATOMIC UNITS

R_{NeH} \ R_{HH}	1.4	1.6	1.8	2.0	2.2	2.4
1.4	5.36459	4.30526	3.61708	3.16845	2.87969	2.70024
1.6	3.02380	2.15644	1.62025	1.29288	1.10147	1.00032
1.8	1.83614	1.10908	0.69117	0.46441	0.35864	0.32981
2.0	1.22709	0.59111	0.25586	0.10414	0.06634	0.09788
2.2	0.92364	0.33960	0.05628	-0.04514	-0.03480	0.04215
2.4	0.78497	0.22704	-0.02746	-0.09843	-0.05710	0.05084
2.6	0.73277	0.18516	-0.05492	-0.10876	-0.04894	0.07831
2.8	0.72189	0.17728	-0.05628	-0.10142	-0.03100	0.10740
3.0	0.72951	0.18380	-0.04731	-0.08782	-0.01224	0.13214
3.4	0.75643	0.20691	-0.02393	-0.06199	0.01795	0.16667
4.0	0.78715	0.23383	0.00190	-0.03616	0.04432	0.19386
4.4	0.79993	0.24553	0.01305	-0.02501	0.05520	0.20447
4.8	0.80863	0.25368	0.02094	-0.01767	0.06254	0.21154
5.0	0.81189	0.25667	0.02366	-0.01468	0.06526	0.21426
5.5	0.81760	0.26238	0.02909	-0.00979	0.06988	0.21861
6.0	0.8202	0.2652	0.0316	-0.0074	0.0722	0.2208
7.0	0.8230	0.2680	0.0342	-0.0048	0.0746	0.2232
8.0	0.8238	0.2691	0.0352	-0.0039	0.0755	0.2241
9.0	0.8243	0.2692	0.0356	-0.0035	0.0759	0.2246
10.0	0.8246	0.2692	0.0358	-0.0032	0.0763	0.2250

TABLE III (Continued)

R_{NeH} \ R_{HH}	2.8	3.0	3.4	4.0	4.4	4.8
1.4	2.54036	2.51752	2.52214	2.56456	2.58985	2.60861
1.6	0.95138	0.96660	1.02316	1.10554	1.14361	1.16971
1.8	0.39045	0.44592	0.56066	0.69171	0.74691	0.98253
2.0	0.25803	0.35320	0.52939	0.71727	0.79340	0.84180
2.2	0.28386	0.41410	0.64957	0.89944	1.00113	1.06585
2.4	0.35184	0.51008	0.79694	1.10854	1.23959	1.32388
2.6	0.41845	0.59628	0.92201	1.28908	1.45059	1.55772
2.8	0.47120	0.66099	1.01310	1.42312	1.61291	1.74451
3.0	0.50873	0.70558	1.07265	1.51122	1.72357	1.87801
3.4	0.55250	0.75371	1.13138	1.59333	1.82907	2.01287
4.0	0.58023	0.78117	1.15748	1.62080	1.86143	2.05448
4.4	0.58975	0.79014	1.16482	1.62542	1.86469	2.05747
4.8	0.59600	0.79585	1.16944	1.62814	1.86659	2.05828
5.0	0.59845	0.79803	1.17107	1.62950	1.86741	2.05883
5.5	0.6023	0.8016	1.1741	1.6317	1.8690	2.0596
6.0	0.6049	0.8036	1.1760	1.6332	1.8701	2.0607
7.0	0.6073	0.8058	1.1779	1.6352	1.8723	2.0623
8.0	0.6081	0.8066	1.1789	1.6362	1.8736	2.0636
9.0	0.6084	0.8073	1.1796	1.6371	1.8745	2.0648
10.0	0.6086	0.8078	1.1803	1.6379	1.8753	2.0660

TABLE III (Continued)

R_{NeH} \ R_{HH}	5.0	5.5	6.0	7.0	8.0	9.0	10.0
1.4	2.61568	2.62900	2.6391	2.6523	2.6591	2.669	2.666
1.6	1.17923	1.19609	1.2050	1.2175	1.2260	1.233	1.239
1.8	0.79531	0.81679	0.8297	0.8460	0.8554	0.862	0.867
2.0	0.85866	0.88667	0.9027	0.9210	0.9318	0.940	0.947
2.2	1.08814	1.12458	1.1425	1.1623	1.1767	1.188	1.199
2.4	1.35325	1.40110	1.4232	1.4486	1.4667	1.481	1.492
2.6	1.59551	1.65723	1.6900	1.7209	1.7412	1.757	1.771
2.8	1.79209	1.87149	1.9043	1.9440	1.9720	1.994	2.130
3.0	1.93593	2.03272	2.0740	2.1210	1.1545	2.183	2.208
3.4	2.08683	2.2103	2.270	2.338	2.387	2.427	2.464
4.0	2.13550	2.2709	2.362	2.460	2.527	2.584	2.636
4.4	2.13849	2.2732	2.372	2.497	2.574	2.635	2.689
4.8	2.13904	2.2747	2.381	2.517	2.598	2.664	2.721
5.0	2.13931	2.2752	2.381	2.522	2.606	2.673	2.731
5.5	2.1405	2.2761	2.384	2.531	2.618	2.688	2.746
6.0	2.1412	2.2768	2.386	2.534	2.621	2.692	2.751
7.0	2.1427	2.2780	2.388	2.536	2.623	2.695	2.754
8.0	2.1439	2.2790	2.389	2.537	2.624	2.696	2.755
9.0	2.1450	2.2797	2.390	2.538	2.625	2.697	2.756
10.0	2.1462	2.2803	2.391	2.538	2.626	2.697	2.757

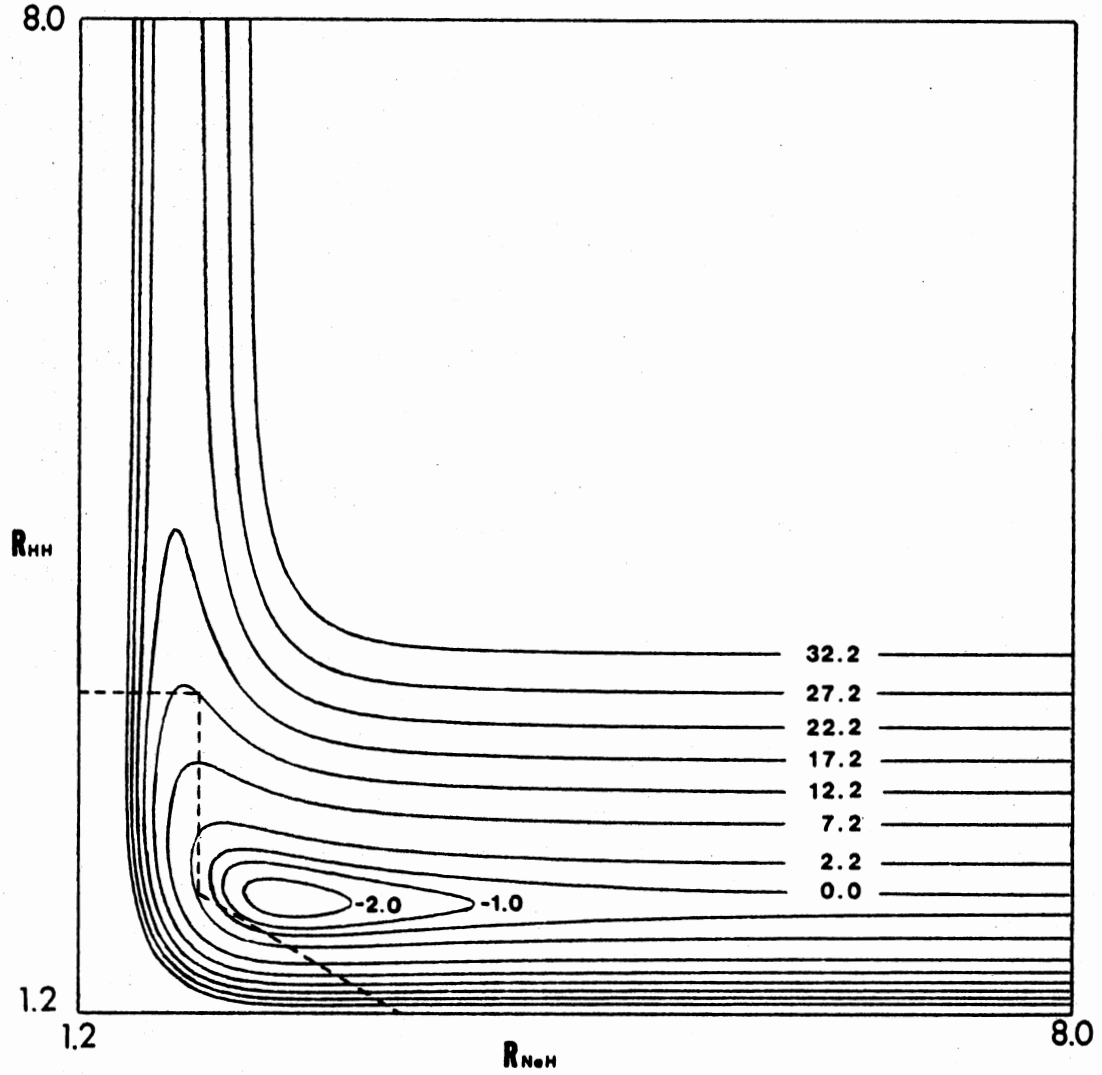

Figure 5. Contour Plot of the SAI Potential-Energy Surface for the Collinear NeH_2^+ System. The boundaries of the inner repulsive wall are indicated by the dashed line. Contours are in kcal/mole. Distances are in atomic units

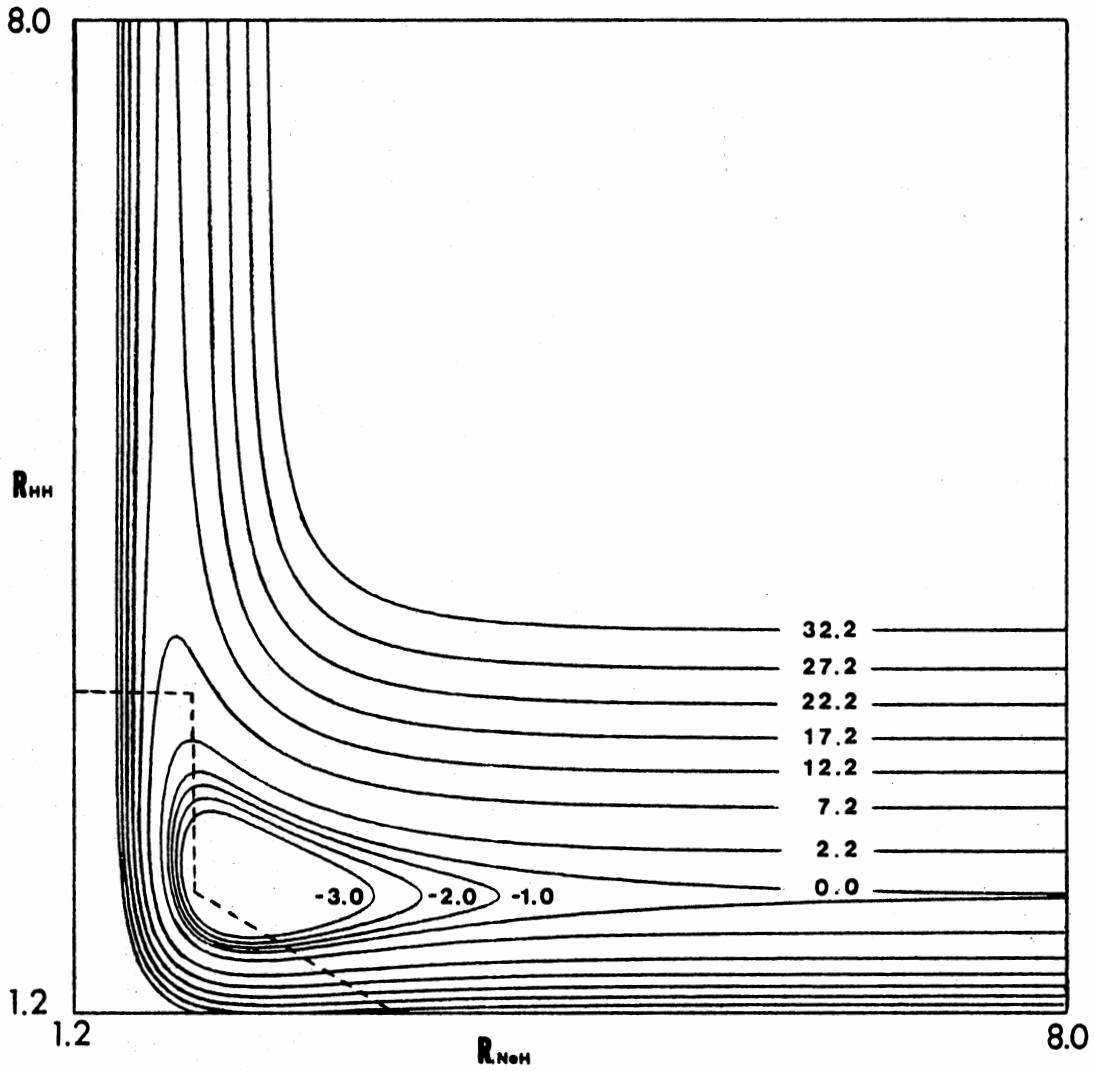

Figure 6. Contour Plot of the DIM Potential-Energy Surface Calculated by Hayes et al for the Collinear NeH_2^+ System. The boundaries of the inner repulsive wall are indicated by the dashed line. Contours are in kcal/mole. Distances are in atomic units

studies. The parameters for this surface, calculated by Hayes et al (15), are given in Table II.

The He - CO_2 System

The calculation of an ab initio potential-energy surface for the He - CO_2 rigid rotor system was a straightforward, but formidable, task. In principle, the potential energy must be obtained as a function of each of the six interatomic distances shown in Figure 7a. Fortunately, the dimensionality of the problem can be reduced from six to two by restricting the CO_2 molecule to be a rigid rotor. This is a reasonable approximation since rotationally inelastic scattering is affected mainly by the variables θ and R (see Figure 7b), the angle which helium makes with the CO_2 bond axis and the distance from helium to the CO_2 center of mass, respectively. Not only is the size of the calculation thereby reduced, but now a numerical interpolation technique, such as the cubic splinefit, can be used to generate the full potential-energy surface. This ensures a more accurate and unbiased representation of the entire ab initio surface than would have been possible using an analytic function to fit the energy values.

As was the case in the calculation of potential energies in the NeH_2^+ system, Gaussian-70 (52) was used to implement the LCAO-MO-SCF calculation of ab initio potential energies in the He - CO_2 rigid rotor system. In all calculations CO_2 was held at its linear equilibrium geometry (R_{C-O} = 1.1611 Å). The basis sets used in describing the four atoms in the system are shown in Table IV and, with the exception of helium, are taken directly from the basis sets provided in the Gaussian-70 program. The basis set used for helium was a minimal basis set

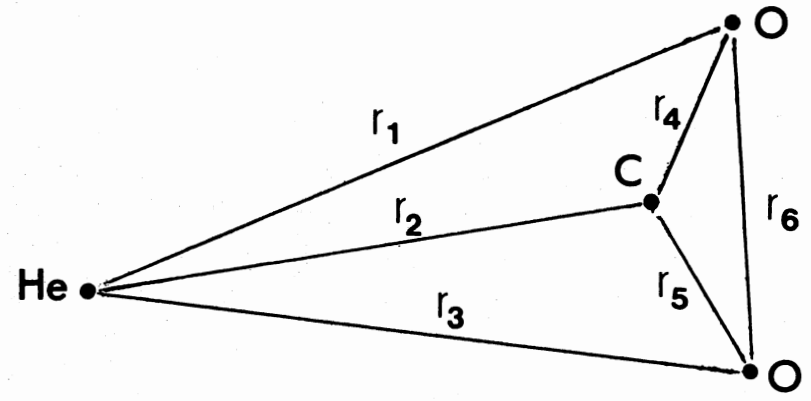

(a)

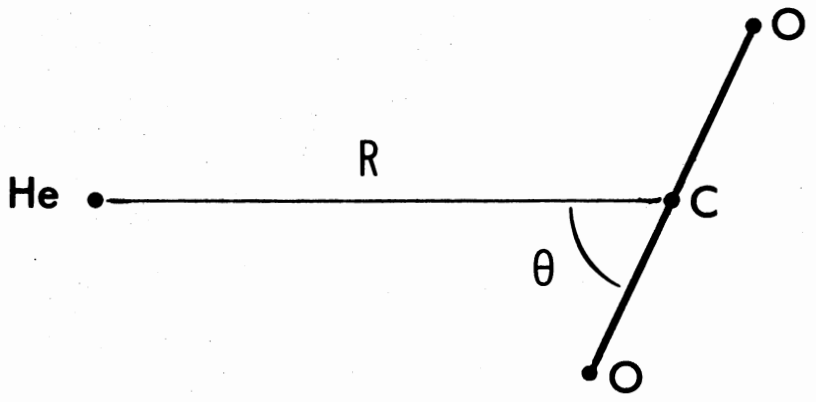

(b)

Figure 7. The He - CO_2 System. a) The full set of interatomic distances necessary to describe the He - CO_2 geometry. b) The two variables necessary to describe the He - CO_2 rigid rotor system

TABLE IV

THE BASIS SET EMPLOYED IN THE LCAO-MO-SCF CALCULATION OF POTENTIAL ENERGIES IN THE He - CO_2 SYSTEM[a]

Atom	Orbital	n	Exponent	s Coefficient	p Coefficient
He[b]	1s	6	0.193849	0.267680	
			0.589851	0.468440	
			1.879204	0.298010	
			6.633653	0.109640	
			28.95149	0.024650	
			192.4388	0.003300	
C[c]	1s	6	3.16393	0.362312	
			9.28666	0.467941	
			29.2101	0.232184	
			103.949	0.0688426	
			457.369	0.0140373	
			3047.52	0.00183474	
	2sp	3	0.544249	1.14346	0.744308
			1.88129	-0.160854	0.316424
			7.86827	-0.119332	0.0689991
	2sp'	1	0.168714	1.000000	1.000000
O	1s	6	5.79963	0.358521	
			16.8976	0.470193	
			52.9645	0.232714	
			188.047	0.0684450	
			825.235	0.0139502	
			5484.67	0.00183107	

TABLE IV (Continued)

Atom	Orbital	n	Exponent	s Coefficient	p Coefficient
O	2sp	3	1.01376	1.13077	0.727159
			3.59993	-0.148026	0.339753
			15.5396	-0.110777	0.0708742
	2sp'	1	0.270006	1.000000	1.000000

[a]The form for each orbital is $\phi_k^{STO} = \sum_{i=1}^{n} f(x,y,z)\, a_{ki}\, \exp(-\alpha r^2)$, where $f(x,y,z) = 1$ for s orbitals and $f(x,y,z) = x,y,z$ for p orbitals. For the valence shell of carbon and oxygen, the s and p orbitals have the same exponent and are shown together.

[b]Reference 53

[c]The basis set was taken directly from the extended basis sets of Gaussian-70, which in turn were taken from W. J. Hehre, R. Ditchfield, and J. A. Pople, J. Chem. Phys. 56, 2275 (1972).

calculated by Huzinaga (53) and was chosen over the bases provided by Gaussian-70 because of its small size and higher accuracy. Although a minimal basis was sufficient for the description of helium, an extended basis set was required for CO_2 in order to allow for anisotropy in the valence shell.

For both helium and CO_2, the basis sets consisted of Slater-type orbitlas (STO's) approximated by expansions of gaussian-type orbitals. For the valence shells of the carbon and oxygen atoms, two STO's were used: one approximated by a three-gaussian expansion and the other by a single gaussian (31G). For the 1s orbital of helium and the inner orbitals of CO_2, six gaussians were used, the number being determined from comparison of potential-energy values obtained using STO's consisting of four, five, and six gaussians. This comparison, shown in Table V, indicates the importance of using the six-gaussian expansion for helium (STO-6G): the energy is lowered 0.016 eV in changing from a four- to a six-gaussian representation. Conversely, the number of gaussians in the inner orbitals of CO_2 did not have a very large effect on the interaction potential and, since the calculation times also did not vary much, the more extensive six-gaussian expansion for the inner orbitals was chosen for the surface computations. This extended basis set for CO_2 is denoted 6-31G.

Ab initio potential energies were calculated for 256 geometries of the He - CO_2 system and are shown in Table VI. The starred values were obtained from extrapolation of ln V vs. R plots. Since the behavior of the potential energy at small R is very nearly exponential (see Figure 8), these values should be accurate enough to be used with the ab initio energies. These extrapolated potential energies were included mainly to

TABLE V

COMPARISON OF TIMES AND ACCURACIES OF THE DIFFERENT BASIS SETS FOR HELIUM AND CO_2

Basis CO_2[a]	He[b]	$E_{R=2\mathring{A}}$(a.u.)[c]	E_∞(a.u.)[d]	ΔE(eV)	Time(sec)[e]
6-31G	STO-4G	-190.357275	-190.370150	0.35020	262
	STO-5G	-190.361565	-190.374384	0.36228	248
	STO-6G	-190.362630	-190.376106	0.36655	266
5-31G	STO-4G	-190.318970	-190.331839	0.35004	235
	STO-5G	-190.323261	-190.336573	0.36209	243
	STO-6G	-190.324327	-190.337795	0.36633	253
4-31G	STO-4G	-190.170252	-190.183125	0.35015	229
	STO-5G	-190.174547	-190.187859	0.36214	245
	STO-6G	-190.175618	-190.189080	0.36617	238

[a] From the bases provided in Gaussian-70

[b] Reference 53

[c] All energies are for helium perpendicular to the CO_2 bond axis ($\theta = 90°$).

[d] E_∞ is taken to be the He - CO_2 interaction energy at R = 15 $\mathring{A}$.

[e] The time is that required to calculate $E_{R=2\mathring{A}}$.

TABLE VI

LCAO-MO-SCF POTENTIAL ENERGIES FOR THE He - CO_2 RIGID ROTOR SYSTEM. ENERGIES ARE MEASURED IN eV FROM THE ENERGY OF CO_2 AND HELIUM AT INFINITE SEPARATION.[a] DISTANCES ARE IN Å.[b]

R	θ = -10°	θ = -5°	θ = 0°	θ = 5°	θ = 10°	θ = 20°
1.8	50.060*	72.473*	(115.957)	(72.473)	(50.060)	(36.716)
2.0	20.973*	27.200*	(39.774)	(27.200)	(20.973)	(16.171)
2.2	9.711*	11.980*	(15.229)	(11.980)	(9.711)	(7.413)
2.4	4.407*	5.276*	(6.509)	(5.276)	(4.407)	(3.432)
2.6	2.040*	2.395*	(2.727)	(2.395)	(2.040)	1.64023
2.8	0.99736*	1.08053*	1.11010	1.08053	0.99736	0.73156
3.0	0.43016*	0.46410*	0.47610	0.46410	0.43016	0.32000
3.2	0.18228*	0.19604*	0.20086	0.19604	0.18228	0.13699
3.4	0.07574*	0.08123*	0.08316	0.08123	0.07574	0.05735
3.7	0.01946*	0.02082*	0.02131	0.02082	0.01946	0.01481
4.0	0.00475*	0.00507*	0.00518	0.00507	0.00475	0.00363
4.3	0.00113*	0.00116*	0.00118	0.00116	0.00113	0.00088
4.7	0.00010*	0.00010*	0.00010	0.00010	0.00010	0.00007
5.0	-0.00001*	-0.00001*	-0.00001	-0.00001	-0.00001	-0.00001
5.5	-0.00001*	-0.00001*	-0.00003	-0.00001	-0.00001	-0.00001
6.0	-0.00001*	-0.00001*	-0.00004	-0.00001	-0.00001	-0.00001

TABLE VI (Continued)

R	θ = 30°	θ = 40°	θ = 50°	θ = 60°	θ = 70°
1.8	(18.788)	(9.424)	(4.633)	2.27992	1.31758
2.0	(9.054)	(4.633)	2.27799	1.17204	0.65562
2.2	(4.363)	2.30535	1.15115	0.58291	0.31611
2.4	2.13043	1.12558	0.56346	0.28107	0.14806
2.6	0.99358	0.53352	0.26747	0.13139	0.06742
2.8	0.45205	0.24577	0.12293	0.05956	0.02977
3.0	0.20070	0.10985	0.05471	0.02604	0.01274
3.2	0.08678	0.04764	0.02352	0.01103	0.00529
3.4	0.03657	0.02003	0.00983	0.00453	0.00216
3.7	0.00951	0.00518	0.00249	0.00113	0.00048
4.0	0.00233	0.00127	0.00059	0.00020	0.00004
4.3	0.00059	0.00026	0.00010	0.00004	-0.00004
4.7	0.00002	-0.00001	-0.00004	-0.00004	-0.00004
5.0	-0.00004	-0.00004	-0.00004	-0.00004	-0.00004
5.5	-0.00004	-0.00004	-0.00004	-0.00004	-0.00004
6.0	-0.00004	-0.00003	-0.00004	-0.00004	-0.00004

TABLE VI (Continued)

R	θ = 80°	θ = 85°	θ = 90°	θ = 95°	θ = 100°
1.8	0.89547	0.80505	0.77614	0.80505*	0.89547*
2.0	0.43002	0.38188	0.36653	0.38188*	0.43002*
2.2	0.20021	0.17564	0.16792	0.17564*	0.20021*
2.4	0.09073	0.07870	0.07481	0.07870*	0.09073*
2.6	0.04011	0.03445	0.03257	0.03445*	0.04011*
2.8	0.01729	0.01484	0.01391	0.01484*	0.01729*
3.0	0.00733	0.00616	0.00578	0.00616*	0.00733*
3.2	0.00295	0.00246	0.00233	0.00246*	0.00295*
3.4	0.00113	0.00094	0.00086	0.00094*	0.00113*
3.7	0.00023	0.00018	0.00015	0.00018*	0.00023*
4.0	-0.00001	-0.00004	-0.00004	-0.00004*	-0.00001*
4.3	-0.00004	-0.00004	-0.00005	-0.00004*	-0.00004*
4.7	-0.00004	-0.00004	-0.00005	-0.00004*	-0.00004*
5.0	-0.00004	-0.00004	-0.00004	-0.00004*	-0.00004*
5.5	-0.00004	-0.00004	-0.00004	-0.00004*	-0.00004*
6.0	-0.00004	-0.00004	-0.00004	-0.00004*	-0.00004*

[a]As in Table V, the interaction energy between helium and CO_2 at a separation of 15 Å is taken to be E_∞.

[b]CO_2 is held fixed in a linear configuration with each C-O bond length = 1.1611 Å.

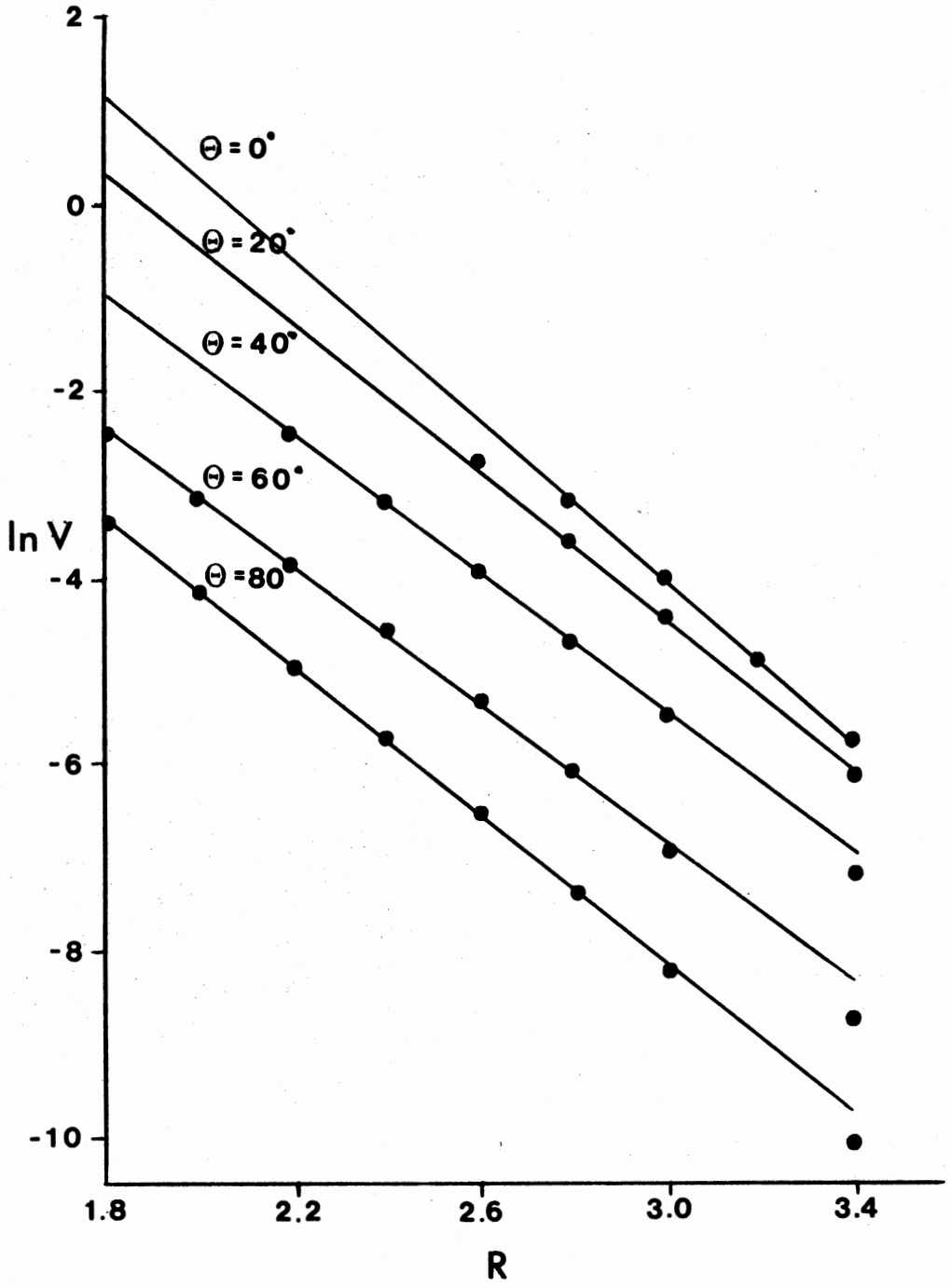

Figure 8. Ln V Versus R Plots for Several He - CO_2 Angles. The potential is in atomic units and the distances in Å

fill out the rectangular grid required by the spline-fitting procedure; the trajectories will sample only those contours <1 eV. Furthermore, the values for $\theta < 0°$, $\theta > 90°$, and $R > 5$ Å were included to increase the accuracy of the two-dimensional cubic spline-fitting procedure near the edges of the (R,θ) grid. The actual potential-energy surface covers only the range $\theta = 0° - 90°$, $R = 1.8 - 5.0$ Å; however, no further energies were needed since the symmetry of the He - CO_2 rigid rotor system allows the generation of the full potential-energy surface from this one quadrant.

The potential-energy surface for the He - CO_2 system is shown in Figure 9a. The positions of the carbon and oxygen atoms are fixed, as indicated, and the contours depict the potentials that helium experiences as it approaches CO_2 from a given angle.

To impart an idea of how accurately the spline-fitted surface reflects the actual ab initio values, ab initio potential-energy values were calculated for a set of ten random geometries likely to be sampled in the trajectory studies. The potential-energy values for the same points were then calculated using the two-dimensional splinefit and the original 256 ab initio points. The results are shown in Table VII and indicate how well the cubic spline procedure works in the two-dimensional case.

Because part of the study of rotationally inelastic scattering in the He - CO_2 system involves a comparison between the theoretical results obtained from the spline-fitted ab initio (SAI) surface calculated here and the electron gas (EG) surface of Parker, Snow, and Pack (16)[1]

---

[1]The complete details of Parker, Snow, and Pack's calculation of the EG surface are given in Appendix A.

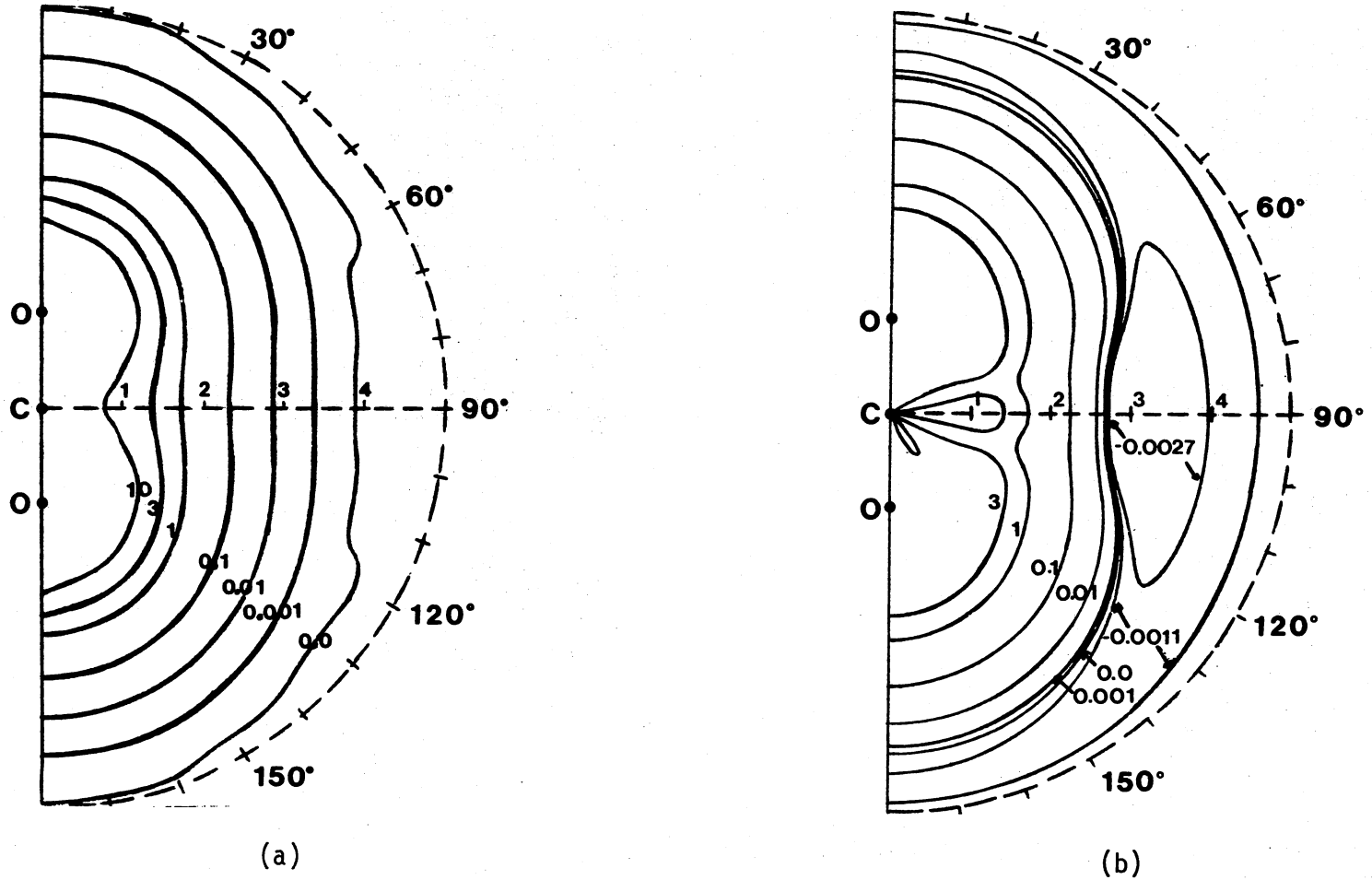

(a) (b)

Figure 9. Contour Plots of the Potential-Energy Surfaces for the He - CO_2 Rigid Rotor System. (a) SAI surface, and (b) Electron Gas surface. The positions of the carbon and oxygen atoms are shown. Energy contours are in eV and distances are in Å

TABLE VII

EVALUATION OF THE ACCURACY OF THE SPLINE-FITTED POTENTIAL-ENERGY SURFACE. ENERGIES ARE IN eV AND DISTANCES IN Å.[a]

θ	R	$\Delta E_{ab\ initio}$	ΔE_{Spline}
78.299	3.077	0.005564	0.005631
49.520	2.641	0.236628	0.237064
67.279	2.356	0.206354	0.206269
42.185	2.483	0.714804	0.712959
53.822	4.801	-0.000039	-0.000047
35.311	2.769	0.374586	0.373020
23.192	3.164	0.140530	0.141062
6.750	3.558	0.039156	0.038507
17.904	4.217	0.001348	0.001381
88.333	2.186	0.178420	0.178263
		Standard deviation = 0.000757 eV	

[a]All energies are relative to E_∞ = -190.376106 a.u.

(see Figure 9b), the differences between the two surfaces should be noted. An obvious difference is that the SAI surface contains no attractive interactions, while the EG surface contains a shallow, elliptically-shaped well which has a depth of 0.0013 eV at (R = 4.66 Å, θ = 0°) and of 0.00824 eV at (R = 3.02 Å, θ = 90°). The absence of this feature on the SAI surface is due to the neglect of electron correlation in the calculation of the ab initio energies, i.e., no configuration interaction was employed in the ab initio calculations. This is clearly seen in Figure 10, semilog plots of potential energy as a function of the He - C distance at θ = 0° and θ = 90°. In each case, the energies plotted are the original values from which the respective potential-energy surfaces were fitted. In the case of the ab initio values, the surface passes through each ab initio point; however, the values obtained using the electron gas approximation were fitted using an expansion in Legendre polynominals with the coefficients fitted to a continuous function of R

$$V(R,\theta) = \sum_{n \text{ even}} v_n(R)\, P_n(\cos\theta),$$

and the EG surface does not pass directly through the original values. Furthermore, the electron gas potential is divided into two parts

$$V_{EG}(R,\theta) = V^{HF}(R,\theta) + aV^{COR}(R,\theta),$$

where the first term is the Hartree-Fock energy and the second the correlation energy scaled up to fit a Van der Waal's potential.

Shown in Figure 10 for each angle are the ab initio potential, V_{EG}, and V^{HF}. Comparing the ab initio potential and V^{HF} allows a direct measure of the relative accuracy of the two calculations and, clearly, the two sets of values are in very good agreement at all the geometries

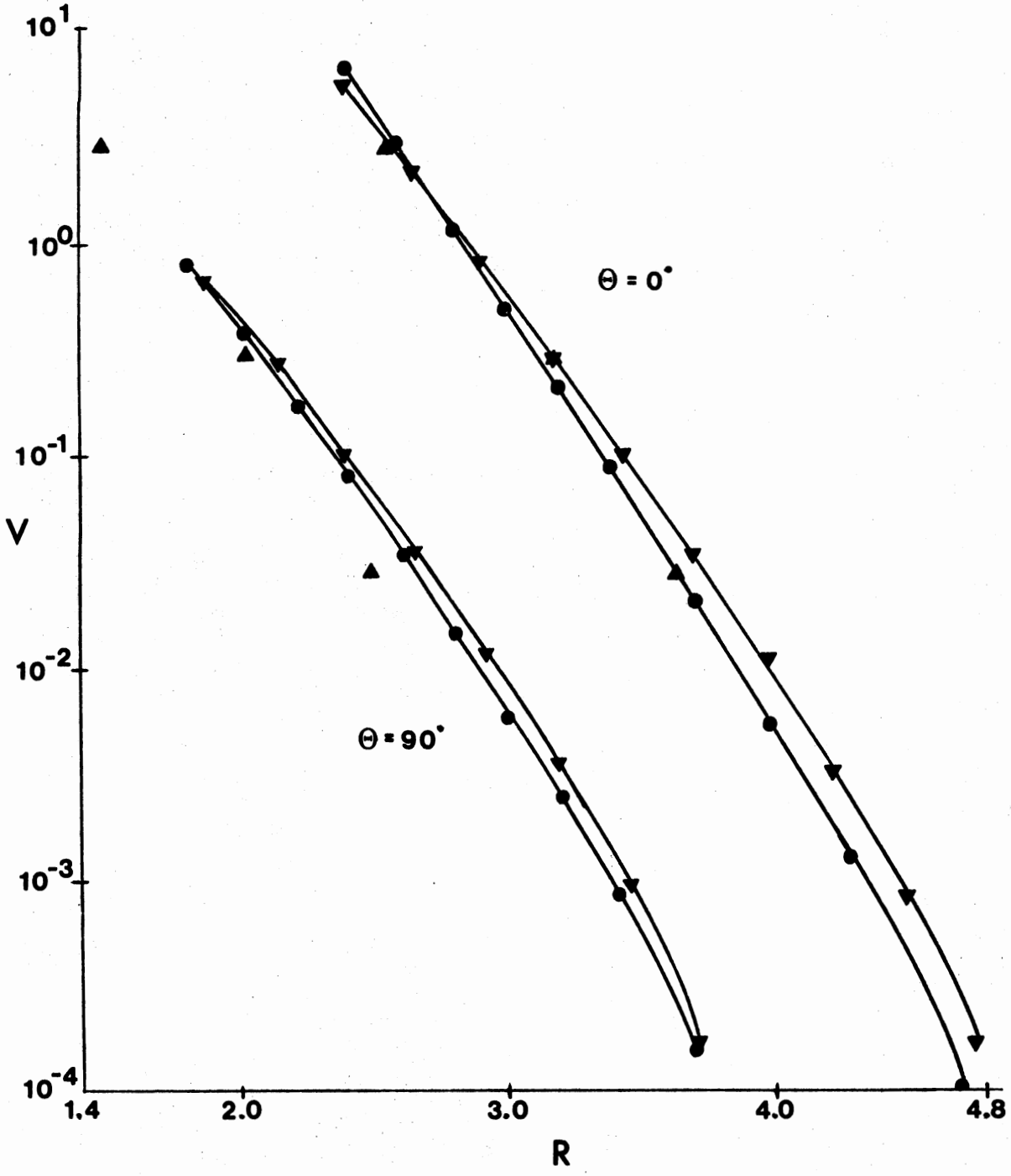

Figure 10. Comparison of Ab Initio and Electron Gas Potential Energies at $\theta = 0°$ and $\theta = 90°$. The circles represent the ab initio values, the triangles the electron gas potential, and the inverted triangles the electron gas values with the correlation energy excluded. The distances are in Å and the energies are in eV

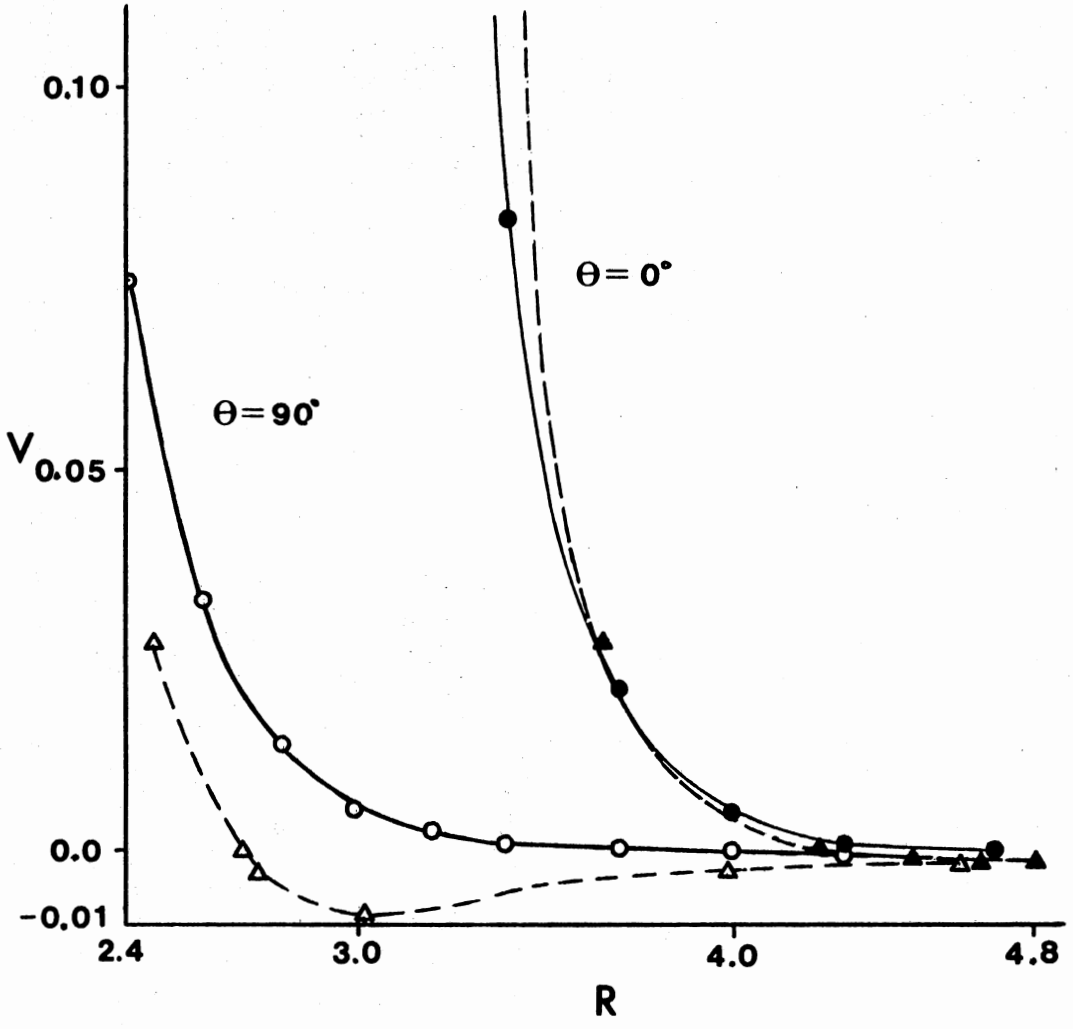

Figure 11. A Comparison of the Potential-Energy Contours of the SAI and EG Surfaces at $\theta = 0°$ and $\theta = 90°$. The circles represent points on the SAI surface and the triangles points on the EG surface. Energies are in eV and distances are in Å

shown. The ab initio potential is slightly steeper than V^{HF} and, for small R, more repulsive. The effect of adding the correlation energy to V^{HF} is reflected in the three V_{EG} points at each angle: the ab initio potential and V_{EG} are in near coincidence for small to moderate values of R, while at larger distances V_{EG} shows the increasing influence of the attractive V^{COR} term and diverges from the ab initio energies. Indeed, additional V_{EG} points could not be shown in Figure 10 because the values became negative. This behavior is shown more clearly in Figure 11, a plot of the behavior of the two surfaces at $\theta = 0°, 90°$. With the exception of the shallow well on the EG surface, the inclusion of correlation energy does not radically affect the description of the He - CO_2 interaction. This was assumed at the start of the ab initio calculations, since both helium and carbon dioxide are closed-shell systems and no extensive electronic rearrangements occur during a rotationally inelastic collision. The relative importance of the attractive well will become apparent upon comparison of the theoretical results obtained from the SAI and EG surfaces.

CHAPTER III

EFFECTS OF SURFACE TOPOLOGY ON REACTION DYNAMICS IN THE HeH_2^+ AND NeH_2^+ SYSTEMS

The course of the study of collision dynamics in the HeH_2^+ system was outlined in the first chapter and indicates that the differences between the results obtained on the SAI and DIM surfaces were due to small differences between the potential-energy surfaces themselves. Since the quasiclassical trajectory (QCT) method was used in these calculations, quantum mechanical (QM) calculations must be performed on the two surfaces so that the accuracy of the QCT studies may be assessed and the results confirmed. The following section is the body of a paper published by Chemical Physics Letters that describes the QM investigation of the reaction dynamics of the HeH_2^+ system (57).

Quantum Mechanical Scattering Calculations: The $He + H_2^+(v=0,1,2) \rightarrow HeH^+ + H$ Reaction

The QM reaction probabilities for the reaction

$$He + H_2^+(v=0,1,2) \rightarrow HeH^+ + H \qquad (R1)$$

have been computed on both the SAI and DIM surfaces using the time-dependent procedure described by McCullough and Wyatt (12). It has been shown that cubic spline interpolation is very accurate for such all-channel time-dependent QM calculations (8). The method involves the solution of the time-dependent Schrödinger equation by successive use of

the unitary time-evolution operator $U(\Delta t)$:

$$U(\Delta t) = [1+(1\Delta t/2h)H]^{-1}[1-(i\Delta t/2h)H], \qquad \text{(III-1)}$$

where H is the system Hamiltonian. The initial wavefunction of the system at t = 0 is assumed to be

$$\Psi(t_o=0) = \phi(q_1)X_v(q_2), \qquad \text{(III-2)}$$

where $X_v(q_2)$ is the vth state vibrational wavefunction for the H_2^+ Morse oscillator, and $\phi(q_1)$ is a minimum normalized guassian wavepacket. The functional forms for $\phi(q_1)$ and $X_v(q_2)$ have been previously given (54). Successive operation by $U(\Delta t)$ n times upon $\Psi(t_o)$ yields the wavefunction at $t_o + n\Delta t$:

$$\Psi(t_o + n\Delta t) = [U(\Delta t)]^n \Psi(t_o). \qquad \text{(III-3)}$$

The QM reaction probability, P_{QM}, is computed by

$$P_{QM} = \int_{\text{products}} \Psi^*(t=\infty)\Psi(t=\infty)d\tau , \qquad \text{(III-4)}$$

where the integral is taken over the configuration space corresponding to products (HeH^+ + H). The details of the procedure have been given by McCullough and Wyatt (12) and further discussed by Kellerhals et al (54).

All computations were performed on an IBM 360/65 computer. Completion of a reaction for a given set of conditions generally required from 350 to 550 time steps, where one time step was 1.07750×10^{-16}s. Computation of a reaction probability at a given total energy and vibrational state required from 4 - 6 hours of CPU time. The procedure employed to check the numerical accuracy of the method has already been described (54), and the accuracy of the present results is comparable to that previously reported (54).

Figures 12a and 12b show the distribution of probability density

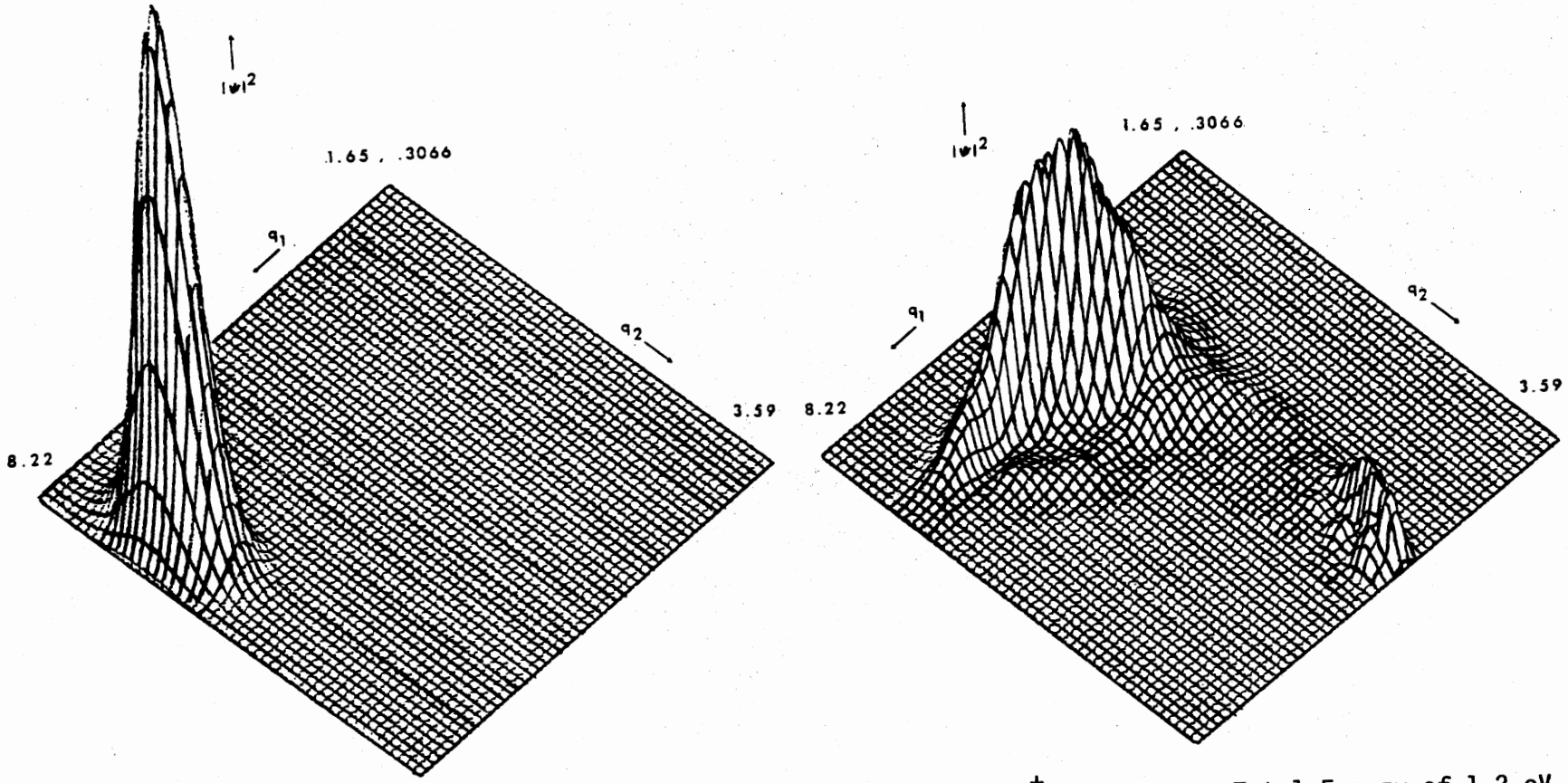

Figure 12. Probability Densities on the SAI Surface for the HeH_2^+ System at a Total Energy of 1.2 eV and v=0. a) Time = 0. b) Time = 4.1 X 10^{-14} s

at the beginning and end of a calculation on the SAI surface, at a total energy of 1.2 eV with H_2^+ initially in the v=0 vibrational state. The variables q_1 and q_2 are the distance from helium to the H_2^+ center of mass and a mass-scaled H_2^+ internuclear distance, respectively (12) (54). In Figure 12a the single peak represents the initial H_2^+ Morse oscillator probability density in the v=0 state. Computations involving the vth excited vibrational state will exhibit (v+1) such peaks aligned along the q_2 axis with v nodes between them. In Figure 12b the probability density is seen to divide into two distinguishable volumes. The product configuration space is the region at large q_2, and the reaction probability computed from Eq (III-4) is simply the total volume under the wavepacket in this region.

To some extent the definition of the product configuration space is arbitrary. In the v=0 case, the distinction between reactant and product configurations is reasonably clear. However, for excited vibrational states of H_2^+, the resolution of the final-state wavefunction into reactants and products is more difficult due to the reflection of the wavepacket from the edges of the rectangular grid over which the time-dependent Schrödinger equation is solved. This effect is illustrated in Figure 13 where we plot $P_{QM}(t)$ computed from Eq (III-4) at time t on the SAI surface versus time. As can be seen, with H_2^+ initially in the v=0 vibrational state, P_{QM} rises to its final value of 0.0974 after 4.31 X 10^{-14} s and remains constant thereafter. The final reaction probability in this case is therefore unequivocal. For the v=1 and v=2 states, however, $P_{QM}(t)$ can be seen to rise to a maximum and then slowly decrease due to reflection of the wavepacket from the edges of the grid, as mentioned above. For these cases, we take P_{QM} at the maximum to be the

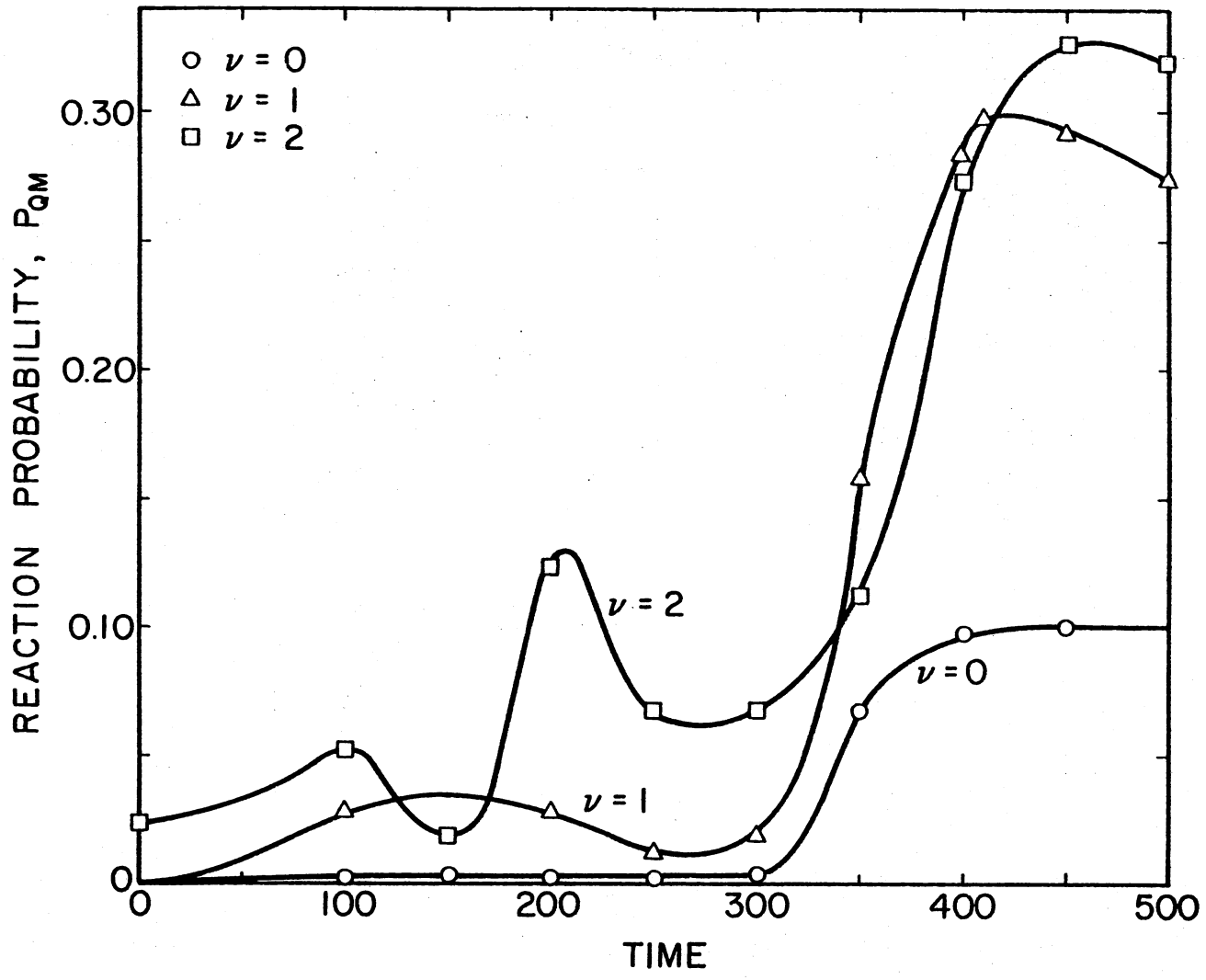

Figure 13. Reaction Probability as a Function of Time on the SAI Surface for the v=0,1,2 Vibrational States of H_2^+ at a Total Energy of 1.2 eV. One time unit represents 1.0775 X 10^{-16} s

final reaction probability. This choice, although logical, clearly introduces some error into the computed probabilities. Similar results are also obtained for calculations on the DIM surface. The structure in the P_{QM} curve at small t is due to the vibrational transverse motion of the wavepacket which becomes more pronounced for the higher vibrational states.

Table VIII shows the results of both the present time-dependent QM and previously reported QCT calculations of the reaction probability for R1 at a total energy of 1.2 eV. As can be seen, both the QM and QCT results on the SAI surface predict a significant enhancement of the reaction probability for R1 as the total available energy is selectively partitioned into H_2^+ vibrational motion. In addition, the magnitudes of the QM and QCT results are comparable although the QM results are uniformly slightly larger. Thus, the large discrepancies sometimes noted in collinear systems between QM and QCT computed reaction probabilities are not present here even though the HeH_2^+ potential-energy surface is asymmetric (54).

In contrast to the above, the QM and QCT calculations on the analytical DIM surface (27) indicate the absence of vibrational enhancement of the reaction probability of R1. This result is in accord with conclusions previously drawn by Kouri and Baer (29a). The relative magnitudes of the QM and QCT values are comparable although the time-dependent QM results are uniformly larger, as was the case on the SAI surface.

The largest single difference between the time-dependent quantum calculations on the two surfaces is the computed reaction probability with H_2^+ in the v=0 vibrational state. The reaction probability for this case is over four times larger for the DIM surface than for the

TABLE VIII

TIME-DEPENDENT QM AND QCT COMPUTED REACTION PROBABILITIES FOR R1 AT 1.2 eV ON THE SAI AND DIM POTENTIAL-ENERGY SURFACES

H_2^+ vibrational state, v	Reaction Probability			
	QM[a]		QCT[b]	
	SAI	DIM	SAI	DIM
0	0.0974	0.406	0.030	0.330
1	0.291	0.413	0.210	0.215
2	0.321	0.303	0.290	0.235

[a]This work

[b]Reference 30

SAI surface. The final-state probability density on the DIM surface, shown in Figure 14, is seen to be dramatically different from that for the SAI surface, shown in Figure 12b. The features of the potential-energy surface primarily responsible for these differences have recently been determined by Sathyamurthy et al (31). This work is discussed in the following section.

In Table IX the present time-dependent QM calculations on the DIM surface are compared with the close-coupling results previously reported by Kouri and Baer (29a) (55). Although the qualitative trends are identical for both calculations, the time-dependent results are uniformly larger. This discrepancy arises from the manner in which the energy of the HeH_2^+ system enters the two QM calculations. In a close-coupling calculation, the energy of the HeH_2^+ system is exactly specified. In a wavepacket calculation, however, the superposition of plane waves that occurs in the formation of the wavepacket causes the energy of the HeH_2^+ system to become slightly diffused. The wavepacket calculation, therefore, gives a result that is an average over a small range of energies and should not be expected to agree exactly with the close-coupling result.

The present results confirm our previously drawn conclusions that were based solely on QCT calculations on the SAI surface (5a) (30) (56). Extremely small differences in the potential-energy surface can produce drastic alterations in the computed reaction dynamics. Consequently, it is necessary to employ accurate procedures in both the surface calculations and interpolation. In the present case, the SCF ab initio collinear surface reported by Brown and Hayes (26) is sufficiently accurate

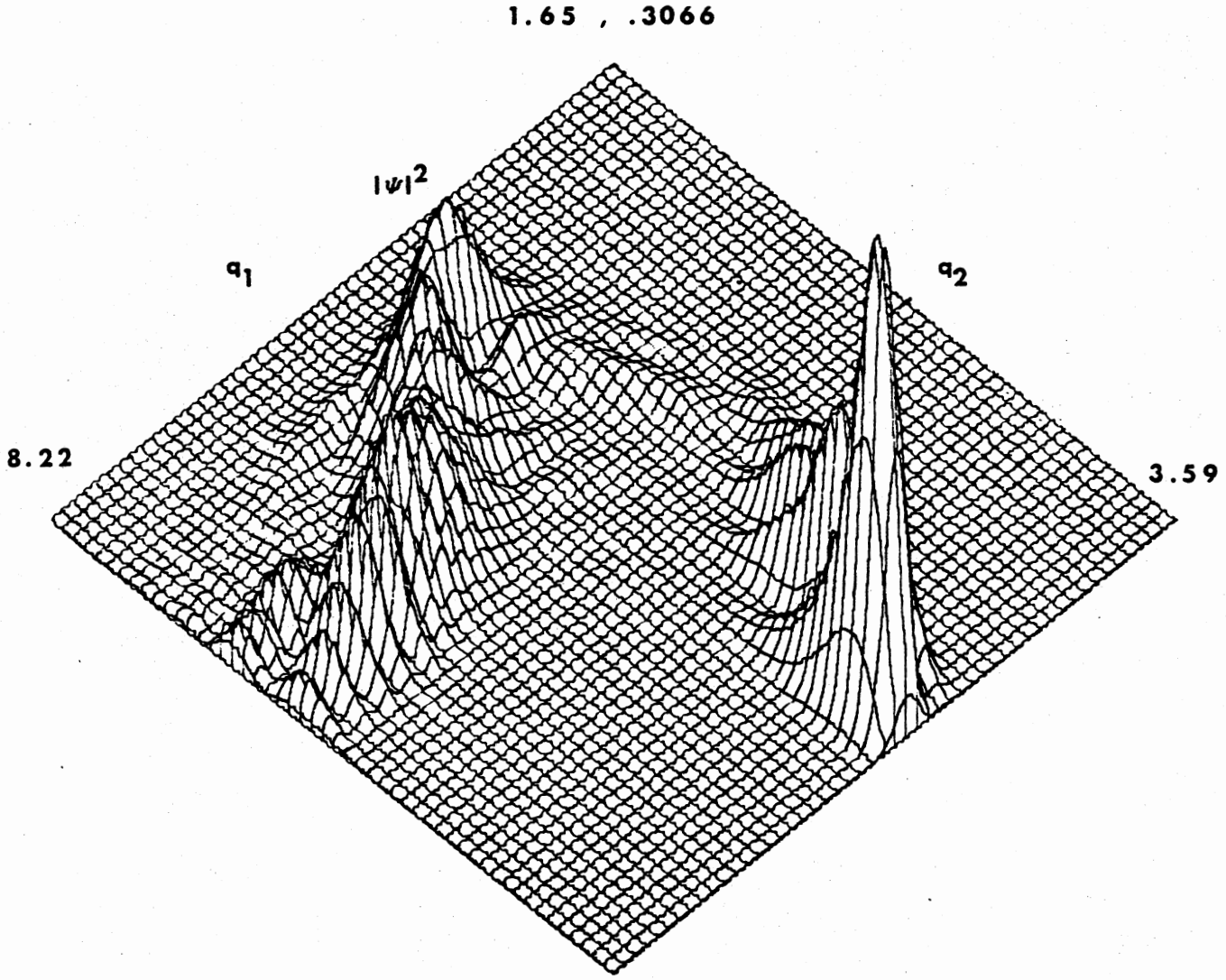

Figure 14. Probability Density at t=4.31 X 10^{-14} s on the DIM Surface. The total energy is 1.2 eV and v(H_2^+)=0

TABLE IX

COMPARISON OF TIME-DEPENDENT AND CLOSE-COUPLING QM RESULTS ON THE DIM SURFACE AT 1.2 eV

H_2^+ vibrational state, v	QM Reaction Probability	
	Time-dependent[a]	Close-coupling[b]
0	0.406	0.28
1	0.413	0.36
2	0.303	0.23

[a]This work

[b]References 29a and 55

to permit qualitatively correct trends to be predicted from QM calculations provided an accurate interpolation procedure is employed.

The Origin of the Dynamical Differences Observed in Studies of the HeH_2^+ Reactive System on Spline-fitted Ab Initio and Diatomics-in-Molecules Surfaces[1]

The potential-energy surface has clearly been shown to play a key role in the theoretically determined collision dynamics for the collinear HeH_2^+ system. However, the topological features of the surface that are critical to this influence are not known. The SAI and DIM surfaces are nearly identical with regard to such features as the location of entrance and exit channels, the position and height of the barrier to the reaction, and the placement and curvature of the minimum energy path. Indeed, a comparison of Figures 15 and 16 shows that the contour plots for the two surfaces are nearly superimposable. Thus, an investigation of the critical differences in these surfaces must begin at a point where the behavior of QCT's performed in earlier studies diverges most sharply. Table VIII indicates that both QM and QCT results differ most markedly for the vibrational ground state of H_2^+. This was also found to be true for the other energies at which QCT's were performed. Thus, the effects of the differences between the SAI and DIM surfaces should be maximized if the vibrational energy of H_2^+ is suppressed altogether, i.e., if zero-point energy is excluded. Accordingly, individual

---

[1]The complete details of this study may be found in Appendix B.

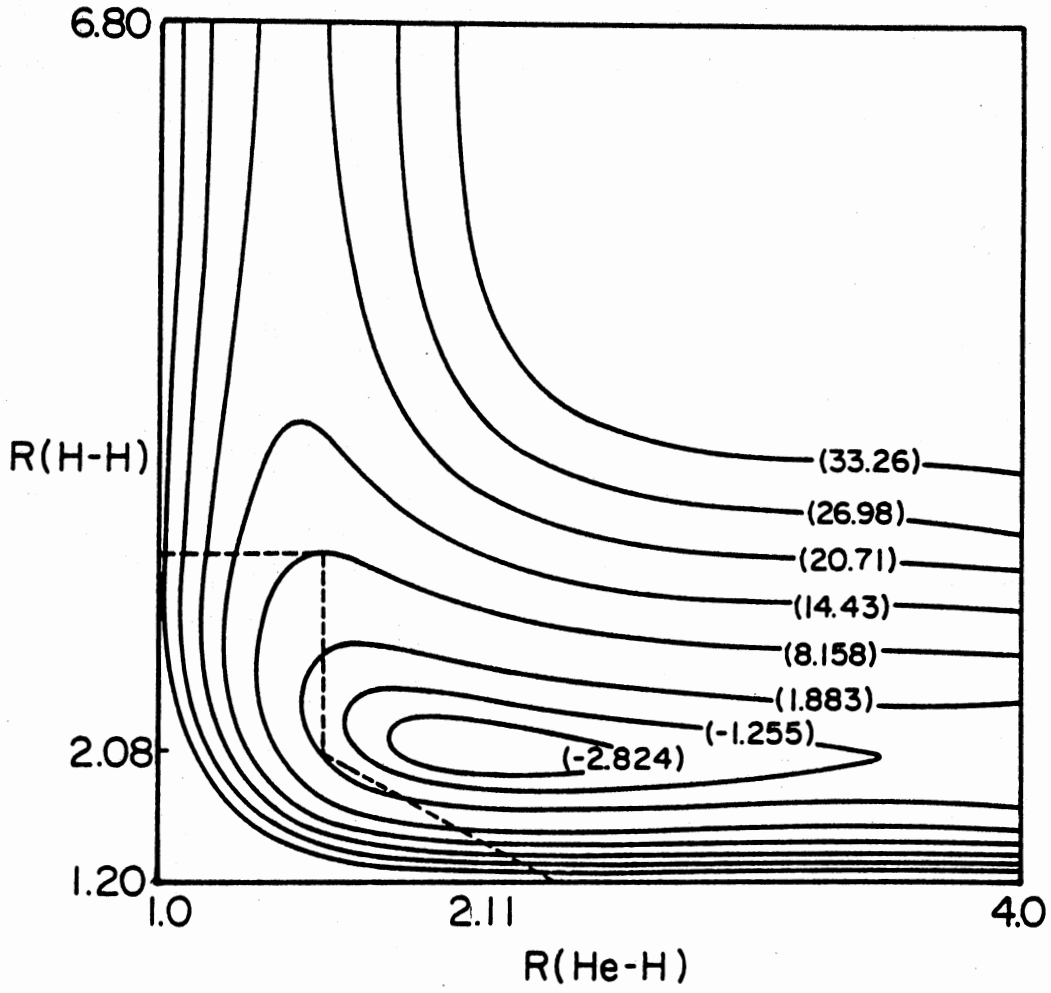

Figure 15. The SAI Surface for the Collinear HeH_2^+ System. The region to the lower left of the dashed line is replaced with the corresponding potential-energy values from the SDIM surface to form the CPS1 surface. Distances are in a.u. Energies are in kcal/mole relative to the He + H_2^+ asymptotic limit

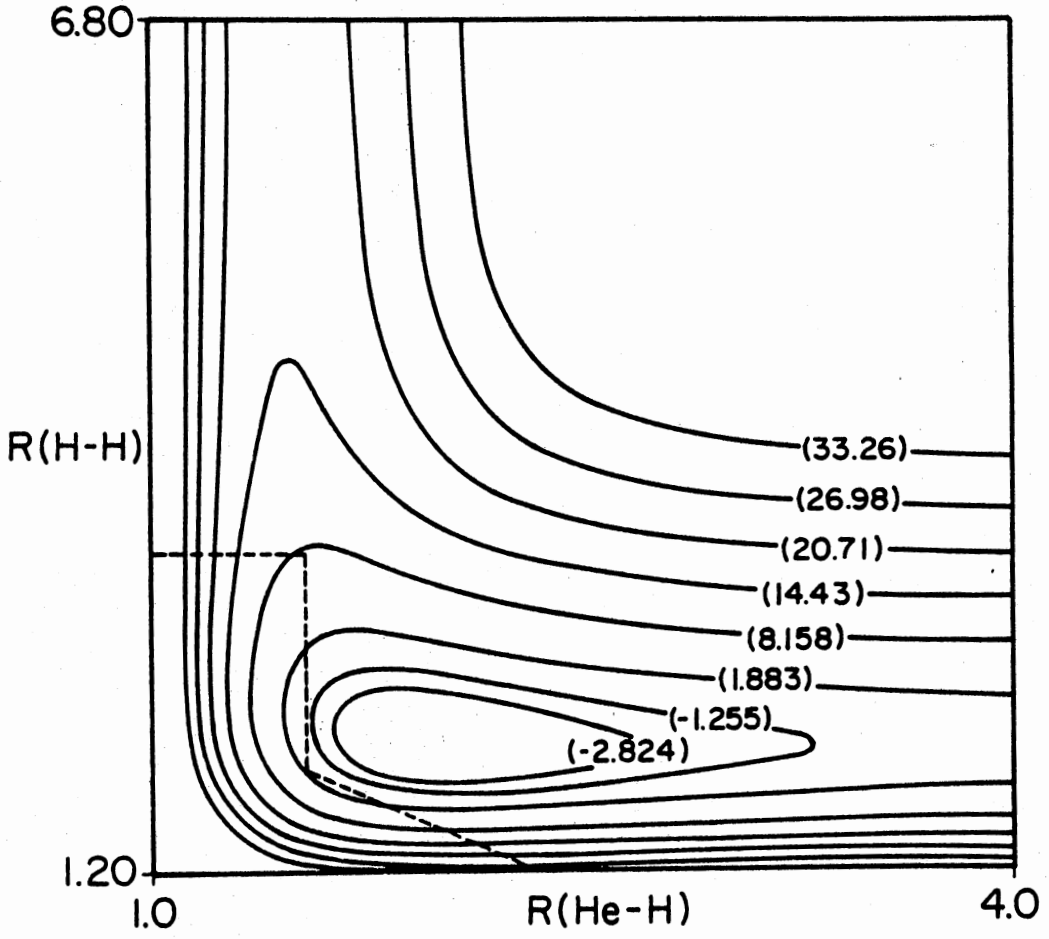

Figure 16. The (S)DIM Surface for the Collinear HeH_2^+ System. The region to the lower left of the dashed line is replaced with the corresponding potential-energy values from the SAI surface to form the CPS2 surface. Distances are in a.u. Energies are in kcal/mole relative to the He + H_2^+ asymptotic limit

trajectories were calculated on both surfaces at total energies of 1.1 and 1.2 eV with H_2^+ vibration completely suppressed. Plots of these trajectories were then superimposed on the appropriate potential-energy surfaces. These are shown in Figures 17 and 18.

A comparison of the trajectories on the SAI and DIM surfaces at 1.1 eV (Figure 17) showed major differences in behavior. The trajectory on the SAI surface was straightforward and simple. The system moved through the reactant valley toward the interaction region, encountered the inner repulsive wall of the surface, and rebounded into the reactant region with H_2^+ now vibrationally excited. The trajectory on the DIM surface was quite different. Although behaving in the same manner as the SAI trajectory while passing through the reactant region, the DIM trajectory diverged sharply from the SAI trajectory upon meeting the inner repulsive wall. In this case, the system did not move at once toward the reactant channel but rather toward the product channel, where it remained temporarily. Although the trajectory was ultimately nonreactive, it was much more complex and long-lived than the SAI trajectory. This behavior was even more apparent at 1.2 eV (Figure 18). Here the SAI trajectory was very nearly identical to its 1.1 eV counterpart; however, the DIM trajectory nearly became reactive. The system moved far into the product channel before insufficient translational energy in the products prevented their separation and forced the system to return to the reactant configuration.

This comparison strongly indicated that the inner repulsive walls of the surfaces were playing a major role in the influence of the dynamical outcome of the QCT studies. The differing curvatures of this

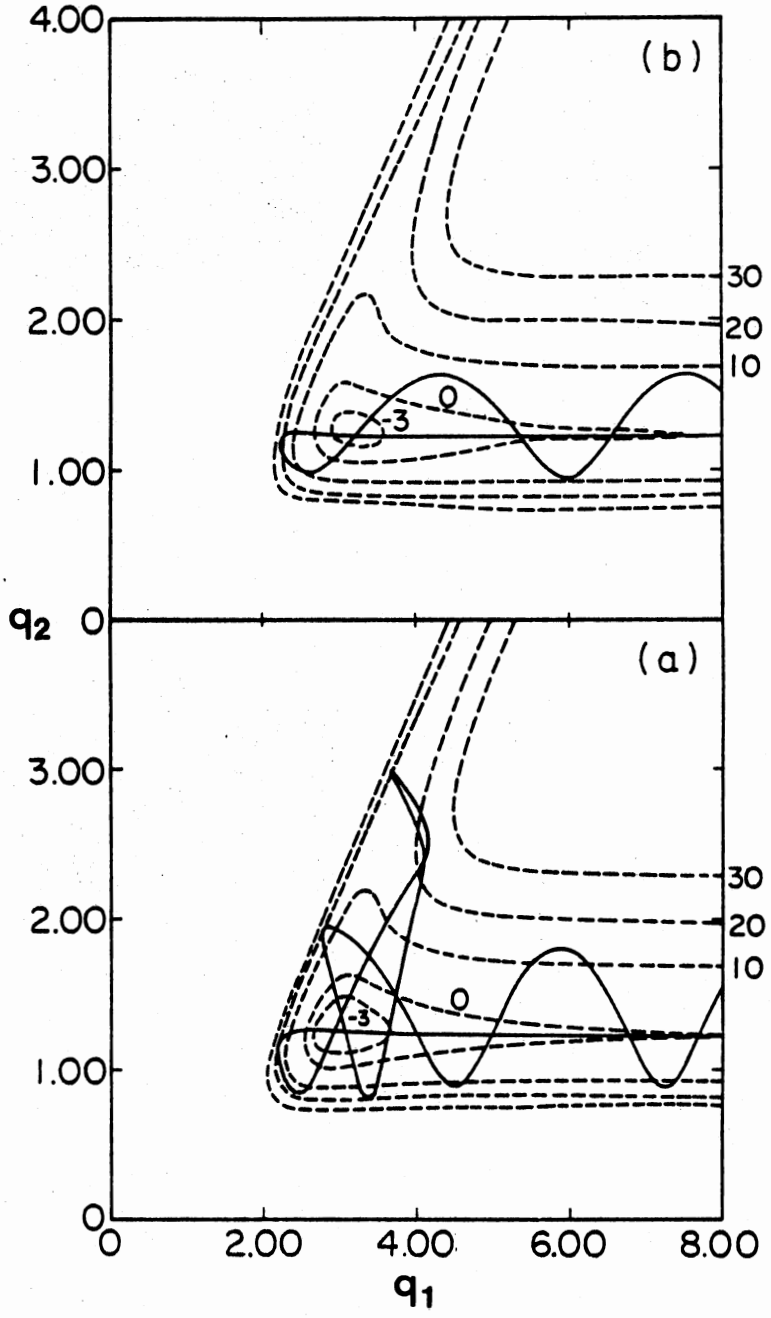

Figure 17. Vibrationless Trajectories on the (a) DIM and (b) SAI Surfaces at a Total Energy of 1.1 eV. The potential-energy contours (---) are in kcal/mole. Distances are in a.u.

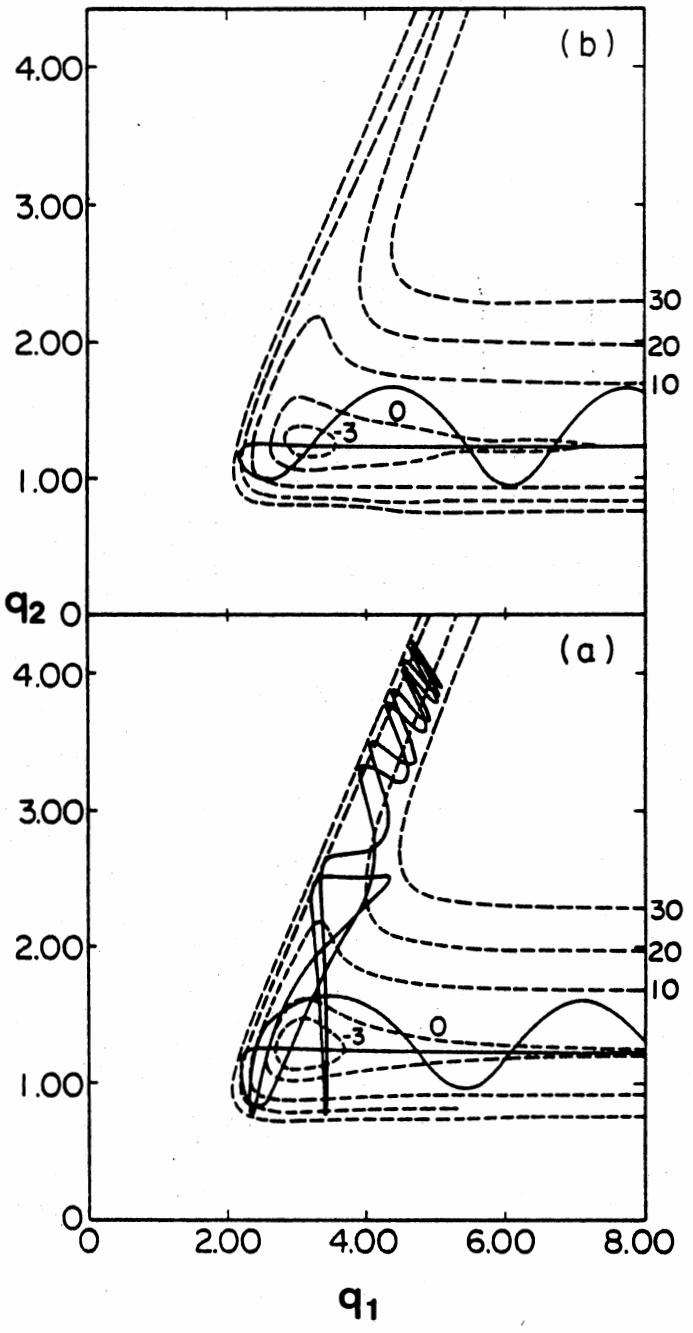

Figure 18. Vibrationless Trajectories on the (a) DIM and (b) SAI Surfaces at a Total Energy of 1.2 eV. The potential-energy contours (---) are in kcal/mole. Distances are in a.u.

region on the two surfaces apparently caused trajectories on the SAI surface largely to be reflected back into the reactant channel and caused trajectories on the DIM surface to be diverted into the product channel, thus allowing the DIM trajectory a greater chance of reactivity. Furthermore, it is known that the short-range repulsive potential is the main factor in determining the effectiveness of translational-to-vibrational energy transfer (58), the process occurring the HeH_2^+ system. However, these studies of the individual trajectories do not prove that the inner repulsive wall is the only feature of the surfaces that is influencing the behavior of the trajectories. Because the SAI and DIM surfaces do differ slightly, forces received in traversing the entrance channel and attractive well may also have an important influence on the behavior of the system.

To eliminate this possibility, two composite surfaces were devised. In this part of the study the DIM surface was replaced by an SDIM surface, one in which DIM energies were calculated for the same geometries as the ab initio energies, and then spline-fitted to generate the full (S)DIM surface. This change has no effect on the theoretical results (30) and greatly facilitates the generation of the composite surfaces. The first composite surface (CPS1) had the attributes of the SAI surface in all regions except the inner repulsive wall (see Figure 15), where the surface behaved like the SDIM surface. CPS2 was just the reverse, it was effectively an SDIM surface with an SAI inner repulsive wall (see Figure 16). Mathematically, these composite surfaces were effected during the course of a trajectory simply by calculating the trajectory on the appropriate "pure" potential-energy surface (SAI or SDIM) until the system reached the inner wall region, whereupon the trajectory was

continued on the other pure surface as long as the system remained in this region. This jump from one potential-energy surface to the other at the boundaries shown in Figures 15 and 16 did not invalidate the calculation because of discontinuities in the potential energies at these boundaries. The potential energies on both SAI and SDIM surfaces varied smoothly and the chance of the system geometry falling exactly on the boundary was small. The accuracy of this method was confirmed by back-integrating completed trajectories to the initial conditions. In all cases, initial coordinates and momenta were reproduced with no greater than 1% error when an integration step size of 0.539×10^{-16} s was used. It should also be noted that this procedure has been used successfully in the treatment of the $T^* + CH_4$ system investigated by Raff (33a).

Batches of 500 trajectories each were run on the SAI, SDIM, CPS1, and CPS2 surfaces. H_2^+ was initially in its vibrational ground state (including zero-point energy) and all conditions, save the interaction potential, were identical. The results of the QCT study are shown in Table X. The reaction probability on the SAI surface is small for the conditions given; on the SDIM surface the reaction probability is over fifteen times larger. This is exactly what has been found in previous studies. The reaction probability on CPS1, the SAI surface with the SDIM inner repulsive wall, is very close to the probability found on the SDIM surface; for CPS2, the reaction probability mimics that found on the SAI surface. In each case, the results obtained on the composite surface were dictated by the nature of the inner repulsive wall of the surface. However, the reaction probabilities found on the SAI and CPS2 surfaces and on the SDIM and CPS1 surfaces are not identical, indicating that other areas of the potential-energy surface also have

TABLE X

COMPARISON OF REACTION PROBABILITIES ON THE SAI, SDIM, CPS1, AND CPS2 SURFACES AT A TOTAL ENERGY OF 1.1 eV WITH H_2^+ INITIALLY IN THE v=0 VIBRATIONAL STATE

Surface	Computed Reaction Probability
SAI	0.018
SDIM	0.300
CPS1	0.368
CPS2	0.008

a role in determining the dynamical outcome of the reaction, although to a much smaller extent.

The data in Table X clearly proves that the results obtained on the DIM surface differ qualitatively from both experiment and the calculations on the SAI surface because the curvature of the potential-energy contours for the collinear HeH_2^+ system was not accurately represented in the region of the inner repulsive wall by the DIM functional fit to the ab initio values. Thus, it is very important that the investigation of vibrational energy transfer in collinear systems of this type be carried out on a potential-energy surface in which the ab initio energies have been represented as accurately as possible, for instance, by use of the cubic spline interpolation procedure. This technique results in a surface which passes through all the calculated ab initio energies and thus provides a reliable representation of all of the topological features of the potential-energy surface.

A Quasiclassical Study of Collision Dynamics in the NeH_2^+ System

An obvious question that arises from the studies so far presented is that of the scope of their validity. Does the collinear system still give an accurate representation of the reaction dynamics of the three-dimensional system? Is it necessary to use the more complicated spline-fitting procedure to generate the potential-energy surfaces from ab initio values for larger systems, or will the much simpler analytical function serve adequately? Is the inner repulsive wall always the most critical feature of the surface?

These questions may be answered, at least in part, by considering

a system very similar to the HeH_2^+ system. The reaction between neon and H_2^+

$$Ne + H_2^+(v) \rightarrow NeH^+ + H \qquad (R2)$$

has been found experimentally (22b) to exhibit the same behavior as the HeH_2^+ system, i.e., the reaction is favored when H_2^+ is vibrationally excited. Furthermore, both an SAI (see Chapter II) and a DIM (15) surface exist for this system, making possible an investigation of the reaction dynamics of this system that proceeds along the same lines as the HeH_2^+ investigation.

QCT studies were performed on the collinear SAI_{G-70} and DIM potential-energy surfaces. The trajectories covered a total energy range of 0.94 - 1.4 eV and included the first three vibrational quantum levels of H_2^+. The results are shown in Table XI; each reaction probability is the result of 200 trajectories. The reaction probabilities show the familiar trend displayed by the HeH_2^+ system: the DIM results indicate that vibrational energy in H_2^+ inhibits the reaction, while just the opposite is evidenced by the SAI results. Furthermore, the differences in the two sets of calculations are most pronounced for the vibrational ground state of H_2^+ and decrease as the vibrational energy is increased. Once again, calculations performed on a collinear DIM potential-energy surface have failed to predict the correct qualitative behavior of the reaction system.

The results shown in Table XI also allow another interesting observation. The SAI_{G-70} surface contained only LCAO-MO-SCF energies based on s and p orbitals for neon, while the values calculated by Hayes et al (15) contained d orbitals as well. Therefore, the inclusion of the d orbitals (often called polarizing orbitals) on neon in the calculation

TABLE XI

REACTION PROBABILITIES FOR R2 CALCULATED FROM QUASICLASSICAL TRAJECTORIES ON THE SAI AND DIM SURFACES FOR THE COLLINEAR SYSTEM

H_2^+ vibrational state, v	Total Energy (eV)	Reaction Probability	
		SAI	DIM
0	0.94	0.0	0.475
1		0.280	0.365
2		0.225	0.270
0	1.0	0.015	0.510
1		0.335	0.390
2		0.260	0.295
0	1.1	0.115	0.565
1		0.350	0.430
2		0.365	0.345
0	1.2	0.175	0.625
1		0.310	0.470
2		0.395	0.385
0	1.4	0.260	0.710
1		0.355	0.550
2		0.380	0.440

of potential energies is not necessary for a qualitatively correct description of the NeH_2^+ interaction potential. Although this result is not generally true, it certainly indicates that smaller basis sets may be used to give reliable potentials in systems where electron correlation does not play an extensive role.

To determine the role of the inner repulsive wall of the collinear NeH_2^+ surface in the outcome of the studies shown in Table XI, two composite surfaces were formed from the SAI_{G-70} and the SDIM potential-energy surfaces. These surfaces may be visualized from Figures 5 and 6, which show the SAI and SDIM potential-energy surfaces and the boundaries for the inner repulsive walls. The SDIM surface was used instead of the DIM surface in this study for the same reasons as were given before. Trajectories run on the DIM and SDIM surfaces showed identical behavior. Back integration of trajectories on both composite surfaces yielded initial coordinates and momenta within 0.7% of the original values. The integration step size used was 0.539×10^{-15} s on the SAI and SDIM surfaces, and 0.108×10^{-15} s on the composite surfaces. The accuracy of the back integrated values is reassuring in view of the fact that the SAI surface is much shallower than the SDIM surface and the discontinuity between the surfaces much larger than was true for the HeH_2^+ system.

Individual trajectories were computed and plotted for the NeH_2^+ system at a total energy of 1.1 eV. As with the HeH_2^+ system, there is a large difference between trajectories performed on the SAI and SDIM surfaces (see Figure 19). At the inner repulsive wall the SDIM trajectory is deflected directly into the produce channel, while the SAI

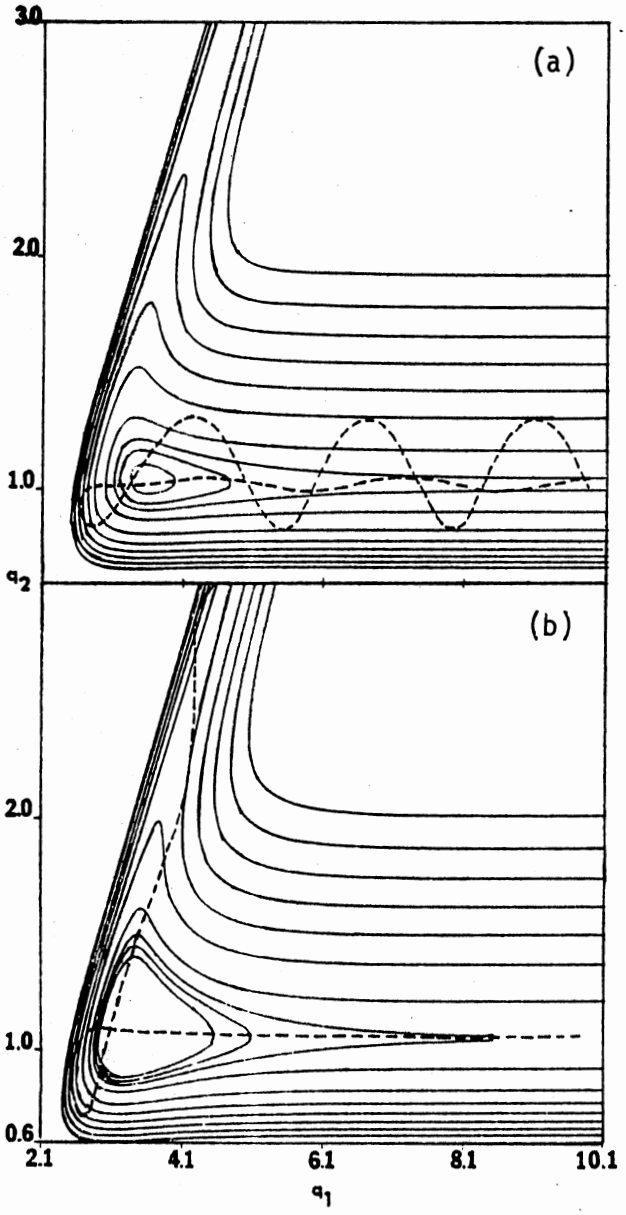

Figure 19. Vibrationless Trajectories for the Collinear NeH_2^+ System at a Total Energy of 1.1 eV on the a) SAI and b) SDIM Surfaces. Distances are in atomic units and the energy contours for the SAI and SDIM surfaces are the same as in Figures 5 and 6, respectively

trajectory is reflected into the reactant channel.[2] A comparison of the SAI and SDIM trajectories with ones performed on the composite surfaces indicates that the inner repulsive wall also has significant influence in the NeH_2^+ system (see Figure 20): the SDIM trajectory becomes non-reactive when the SAI contours replace the SDIM inner wall (CS2 trajectory) while the presence of the SDIM repulsive wall causes the CS1 trajectory to be angled more sharply toward the product channel than was the case for the SAI trajectory.

The results of the trajectory studies performed on each of the four NeH_2^+ potential-energy surfaces are shown in Table XII. It is obvious that in the NeH_2^+ system the inner repulsive wall does not play nearly as significant a role as it did in the HeH_2^+ system. Although the reaction probability does increase when the SAI_{G-70} surface has the SDIM inner wall (CS1), it is still far from the SDIM result. Even less of a change is observed in going from the SDIM surface to the CS2 surface. For the collinear NeH_2^+ system, the short-range repulsive forces of the inner wall region only partially determine the behavior of the system. The effects of medium- and long-range attractions represented by the attractive well and entrance channel, respectively, must be playing a much more influential role in this system than was found in the HeH_2^+ system.

An example of the effects of these other forces is shown in Figure 21. Because the SAI and SDIM surfaces do not have identical entrance

---

[2]The small vibrational motion of H_2^+ occurring during the first half of the trajectory is due to the behavior of the H_2^+ potential at large R_{NeH}. The manner in which the SAI_{G-70} surface was extended to 10 a.u. (see Chapter II) resulted in a displacement of the minimum of the H_2^+ potential to a value slightly less than 2.00 a.u., the minimum of the H_2^+ Morse curve. On the SAI surface, H_2^+ experiences a slight compression force at the start of the trajectory, a force sufficient to start a small oscillatory motion.

trajectory is reflected into the reactant channel.[2] A comparison of the SAI and SDIM trajectories with ones performed on the composite surfaces indicates that the inner repulsive wall also has significant influence in the NeH_2^+ system (see Figure 20): the SDIM trajectory becomes non-reactive when the SAI contours replace the SDIM inner wall (CS2 trajectory) while the presence of the SDIM repulsive wall causes the CS1 trajectory to be angled more sharply toward the product channel than was the case for the SAI trajectory.

The results of the trajectory studies performed on each of the four NeH_2^+ potential-energy surfaces are shown in Table XII. It is obvious that in the NeH_2^+ system the inner repulsive wall does not play nearly as significant a role as it did in the HeH_2^+ system. Although the reaction probability does increase when the SAI_{G-70} surface has the SDIM inner wall (CS1), it is still far from the SDIM result. Even less of a change is observed in going from the SDIM surface to the CS2 surface. For the collinear NeH_2^+ system, the short-range repulsive forces of the inner wall region only partially determine the behavior of the system. The effects of medium- and long-range attractions represented by the attractive well and entrance channel, respectively, must be playing a much more influential role in this system than was found in the HeH_2^+ system.

An example of the effects of these other forces is shown in Figure 21. Because the SAI and SDIM surfaces do not have identical entrance

---

[2]The small vibrational motion of H_2^+ occurring during the first half of the trajectory is due to the behavior of the H_2^+ potential at large R_{NeH}. The manner in which the SAI_{G-70} surface was extended to 10 a.u. (see Chapter II) resulted in a displacement of the minimum of the H_2^+ potential to a value slightly less than 2.00 a.u., the minimum of the H_2^+ Morse curve. On the SAI surface, H_2^+ experiences a slight compression force at the start of the trajectory, a force sufficient to start a small oscillatory motion.

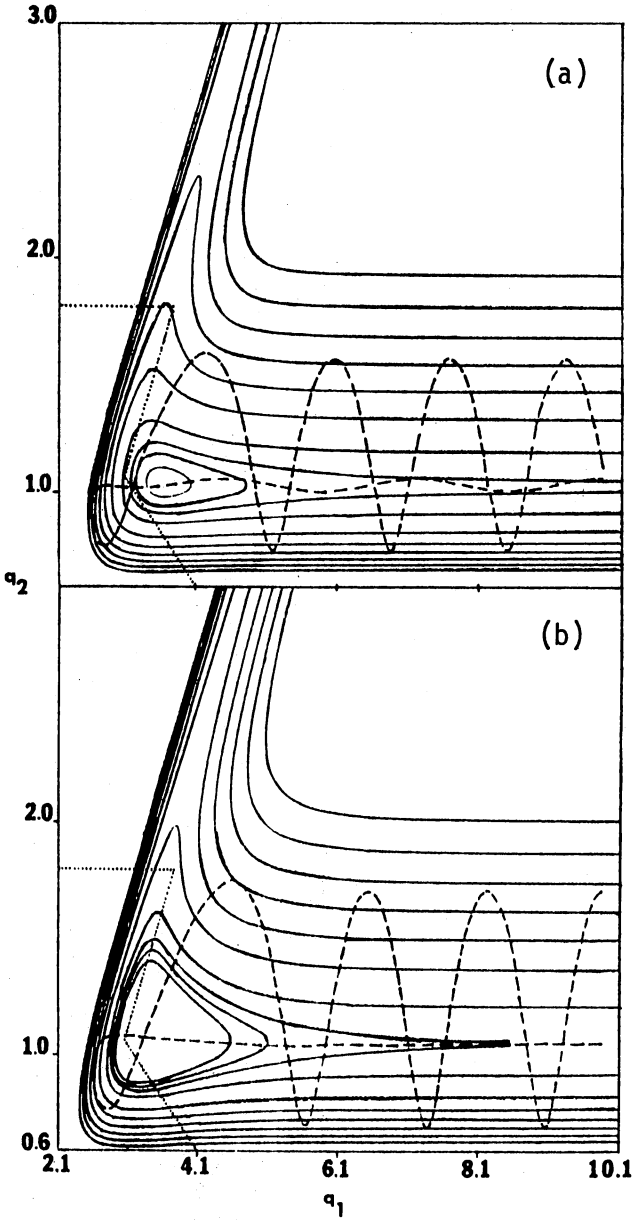

Figure 20. Vibrationless Trajectories for the Collinear NeH_2^+ System at 1.1 eV on the a) CS1 and b) CS2 Surfaces. The dotted lines indicate the boundaries of the inner repulsive wall. Distances and energies are the same as in Figure 19

TABLE XII

COMPARISON OF REACTION PROBABILITIES ON THE SAI, SDIM, CS1, AND CS2 SURFACES AT A TOTAL ENERGY OF 1.1 eV WITH H_2^+ INITIALLY IN THE v=0 VIBRATIONAL STATE

Surface	Computed Reaction Probability
SAI	0.115[a]
SDIM	0.570[a]
CS1	0.300[b]
CS2	0.422[b]

[a]The result of 200 trajectories

[b]The result of 500 trajectories

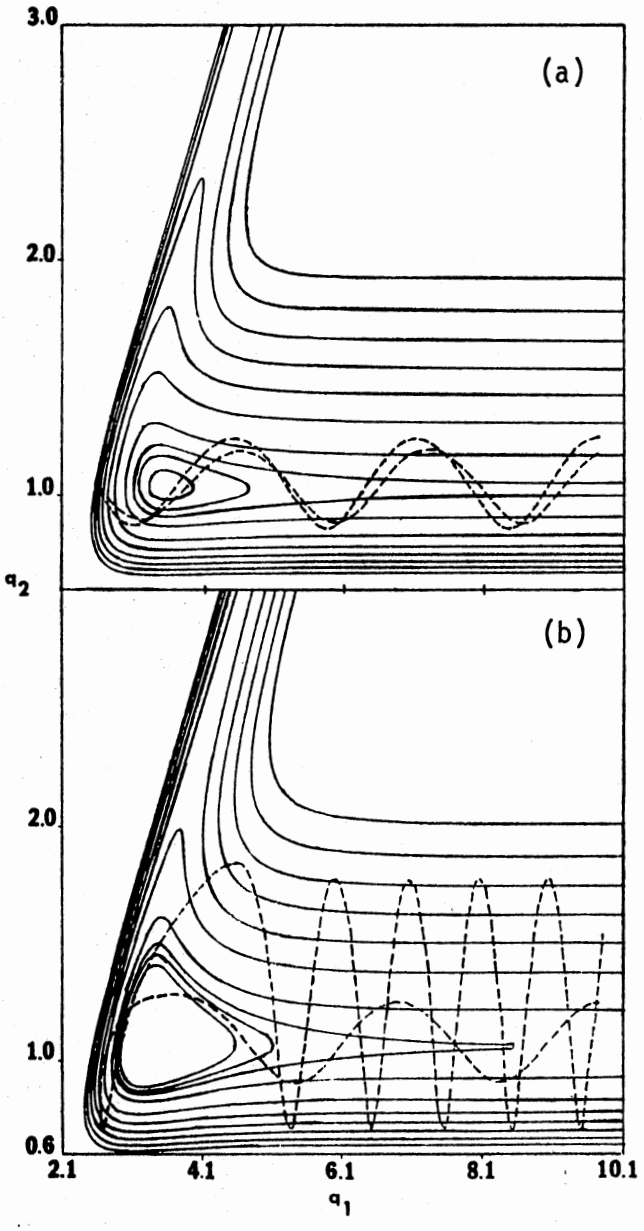

Figure 21. Collinear NeH_2^+ Trajectories on the a) SAI and b) SDIM Surfaces. H_2^+ is in its vibrational ground state. Distances and energies are the same as in Figure 19

channels and attractive wells, trajectories having identical initial conditions will experience slightly different forces in these regions. A comparison of Figures 21a and 21b shows that H_2^+ has a longer vibrational period on the SDIM surface; furthermore, the large attractive well on the SDIM surface prolongs the H_2^+ vibration even more. The net effect of the forces on the incoming SDIM trajectory is to bring the system to the inner wall with a large fraction of HeH^+ - H Motion. This motion is parallel to the paroduct channel and results in a deflection toward this region. The SAI trajectory encounters the inner repulsive wall at a much more perpendicular angle due to the larger amount of He - H_2^+ motion present in the trajectory, and the system is deflected directly into the reactant channel. Although neither trajectory is reactive, the SDIM trajectory exhibits a much greater reactive potential.

It is fortunate that the inner repulsive wall does not appear to be as critical to other reactive systems as it is to the HeH_2^+ system, because the accurate representation of the curvature of this region is very difficult to accomplish even using ab initio methods, due to the importance of electron correlation in this region.

Conclusions

The results of the QM and QCT studies of the HeH_2^+ system and of the QCT studies on the NeH_2^+ system revealed several important facts. The dynamical behavior of vibrational energy transfer systems, such as HeH_2^+ and NeH_2^+, can be obtained from theoretical studies of the collinear system provided an accurate ab initio potential-energy surface is used. The generation of a sufficiently accurate surface from ab initio energies can be accomplished using interpolation with cubic

splines. Because the course of the reaction involves only the transfer of a proton, no extensive electronic changes occur in the system and correlation effects are relatively constant over the potential-energy surface. Thus, the ab initio values need not include configuration interaction and may be calculated using an LCAO-MO-SCF procedure. Indeed, the study of the NeH_2^+ system showed that extensive basis sets for the larger atoms in the system (neon, for instance) are not necessary to produce an ab initio surface which gives qualitatively correct dynamical results.

The SAI surface is required in the study of the collinear HeH_2^+ system because it accurately reproduces the curvature of the inner repulsive wall, while the DIM fit to the collinear energies does not. For the NeH_2^+ system, an ab initio surface is again required if reliable results are to be obtained from a study of the theoretical system; however, the curvature of the inner repulsive wall is not nearly as important. Medium- and/or long-range attractions apparently play a more significant part in determining the reaction dynamics of this system than in the HeH_2^+ system. Since an accurate representation of the inner repulsive wall for the collinear system is difficult using ab initio methods which do not include configuration interaction, and impossible using the present form of the diatomics-in-molecules interaction, it would be fortunate if the conclusions drawn from the NeH_2^+ study are found to be generally applicable.

There do remain several questions as yet unanswered. The effects of the entrance channel and attractive well of both the collinear HeH_2^+ and NeH_2^+ surfaces on the theoretically determined reaction dynamics of the systems need to be determined. In addition, the importance of the

inner repulsive wall should be more clearly defined: is it generally a critical feature of the potential-energy surface, as was found for the HeH_2^+ system, or does it play a less influential role, as was found for NeH_2^+ systems? The study of systems with potential-energy surfaces similar to these will determine more conclusively the relative influence of the various features of the potential-energy surface.

CHAPTER IV

A QUASICLASSICAL TRAJECTORY STUDY OF ROTATIONALLY INELASTIC SCATTERING IN THE He - CO_2 RIGID ROTOR SYSTEM

A major goal in the theoretical study of reactive and nonreactive scattering is the discovery of computational methods which quickly and accurately characterize the behavior of the system. These methods may be divided into two principal areas: those that deal with the representation of the potential energy of the system, and those that treat the actual calculation of scattering cross sections, rates, etc. The studies of reactive scattering in the HeH_2^+ and NeH_2^+ systems focussed on the first of these areas, i.e., the studies tested the suitability of the diatomics-in-molecules approximation of the potential energy of the systems. The study of rotationally inelastic scattering in the He - CO_2 rigid rotor system also focusses upon the first area. In this case, the potential of the system is calculated by assuming that the electron densities of helium and CO_2 remain undistorted at all system geometries and that the energy densities may be represented by those of a uniform electron gas. This electron gas (EG) approximation allows a much faster calculation of the potential than is possible using present ab initio methods; however, no comparison of the accuracies of the EG and ab initio potentials has yet been made. Such a comparison is reported in this work and is effected by using the QCT method to calculate scattering

cross sections on both the EG and ab initio potential-energy surfaces, followed by a comparison of the results with those obtained from an experimentally determined potential. Before the results of this study are presented, the details of the QCT treatment of the He - CO_2 rigid rotor system will be given.

Calculational Methods

The quasiclassical trajectory method has been described by Bunker (59) and by Porter and Raff (13b), and has been applied to rare gas-CO_2 systems by Suzukawa (43). The major steps in a QCT study are the determination of a suitable potential and its derivatives, the selection of the initial conditions for the system, integration of the equations of motion, the determination of the final states of the system, and finally, the calculation of mean energy changes, cross sections, and rate constants.

The Potential Energy and Its Derivatives

In Chapter II, ab initio energies for the He - CO_2 rigid rotor system were calculated and the cubic spline interpolation procedure used to generate the full two-dimensional surface. Thus, the interaction potential is known for any geometry within the (R,θ) grid. For the QCT method to be used, however, it is the gradient of the potential rather than the potential energy itself that must be known. In other words, the values for $\partial V_{inter}/\partial Q_i$, the partial derivatives of the potential with respect to the spatial coordinates of helium and CO_2 (see Figure 22), must be known.

The total potential of the He - CO_2 system is simply the interaction

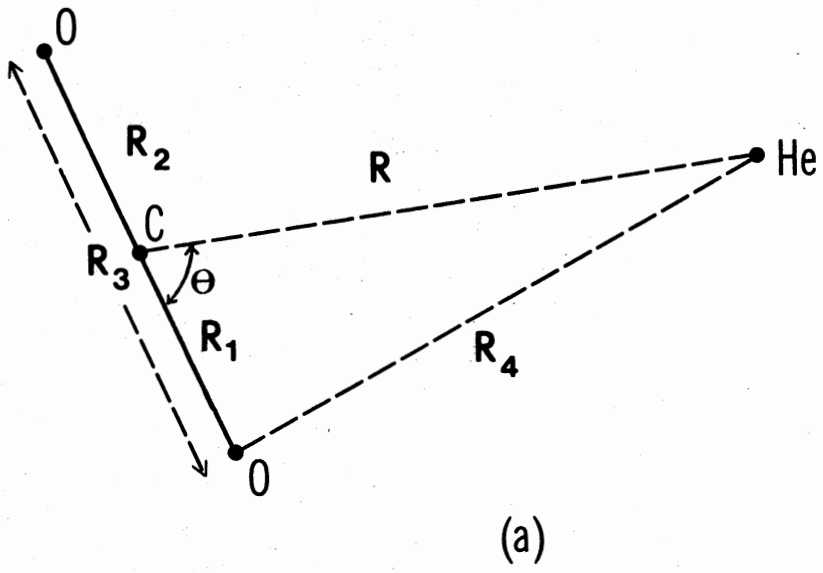

(a)

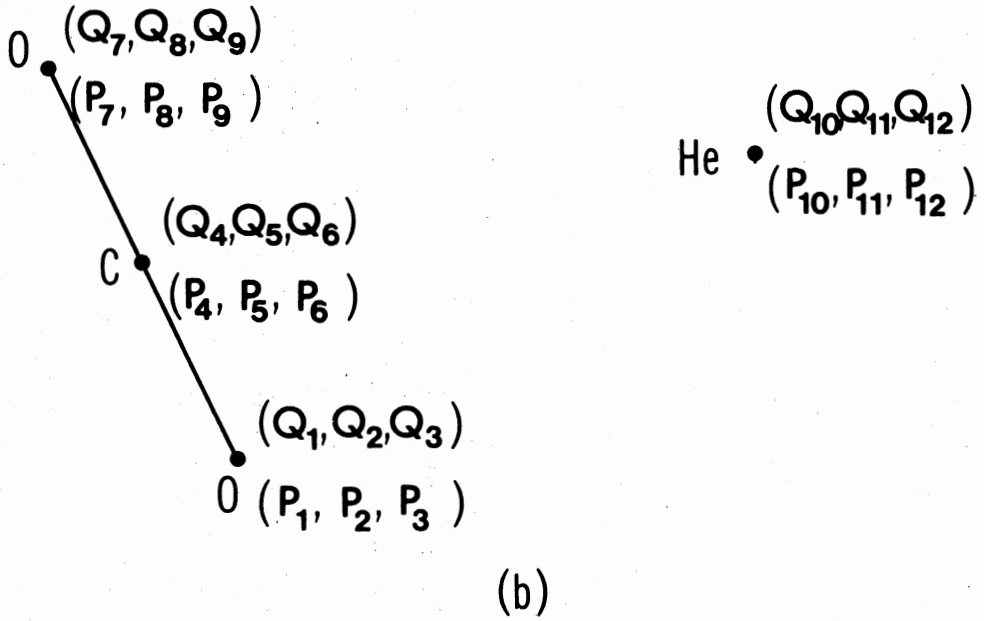

(b)

Figure 22. The He - CO_2 Rigid Rotor System. (a) The R_i denote interatomic distances important in determining derivatives to the interaction potential. (b) The Q_i and P_i are the Cartesian coordinates and conjugate momenta of CO_2 in the space-fixed frame

potential calculated in Chapter II

$$V = V_{inter}(R,\theta) \ , \tag{IV-1}$$

since CO_2 is fixed in its (00°0) equilibrium position by the rigid rotor requirement. Thus, the chain rule yields

$$\frac{\partial V}{\partial Q_i} = \frac{\partial V}{\partial R}\text{inter}\ \frac{\partial R}{\partial Q_i} + \frac{\partial V}{\partial \theta}\text{inter}\ \frac{\partial \theta}{\partial Q_i} \qquad (i=1,2,\ldots,12), \tag{IV-2}$$

where

$$\begin{aligned} R &= [(Q_4-Q_{10})^2 + (Q_5-Q_{11})^2 + (Q_5-Q_{12})^2]^{1/2} \\ R_1 &= [(Q_4-Q_1)^2 + (Q_5-Q_2)^2 + (Q_6-Q_3)^2]^{1/2} \\ R_4 &= [(Q_1-Q_{10})^2 + (Q_2-Q_{11})^2 + (Q_3-Q_{12})^2]^{1/2} \end{aligned} \tag{IV-3}$$

and

$$\theta = \cos^{-1}\left[\frac{R_1^2 + R^2 - R_4^2}{2R_1R}\right] \ . \tag{IV-4}$$

The derivatives of the interaction potential shown on the right-hand side (RHS) of Eq (IV-2) are obtained directly from the splinefit of the <u>ab initio</u> energies. The $\partial R/\partial Q_i$ may be obtained from Eq (IV-3) in a straightforward manner, whereas the $\partial\theta/\partial Q_i$ require further use of the chain rule:

$$\frac{\partial \theta}{\partial Q_1} = \frac{\partial \theta}{\partial R_1}\frac{\partial R_1}{\partial Q_1} + \frac{\partial \theta}{\partial R}\frac{\partial R}{\partial Q_i} + \frac{\partial \theta}{\partial R_4}\frac{\partial R_4}{\partial Q_1} \ , \tag{IV-5}$$

where

$$\begin{aligned} \frac{\partial \theta}{\partial R_1} &= \frac{R\cos\theta - R_1}{R_1R\sin\theta} \\ \frac{\partial \theta}{\partial R} &= \frac{R_1\cos\theta - R}{R_1R\sin\theta} \\ \frac{\partial \theta}{\partial R_4} &= \frac{R_4}{R_1R\sin\theta} \ . \end{aligned} \tag{IV-6}$$

It should be noted that the splinefit of the ab initio energies yields $\partial V_{inter}/\partial\theta$ in eV/degree, while the $\partial\theta/\partial Q_i$ are in radians/distance; therefore, a factor of $180/\pi$ must be used in evaluating Eq (IV-2).

Separation of Rotation and Translation

In order that meaningful energy transfer values may be calculated from the computed trajectories, the rotation of the CO_2 molecule must be separated from its translational motion. This is accomplished rigorously by using two coordinate systems in the description of the He - CO_2 system: the space-fixed XYZ system and the molecule-fixed xyz system (Figure 23a and 23b). The orientation of the xyz system is given by the Eulerian angles α and β (Figure 23c), and the vector $\underset{\sim}{R}_{CO_2}$ denotes the position of its origin relative to the XYZ frame. The origin of the xyz system is the CO_2 center of mass and the system rotates with angular velocity $\underset{\sim}{\omega}$. The CO_2 molecule lies along the z axis with the carbon atom at the origin and remains fixed in this position. If $\underset{\sim}{r}_i$ denotes the position of atom i in xyz, then the total velocity of each atom is given by

$$\underset{\sim}{v}_i = \dot{\underset{\sim}{R}}_{CO_2} + \underset{\sim}{\omega} \times \underset{\sim}{r}_i \qquad \begin{matrix} i = 0,C,0 \\ 1,2,3 \end{matrix} \qquad \text{(IV-7)}$$

where the dot above $\underset{\sim}{R}_{CO_2}$ denotes the time derivative. The velocity of helium is

$$\underset{\sim}{v}_{He} = \dot{\underset{\sim}{R}}_{He} \quad . \qquad \text{(IV-8)}$$

$\underset{\sim}{R}_{He}$ is the position vector for helium in XYZ. The kinetic energies of helium and CO_2 may now be found

$$T_{He} = 1/2\ m_{He}\ (\dot{R}_{He})^2 \qquad \text{(IV-9)}$$

$$T_{CO_2} = 1/2\ (\dot{R}_{CO_2})^2 \sum_{i=1}^{3} m_i + \dot{\underset{\sim}{R}}_{CO_2} \cdot \underset{\sim}{\omega} \times \sum_{i=1}^{3} m_i\ \underset{\sim}{r}_i + 1/2 \sum_{i=1}^{3} m_i\ (\underset{\sim}{\omega} \times r_i) \cdot (\underset{\sim}{\omega} \times \underset{\sim}{r}_i) \quad . \qquad \text{(IV-10)}$$

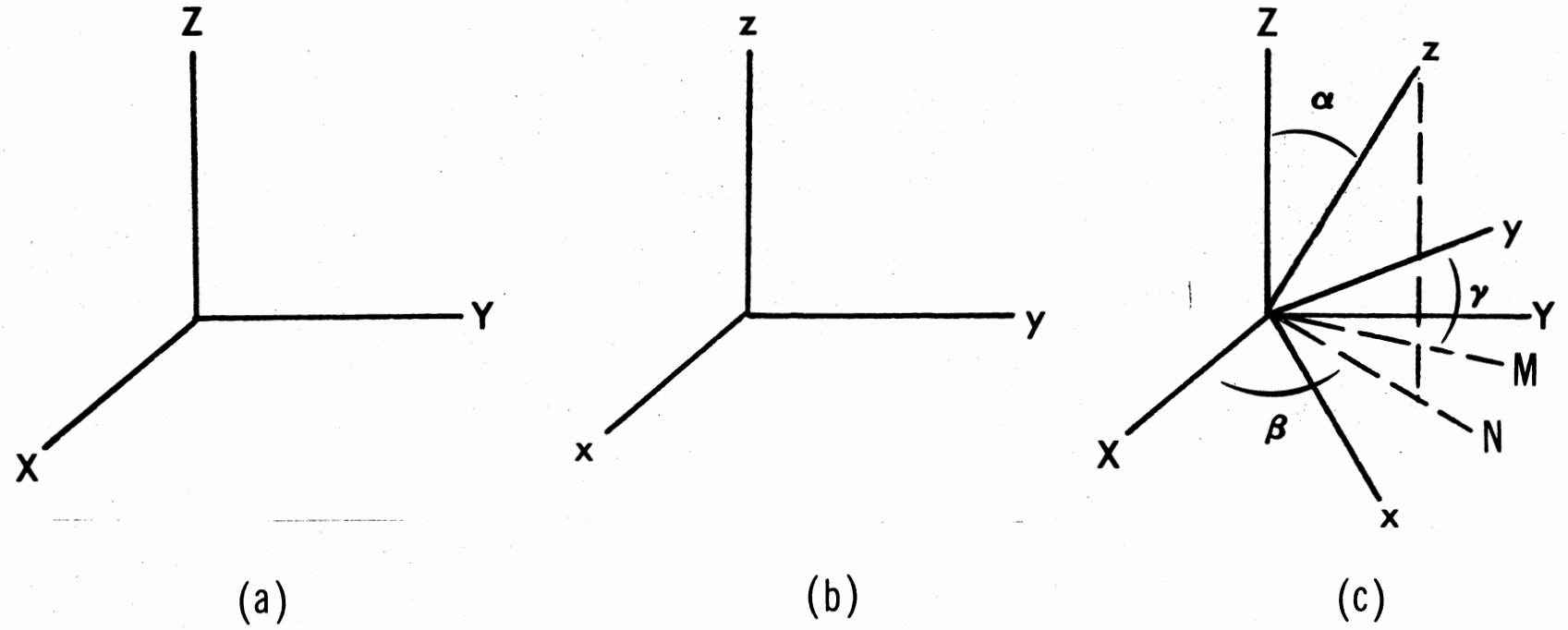

Figure 23. Cartesian Coordinate Systems Used in the Calculation, (a) Space-fixed XYZ, (b) molecule-fixed xyz, and (c) the Eulerian angles giving the orientation of xyz relative to XYZ. The lines in (c) containing M and N are in the XY plane

The mass of helium is given by m_{He}, and m_i are the masses of the atoms in CO_2. The expression for the kinetic energy of CO_2 may be simplified by noting that the origin of xyz is the CO_2 center of mass and that, as a result, the second term vanishes. Furthermore, the moments of inertia

$$\begin{aligned} I_{xx} &= \sum_{i=1}^{3} m_i (y_i^2 + z_i^2) \\ I_{yy} &= \sum_{i=1}^{3} m_i (x_i^2 + z_i^2) \\ I_{zz} &= \sum_{i=1}^{3} m_i (x_i^2 + y_i^2) \end{aligned} \qquad \text{(IV-11)}$$

and the products of inertia

$$\begin{aligned} I_{xy} &= \sum_{i=1}^{3} m_i x_i y_i \\ I_{yz} &= \sum_{i=1}^{3} m_i y_i z_i \\ I_{xz} &= \sum_{i=1}^{3} m_i x_i z_i \end{aligned} \qquad \text{(IV-12)}$$

may be used to expand the last term in the equation for T_{CO_2}

$$1/2 \sum_{i=1}^{3} m_i (\underset{\sim}{\omega} \times \underset{\sim}{r}_i) \cdot (\underset{\sim}{\omega} \times \underset{\sim}{r}_i) = 1/2 \, (\omega_x^2 I_{xx} + \omega_y^2 I_{yy} + \omega_z^2 I_{zz}) - (\omega_x \omega_y I_{xy} + \omega_x \omega_z I_{xz} + \omega_y \omega_z I_{yz}). \qquad \text{(IV-13)}$$

Because CO_2 lies along the z axis of xyz, the plane of rotation is perpendicular to the xy plane and $\omega_z = 0$. The RHS of Eq (IV-13) thus reduces further

$$1/2 \sum_{i=1}^{3} m_i (\underset{\sim}{\omega} \times \underset{\sim}{r}_i) \cdot (\underset{\sim}{\omega} \times \underset{\sim}{r}_i) = 1/2 \, I_{xx} (\omega_x^2 + \omega_y^2) \, .$$

The kinetic energy of CO_2 may now be written in a simpler form

$$T_{CO_2} = 1/2 \, (R_{CO_2})^2 \sum_{i=1}^{3} m_i + 1/2 \, I_{xx} (\omega_x^2 + \omega_y^2) \, , \qquad \text{(IV-14)}$$

where the first term is the translational energy of the CO_2 molecule and the second term its rotational energy.

Selection of Initial States

The parameters necessary to determine the initial conditions of the He - CO_2 system are J, the rotational quantum number of CO_2; γ, the orientation of the CO_2 rotation plane; α and β, the CO_2 orientation angles; $\underset{\sim}{V}_r$, the relative velocity of helium with respect to the CO_2 center of mass; b, the impact parameter; and R_s, the initial helium-carbon separation.

In quasiclassical trajectories, J has an integral value at the start of the trajectory but is treated classically for the remainder of the trajectory. J may be specified or it may be taken from a thermal Boltzmann distribution. The latter selection is achieved by choosing

$$J = 1/2\left[-1 + \sqrt{1 - \frac{8IkT}{h^2}\ln(1-\xi_J)}\right], \qquad \text{(IV-15)}$$

where ξ_J is a random number uniformly distributed on the interval [0,1] (13b). Because the configuration of the CO_2 rigid rotor is taken to be that of its vibrational ground state (00°0), the molecule is a boson and J must be even. When selecting J from a thermal Boltzmann distribution, the value obtained from Eq (IV-15) must be put into the appropriate even-integer bin, i.e., J is assigned the value of n which satisfies the following condition

$$n-1 < J \leqslant n+1 \qquad n=0,2,\ldots \quad . \qquad \text{(IV-16)}$$

Once J is determined, the initial rotational energy is calculated using

$$E_{rot} = J(J+1)B - J^2(J+1)^2D \quad . \qquad \text{(IV-17)}$$

The values of the rotational constants B and D are given in Table XIII.

The rotation of the CO_2 molecule occurs in a plane perpendicular to the xy plane and rotated by an angle γ away from the yz plane. The distribution from which γ is selected is thus

TABLE XIII

CONSTANTS FOR THE He - CO_2 SYSTEM

Rotational Constants	
B^a	0.3906 cm^{-1}
D^b	0.00 cm^{-1}
C-O Bond Equilibrium Distance	
r_e^c	1.1611 Å
Atomic Masses	
m_C	12.01 amu
m_O	16.00 amu
m_{He}	4.003 amu

[a] Reference 61, p. 395

[b] Reference 61, p. 14

[c] This value is for the (00°0) vibrational state of CO_2 and was calculated from the Gaussian-70 geometry optimization option using a 6-31G basis.

$$\gamma = 2\pi\xi_\gamma \ , \tag{IV-18}$$

where ξ_γ is again a random number on the interval [0,1]. The components of the CO_2 rotational angular momentum are

$$\begin{aligned} L_x(CO_2) &= |\underset{\sim}{L}| \cos\gamma \\ L_y(CO_2) &= |\underset{\sim}{L}| \sin\gamma \\ L_z(CO_2) &= 0 \end{aligned} \tag{IV-19}$$

and

$$|\underset{\sim}{L}| = \sqrt{2I_{xx}E_{rot}} \ . \tag{IV-20}$$

The angular velocities may also be calculated

$$\begin{aligned} \omega_x &= L_x(CO_2)/I_{xx} \\ \omega_y &= L_y(CO_2)/I_{xx} \\ \omega_z &= 0 \ . \end{aligned} \tag{IV-21}$$

The Eulerian angles α and β specify the initial orientation of the CO_2 molecule. At the start of a trajectory, the carbon atom lies at the origin of XYZ and helium moves toward the CO_2 molecule with a relative velocity $\underset{\sim}{V}_r$. The initial coordinates and momenta of CO_2 expressed in the molecule-fixed frame are

$$\begin{array}{llllll} x_1=0 & p_{x1}=-m_1\omega_y r_e & x_2=0 & p_{x2}=0 & x_3=0 & p_{x3}=m_1\omega_y r_e \\ y_1=0 & p_{y1}=m_3\omega_x r_e & y_2=0 & p_{y2}=0 & y_3=0 & p_{y3}=-m_3\omega_x r_e \\ z_1=-r_e & p_{z1}=0 & z_2=0 & p_{z2}=0 & z_3=r_e & p_{z3}=0 \ , \end{array} \tag{IV-22}$$

and may be transformed into the space-fixed frame by a rotation of α about the Y axis and β about the Z axis

$$\begin{pmatrix} X_i \\ Y_i \\ Z_i \end{pmatrix} = R_Z(\beta)\, R_Y(\alpha) \begin{pmatrix} x_i \\ y_i \\ z_i \end{pmatrix} \tag{IV-23}$$

$$\begin{pmatrix} P^{\dagger}_{Xi} \\ P^{\dagger}_{Yi} \\ P^{\dagger}_{Zi} \end{pmatrix} = R_Z(\beta)\, R_Y(\alpha) \begin{pmatrix} P_{xi} \\ P_{yi} \\ P_{zi} \end{pmatrix} \qquad \text{(IV-24)}$$

The rotation matrices R_Z and R_Y are given in Table XIV. The angles α and β are chosen from the distributions

$$\alpha = \cos^{-1}(1-2\xi_\alpha) \qquad \text{(IV-25)}$$

$$\beta = 2\pi\xi_\beta \quad , \qquad \text{(IV-26)}$$

which result in the proper weighting of the solid angle.

Because the orientation of CO_2 in the space-fixed frame is now completely arbitrary, no loss of generality occurs from placing helium in the YZ plane with the relative velocity vector parallel to the Z axis or from requiring that the center of mass of the system remain stationary. The relative velocity may be chosen from a thermal Boltzmann distribution by taking V_r to be the solution to

$$\frac{2kT}{\mu_{He,CO_2}}(1-\xi_{V_r}) - \left(V_r^2 + \frac{2kT}{\mu_{He,CO_2}}\right)\exp(-\mu_{He,\,CO_2} V_r^2/2kT) = 0 \quad , \qquad \text{(IV-27)}$$

or may be specified for a batch of trajectories (13b). The reduced mass of the He - CO_2 is given by μ_{He,CO_2} and is equal to $m_{He}m_{CO_2}/(m_{He}+m_{CO_2})$. The motion of the He - CO_2 center of mass is

$$\dot{R}_{cm} = \frac{\sum_{i=1}^{4} m_i(X_i + Y_i + Z_i)}{\sum_{i=1}^{4} m_i} \qquad m_4=m_{He} \qquad \text{(IV-28)}$$

$$= m_{He}V_r\hat{Z}/M \quad ,$$

where $M = \sum_{i=1}^{4} m_i$. This motion does not affect the course of a He - CO_2 collision and is subtracted from the velocities of helium and CO_2

$$\underset{\sim}{v}_{He} = m_{He}V_r\hat{Z} - m_{He}V_r\hat{Z}/M$$

TABLE XIV

THE ROTATION MATRICES. THESE MATRICES ROTATE THE COORDINATE AXES COUNTERCLOCKWISE THROUGH AN ANGLE θ ABOUT THE SPECIFIED AXIS

$$R_Y(\theta) = \begin{bmatrix} \cos\theta & 0 & -\sin\theta \\ 0 & 1 & 0 \\ \sin\theta & 0 & \cos\theta \end{bmatrix}$$

$$R_Z(\theta) = \begin{bmatrix} \cos\theta & \sin\theta & 0 \\ -\sin\theta & \cos\theta & 0 \\ 0 & 0 & 1 \end{bmatrix}$$

$$= m_{CO_2} V_r \hat{Z}/M \qquad \text{(IV-29)}$$

$$\underset{\sim}{v}_{CO_2} = -m_{He} V_r \hat{Z}/M \quad , \qquad \text{(IV-30)}$$

where $m_{CO_2} = m_2+2m_1$. The components of the momentum of CO_2 in the space-fixed frame are

$$\begin{aligned} P_{X1} &= P^{\dagger}_{X1} & P_{Z2} &= 0 & P_{X3} &= P^{\dagger}_{X3} \\ P_{Y1} &= P^{\dagger}_{Y1} & P_{Y2} &= 0 & P_{Y3} &= P^{\dagger}_{Y3} \\ P_{Z1} &= P^{\dagger}_{Z1} - \frac{m_1 m_{He}}{M} V_r & P_{Z2} &= \frac{-m_2 m_{He}}{M} V_r & P_{Z3} &= P^{\dagger}_{Z3} - \frac{m_3 m_{He}}{M} V_r \quad , \end{aligned} \qquad \text{(IV-31)}$$

and the initial coordinates and momenta of helium are

$$\begin{aligned} X_4 &= 0 & P_{X4} &= 0 \\ Y_4 &= -b & P_{Y4} &= 0 \\ Z_4 &= -\sqrt{R_s^2 - b^2} & P_{Z4} &= \frac{m_{He} m_{CO_2}}{M} V_r \end{aligned} \qquad \text{(IV-32)}$$

R_s is chosen such that the initial He - CO_2 interaction is negligible and b is taken from a flat distribution

$$b = b_{max} \xi_b \quad , \qquad \text{(IV-33)}$$

where b_{max} must be calculated and is the impact parameter at which energy transfer first becomes negligible.

The relative translational energy of the system may be calculated

$$E_{trans} = 1/2 \; \mu_{He,CO_2} (V_r)^2 \quad . \qquad \text{(IV-34)}$$

The total energy of the system is then

$$E_T = E_{rot} + E_{trans} + V(R_s,\theta) \quad . \qquad \text{(IV-35)}$$

From the initial coordinates and mementa, the components of the total angular momentum are calculated

$$L_X = \sum_{i=1}^{4} (Y_i P_{Zi} - Z_i P_{Yi})$$

$$L_Y = \sum_{i=1}^{4} (Z_i P_{Xi} - X_i P_{Zi}) \qquad \text{(IV-36)}$$

$$L_Z = \sum_{i=1}^{4} (Z_i P_{Yi} - Y_i P_{Zi})$$

Equations of Motion

In order for CO_2 to behave as a rigid rotor during the course of a trajectory, the following mathematical constraints must be enforced

$$R_1 = \text{constant} = r_e$$

$$R_2 = \text{constant} = r_e \qquad \text{(IV-37)}$$

$$R_3 = \text{constant} = R_1 + R_2 \quad .$$

The intramolecular distances R_i are shown in Figure 22a. As a result of these conditions, the motions of the atoms in CO_2 are no longer independent but are related by the following equations

$$dR_1 = 0 = \sum_{i=1}^{9} a_{1i} dQ_i$$

$$dR_2 = 0 = \sum_{i=1}^{9} a_{2i} Q_i \qquad \text{(IV-38)}$$

$$dR_3 = 0 = \sum_{i=1}^{9} a_{3i} dQ_i$$

The a_{ki} are shown in Table XV and are simply the direction cosines of the three bond axes denoted by R_1, R_2, and R_3.

The Lagrangian equations of motion for a system with three constraints is given by Goldstein (60)

$$\frac{\partial L}{\partial Q_i} - \frac{d}{dt} \frac{\partial L}{\partial Q_i} + \sum_{k=1}^{3} \lambda_k a_{ki} = 0 \qquad i=1,2,\ldots,9 \qquad \text{(IV-39)}$$

where L = T-V. The method of Lagrangian multipliers has been used to incorporate Eq (IV-38) into the Lagrangian equations of motion.

TABLE XV

THE COEFFICIENTS a_{ki} USED IN THE RIGID ROTOR CONSTRAINT EQUATIONS: $\sum_{i=1}^{9} a_{ki} dQ_i = 0$

i=	1	2	3	4	5	6	7	8	9
a_{1i}	$\frac{Q_1-Q_4}{R_1}$	$\frac{Q_2-Q_5}{R_1}$	$\frac{Q_3-Q_6}{R_1}$	$-a_{11}$	$-a_{12}$	$-a_{13}$	0	0	0
a_{2i}	0	0	0	$\frac{Q_4-Q_7}{R_2}$	$\frac{Q_5-Q_8}{R_2}$	$\frac{Q_6-Q_9}{R_2}$	$-a_{24}$	$-a_{25}$	$-a_{26}$
a_{3i}	$\frac{Q_7-Q_1}{R_3}+a_{11}$	$\frac{Q_8-Q_2}{R_3}+a_{12}$	$\frac{Q_9-Q_3}{R_3}+a_{13}$	$a_{24}-a_{11}$	$a_{25}-a_{12}$	$a_{26}-a_{13}$	$\frac{Q_1-Q_7}{R_3}-a_{24}$	$\frac{Q_2-Q_8}{R_3}-a_{25}$	$\frac{Q_3-Q_9}{R_3}-a_{26}$

This last term in Eq (IV-39) represents the forces of constraint, thus the equations of motion for the CO_2 rigid rotor are

$$\begin{aligned} \dot{Q}_i &= \partial H/\partial P_i \\ &= P_i/m_i \qquad i=1,2,\ldots,9 \qquad \text{(IV-40)} \\ \dot{P}_i &= \frac{\partial L}{\partial Q_i} + \sum_{k=1}^{3} \lambda_k a_{ki} \\ &= -\frac{\partial V}{\partial Q_i} + \sum_{k=1}^{3} \lambda_k a_{ki} \qquad i=1,2,\ldots,9 \end{aligned}$$

where $H = T+V$ is the classical Hamiltonian for CO_2.[1]

The equations of motion may not be used as yet because the Lagrangian multipliers λ_k are known. The λ_k are determined by requiring that

$$\begin{aligned} \dot{R}_i &= 0 \qquad i=1,2,3 \\ \ddot{R}_i &= 0 \qquad i=1,2,3 \quad . \qquad \text{(IV-41)} \end{aligned}$$

This prevents the bond from stretching or compressing with time. Taking the second derivative of the second of Eqs (IV-3) with respect to time yields

$$\ddot{R}_1 = 0 = \frac{1}{R_1}\left[(\dot{Q}_1-\dot{Q}_4)^2 + (\dot{Q}_2-\dot{Q}_5)^2 + (\dot{Q}_3-\dot{Q}_6)^2\right] + \sum_{i=1}^{9} a_{1i}\ddot{Q}_i \quad . \qquad \text{(IV-42)}$$

The first term represents the centrifugal acceleration of the atoms at either end of the bond, while the second term denotes the linear acceleration of the atoms in the bond. Rewriting the first term as F_1/R_1 and $\ddot{Q}_i$ as $\dot{P}_i/m_i$ yields

$$\ddot{R}_1 = 0 = F_1/R_1 + \sum_{i=1}^{9} a_{1i}\dot{P}_i/m_i \quad . \qquad \text{(IV-43)}$$

Similarly, the other constraints have the forms

$$\ddot{R}_2 = 0 = F_2/R_2 + \sum_{i=1}^{9} a_{2i}\dot{P}_i/m_i \qquad \text{(IV-44)}$$

$$\ddot{R}_3 = 0 = F_1/R_1 + F_2/R_2 - F_3/R_3 + \sum_{i=1}^{9} a_{3i}\dot{P}_i/m_i \quad , \qquad \text{(IV-45)}$$

---

[1] In this section the masses of the atoms of CO_2 are denoted $m_{1-3,7-9} = m_O$ and $m_{4-6} = m_C$.

where

$$F_2 = (\dot{Q}_4-\dot{Q}_7)^2 + (\dot{Q}_5-\dot{Q}_8)^2 + (\dot{Q}_6-\dot{Q}_9)^2$$
$$F_3 = (\dot{Q}_1-\dot{Q}_7)^2 + (\dot{Q}_2-\dot{Q}_8)^2 + (\dot{Q}_3-\dot{Q}_9)^2 \quad . \tag{IV-46}$$

This system of three equations (Eqs (IV-43)-(IV-45)) in three unknowns can be expressed in matrix form after substituting the expression for $\dot{P}$ (Eq (IV-40)) into each of the equations

$$\begin{bmatrix} \sum_{i=1}^{9} a_{1i}a_{1i}/m_i & \sum_{i=1}^{9} a_{1i}a_{2i}/m_i & \sum_{i=1}^{9} a_{1i}a_{3i}/m_i \\ \sum_{i=1}^{9} a_{2i}a_{1i}/m_i & \sum_{i=1}^{9} a_{2i}a_{2i}/m_i & \sum_{i=1}^{9} a_{2i}a_{3i}/m_i \\ \sum_{i=1}^{9} a_{3i}a_{1i}/m_i & \sum_{i=1}^{9} a_{3i}a_{2i}/m_i & \sum_{i=1}^{9} a_{3i}a_{3i}/m_i \end{bmatrix} \begin{bmatrix} \lambda_1 \\ \lambda_2 \\ \lambda_3 \end{bmatrix} =$$

$$\begin{bmatrix} \sum_{i=1}^{9} \frac{a_{1i}}{m_i} \frac{\partial V}{\partial Q_i} - \frac{F_1}{R_1} \\ \sum_{i=1}^{9} \frac{a_{2i}}{m_i} \frac{\partial V}{\partial Q_i} - \frac{F_2}{R_2} \\ \sum_{i=1}^{9} \frac{a_{3i}}{m_i} \frac{\partial V}{\partial Q_i} - \frac{F_3}{R_3} + \frac{F_1}{R_1} + \frac{F_2}{R_2} \end{bmatrix} . \tag{IV-47}$$

More simply, this equation may be expressed as

$$\mathbb{C}\lambda = \mathbb{F} \quad , \tag{IV-48}$$

and its solution is $\lambda = \mathbb{C}^{-1}\mathbb{F}$, where $\mathbb{C}^{-1}$ is found by the following means

$$\mathbb{C}^{-1} = \frac{\mathbb{C}\ \text{adjoint}}{\det \mathbb{C}} \quad . \tag{IV-49}$$

The equations of motion for CO_2 were given in Eq (IV-40); the equations of motion for helium contain no constraints and are

$$\dot{Q}_i = P_i/m_i \qquad i=10,11,12$$

$$\dot{P}_i = -\partial V/\partial Q_i \qquad i=10,11,12 \qquad \text{(IV-50)}$$

where m_{10-12} represents the mass of helium.

The equations of motion are integrated using a fourth-order Runge-Kutta-Gill integration method with integration step sizes ranging from 0.0008 - 0.3 time units. The rigid rotor constraints serve to keep CO_2 within 1-2° of linearity. Table XVI shows the units used in the calculation of the trajectories. A preliminary check of the accuracy of the trajectories is made by monitoring the conservation of total energy and total angular momentum in the system. Total energy is usually conserved to a minimum of three decimal places, while total angular momentum is reproduced to a minimum of eight decimal places in the final state. The accuracy of the calculations is also evaluated by rerunning trajectories at one-half the original step size and by back integration of trajectories to initial conditions. Initial coordinates and momenta are reproduced in the back integration to a minimum of five decimal places, and more often six or seven.

Determination of Final States

The end of the trajectory is reached when the helium-carbon separation exceeds R_s. From integration of the equations of motion, the final coordinates Q_i' and momenta P_i' are known and may be used to find the component of the final total angular momentum L' by substitution into Eq (IV-36). The final velocity of helium is given by

$$\underset{\sim}{v}'_{He} = \frac{1}{m_{He}} \begin{pmatrix} P'_{X4} \\ P'_{Y4} \\ P'_{Z4} \end{pmatrix} , \qquad \text{(IV-51)}$$

and from this the final relative velocity

TABLE XVI

UNITS USED IN THE He - CO_2 QUASICLASSICAL TRAJECTORY COMPUTER CODE[a]

Quantity	Unit	CGS Equivalent[b]
distance	angstrom (Å)	10^{-8} cm
time	time unit (t.u.)	$1.01804287 \times 10^{-14}$ s
velocity	velocity unit (v.u.)	0.9822769×10^{6} cm/s
energy	electron volt (eV)	1.60219×10^{-12} erg
mass	atomic mass unit (amu)	$1.6604345 \times 10^{-24}$ g
momentum	momentum unit	1.631006×10^{-18} dyne-s
angular momentum	angular momentum unit	1.631006×10^{-26} erg-s
Planck's constant, $h/2\pi$	0.0646551 eV/t.u.	$1.0545887 \times 10^{-27}$ erg-s
Boltzmann constant, k	8.61734×10^{-5} eV/°K	1.380662×10^{-16} erg/°K
speed of light, c	3.05201×10^{-4} cm/t.u.	2.99792×10^{10} cm/s

[a]These units are similar to the molecular units used by Raff et al, J. Chem. Phys. 56, 5998 (1972). The units differ only in the unit of distance.

[b]These values are based on the physical constants recommended by the CODATA Task Group on Fundamental Constants and are taken from Physics Today, September, 1974.

$$\underset{\sim}{V}_r' = \frac{M}{m_{CO_2}} \underset{\sim}{v}'_{He} \tag{IV-52}$$

and relative translational energy

$$E'_{trans} = 1/2\ \mu_{He,CO_2} (V_r')^2 \tag{IV-53}$$

may be calculated. The center of mass scattering angle is given by

$$\Omega = \cos^{-1}\left[\frac{(V_r')_Z}{|\underset{\sim}{V}_r'|}\right] \tag{IV-54}$$

because the initial velocity vector is parallel to the Z axis. The final rotational angular momentum of CO_2 is found by separating the motion of its center of mass from its angular motion

$$\begin{aligned} P_{ki}^{rot} &= P'_{ki} - (\underset{\sim}{v}'_{CO_2})_k\ m_i \\ &= P'_{ki} + \frac{m_{He} m_i}{M} (V_r')_k \quad , \quad k=X,Y,Z \end{aligned} \tag{IV-55}$$

and by subtracting the position of the CO_2 center of mass from its atomic coordinates

$$\begin{aligned} X_i^{rot} &= X_i' - \frac{1}{m_{CO_2}} \sum_{i=1}^{3} m_i X_i' \\ Y_i^{rot} &= Y_i' - \frac{1}{m_{CO_2}} \sum_{i=1}^{3} m_i Y_i' \\ Z_i^{rot} &= Z_i' - \frac{1}{m_{CO_2}} \sum_{i=1}^{3} m_i Z_i' \quad . \end{aligned} \tag{IV-56}$$

These coordinates and momenta may then be combined to determine the components of the CO_2 rotational angular momentum

$$\begin{aligned} L'_X(CO_2) &= \sum_{i=1}^{3} (Y_i^{rot} P_{Zi}^{rot} - Z_i^{rot} P_{Yi}^{rot}) \\ L'_Y(CO_2) &= \sum_{i=1}^{3} (Z_i^{rot} P_{Xi}^{rot} - X_i^{rot} P_{Zi}^{rot}) \\ L'_Z(CO_2) &= \sum_{i=1}^{3} (X_i^{rot} P_{Yi}^{rot} - Y_i^{rot} P_{Xi}^{rot}) \quad . \end{aligned} \tag{IV-57}$$

The final rotational energy of CO_2 is then

$$E'_{rot} = \frac{L'(CO_2)^2}{2I_{xx}} \qquad \text{(IV-58)}$$

where $L'(CO_2)^2 = L'_X(CO_2)^2 + L'_Y(CO_2)^2 + L'_Z(CO_2)^2$. The total energy of the system is calculated in the same fashion as at the start of the trajectory (Eq (IV-35)). The final rotational state of CO_2 is the nearest even-integer solution to

$$J(J+1)\hbar^2 = L'(CO_2)^2 \quad . \qquad \text{(IV-59)}$$

The determination of the appropriate even integer is done as described in Eq (IV-16). Finally, the conservation of total energy and of total angular momentum, and the energy transfer from translation and rotation may be calculated

$$\begin{aligned} \Delta E_T &= E'_T - E_T \\ \Delta L_T &= L'_T - L_T \\ \Delta E_{trans} &= E'_{trans} - E_{trans} \\ \Delta E_{rot} &- E'_{rot} - E_{rot} \quad . \end{aligned} \qquad \text{(IV-60)}$$

Statistical Averaging

The calculation of average energy transfer, rotational state transition probabilities, and scattering cross sections requires the solution of multidimensional integrals. For instance, the average rotational energy transfer is found by evaluating

$$\langle \Delta E_{rot} \rangle = \int_{b=0}^{\infty} \int_{\alpha=0}^{\pi} \int_{\beta=0}^{2\pi} \int_{\gamma=0}^{2\pi} \frac{d\gamma}{2\pi} \frac{d\beta}{2\pi} \frac{d(\cos\alpha)}{2} \frac{2\pi b db}{\pi b_{max}^2} \left(\frac{2}{\pi}\right)^{1/2} \left(\frac{\mu}{kT}\right)^{3/2} \langle V_r \rangle^{-1} \; X$$

$$\int_{V_r=0}^{\infty} V_r^3 \exp(\mu V_r^2/2kT)\, dV_r \sum_{J=0,2,\ldots}^{\infty} \frac{2J+1}{Q_J} \exp(-J(J+1)\hbar^2/2IkT) \; X$$

$$\Delta E_{rot}(\gamma,\beta,\alpha,b,V_r,J) \quad . \qquad \text{(IV-61)}$$

Q_J is the rotational partition function for CO_2. If J is not selected from a Boltzmann distribution, the sum over J drops out and $\langle \Delta E_{rot}(J) \rangle$ is obtained for a given initial J state.

These multidimensional integrals are most easily evaluated using a Monte Carlo technique, where the variables of integration are transformed to random numbers ξ_i on the interval [0,1] as was done in Eqs (IV-15,18,25-27,33). The Monte Carlo approximant to the integral in Eq (IV-61) is

$$\langle \Delta E_{rot} \rangle = \frac{2}{N} \sum_{i=1}^{N} \xi_b^i \Delta E_{rot}^i \quad , \tag{IV-62}$$

where ξ_b is the random number used to select the impact parameter; N is the number of trajectories; and ΔE_{rot}^i is the energy transfer calculated in the ith trajectory. The inelastic scattering cross sections are calculated from

$$\sigma_{inel} = \int_0^\infty P_J(b,\Omega)\, 2\pi b db$$

$$\approx \frac{2\pi b_{max}^2}{N} \sum_{i=1}^{N} \xi_b^i \, P_J^i(\xi^i,\Omega^i) \quad , \tag{IV-63}$$

where $P_J(b,\Omega)$ is the probability that rotational energy transfer will occur given the initial state J with impact parameter b and scattering angle Ω. $P_J^i(\xi^i,\Omega^i)$ is the actual probability calculated from the ith trajectory and is zero if $\Delta J=0$, and one if $\Delta J \neq 0$.

The elastic cross sections must be treated more carefully

$$\sigma_{el} = \int_{b=0}^{\infty} \int_{\Omega=0}^{\pi} P_J(b,\Omega)\, 2\pi b db \, \frac{\sin\Omega}{2} \, d\Omega$$

$$\approx \frac{\pi^2 b_{max}^2}{N} \sum_{i=1}^{N} \xi_b^i P_J^i(\xi^i,\Omega^i) \, \sin\Omega^i \tag{IV-64}$$

in order to avoid the counting of undeflected elastic trajectories. The Monte Carlo error is

$$\varepsilon \leq \frac{\left\{ \sum_{i=1}^{N} \xi_b^i (F^i)^2 - \frac{1}{N}\left[\sum_{i=1}^{N} \xi_b^i F^i \right]^2 \right\}^{1/2}}{\sum_{i=1}^{N} \xi_b^i F^i} \times 100 \quad , \qquad \text{(IV-65)}$$

where F^i represents the energy transfer or the rotational state transition probability. There is a 68% probability that the actual error in the integral is less than ε.

Results and Discussion

The QCT's for the He - CO_2 rigid rotor system were performed on an IBM 370/158 computer and used the units shown in Table XVI. A batch of 250 trajectories usually required 1 1/2 - 2 hours of CPU time for completion. The calculation of statistical quantities, such as inelastic or elastic cross sections, incorporated only those trajectories in which the magnitude of rotational energy transfer exceeded the uncertainty in the total energy of the system.

The value for the maximum impact parameter (b_{max}) for inelastic collisions was determined by running batches of 100 trajectories at fixed impact parameter b, beginning at 0.5 Å and increasing by 0.5 Å with each batch of trajectories, until $\Delta J=0$ for every trajectory. The initial rotational quantum number was set at 16; the reaction shell radius R_s was 5.0 Å; and the translational temperature was 300°K. For the ab initio potential, b_{max} was found to be 4.0 Å. Additional trajectories run at 300°K with J selected from a Boltzmann distribution and at 1000°K with J=16 confirmed the choice of b_{max}. The EG potential was found to require a larger b_{max} of 5.0 Å.

For elastic collisions, a larger value of b_{max} was necessary in

order to include trajectories where $\Delta J=0$ but the center of mass scattering angle is greater than zero. In this case, the criterion for selecting b_{max} was that the elastic cross section $\sigma_{el}=0$. Ten trajectories each were run at intervals of 0.5 Å beginning at 4.0 Å on the SAI and EG surfaces. The relative velocity was set at 0.0713 v.u. (700 m/s); J was selected from a Boltzmann distribution at 300°K; and R_s was increased from 6 to 12.5 Å as b increased from 4 to 12 Å. The maximum impact parameter for elastic collisions was found to be 5 Å on the SAI surface and 12 Å on the EG surface.

Calculation of elastic, inelastic, and total integral cross sections for the He - CO_2 rigid rotor system was made at a series of fixed relative velocities and a rotational temperature of 300°K. The velocities ranged from 0.03 to 1.167 v.u. (300 - 11466 m/s) and were chosen to allow a comparison between the cross sections calculated in this work and those calculated quantum mechanically on the EG surface by Parker and Pack (16b). Total cross sections have also been determined by Butz et al (51d) from a molecular beam experiment and fall into this same relative velocity range.

The calculation of the elastic, inelastic, and total integral cross sections for scattering on each of the two He - CO_2 potential-energy surfaces was accomplished by running two batches of trajectories for each relative velocity: one consisting of 250 trajectories in which b_{max} = 4.0 Å, and one consisting of 100 (200) trajectories in which b_{max} = 5 (12) Å (the numbers in parentheses refer to the EG surface). This procedure avoided introducing a large statistical uncertainty into the calculation of inelastic scattering cross sections,

because inelastic scattering occurs over a much smaller magnitude and range of impact parameter than does elastic scattering. The final elastic cross sections were then calculated simply by adding the appropriately weighted elastic cross sections for b = 0 - 4 and b = 4 - b_{max}^{inel}.

The results of the QCT's are shown in Figures 24, 25, and 26. To save computer time, the trajectories on the EG surface for the impact parameter range 0 - 4 Å were begun with an initial He - CO_2 separation of 5 Å, and the initial intermolecular potential at this distance is not quite zero on the EG surface. In effect, the system behaves as though the trajectory had been started with a smaller relative velocity but at a distance where the intermolecular potential is zero. For instance, at R_s = 5 Å the interaction potential on the EG surface averages about -0.0009 eV. A trajectory begun at this point with a relative velocity of 800 m/s behaves essentially the same as one begun at R_s = 12.5 Å--where the interaction is negligible--having a relative velocity of 771 m/s, and requires much less computational time than a trajectory started at 12.5 Å.

The inelastic cross sections calculated from the EG and SAI surfaces are shown in Figure 24. The computed inelastic cross sections include all nonzero rotational transitions. The SAI cross sections are consistently smaller than the EG counterparts, and the difference between the EG and SAI values increases as the relative velocity decreases. Since trajectories on both surfaces are begun at 5 Å, the effect of the long-range potential of the EG surface is negligible. Furthermore, the magnitude of the difference between the EG and SAI inelastic cross sections is seen to decrease with increasing relative

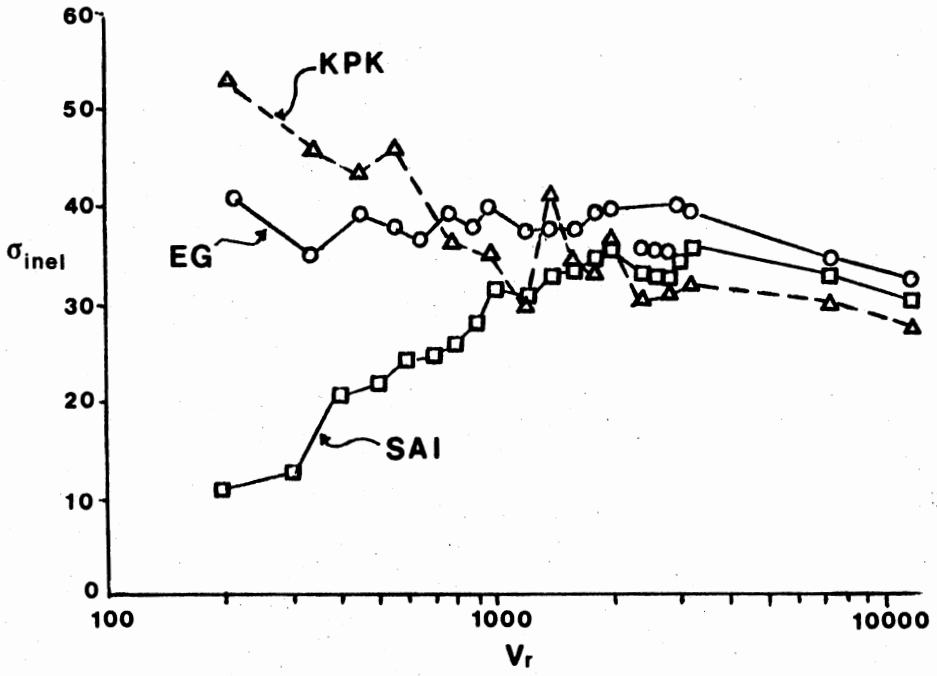

Figure 24. Inelastic Cross Sections for the He - CO_2 System. Squares represent the SAI values, circles the EG values, and triangles the KPK values. Velocities are in m/s and cross sections in $Å^2$

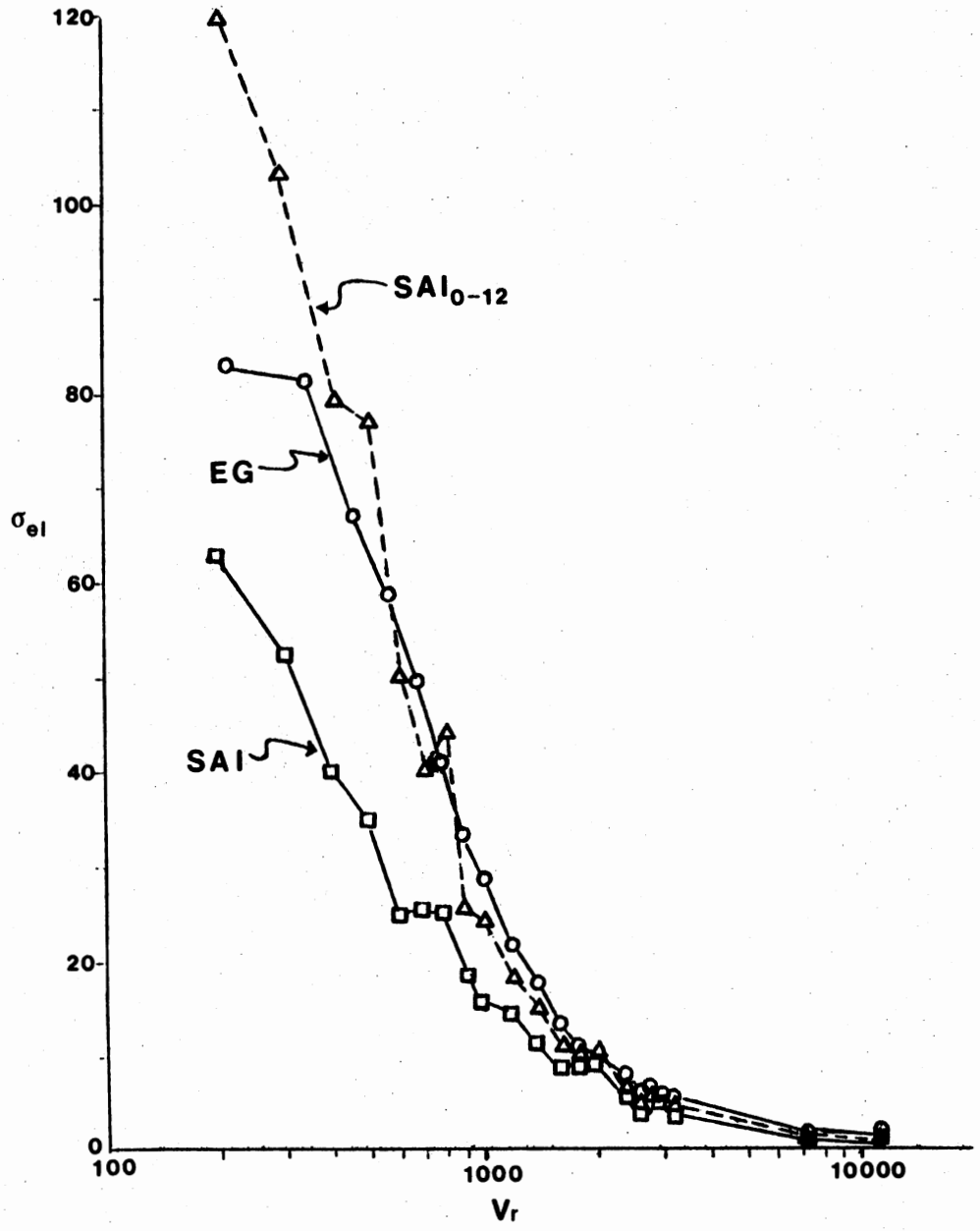

Figure 25. Elastic Cross Sections for the He - CO_2 System. Squares represent the SAI values, circles the EG values, and triangles the SAI_o values with the EG contribution from 5 - 12 Å. Units are the same as in Figure 24

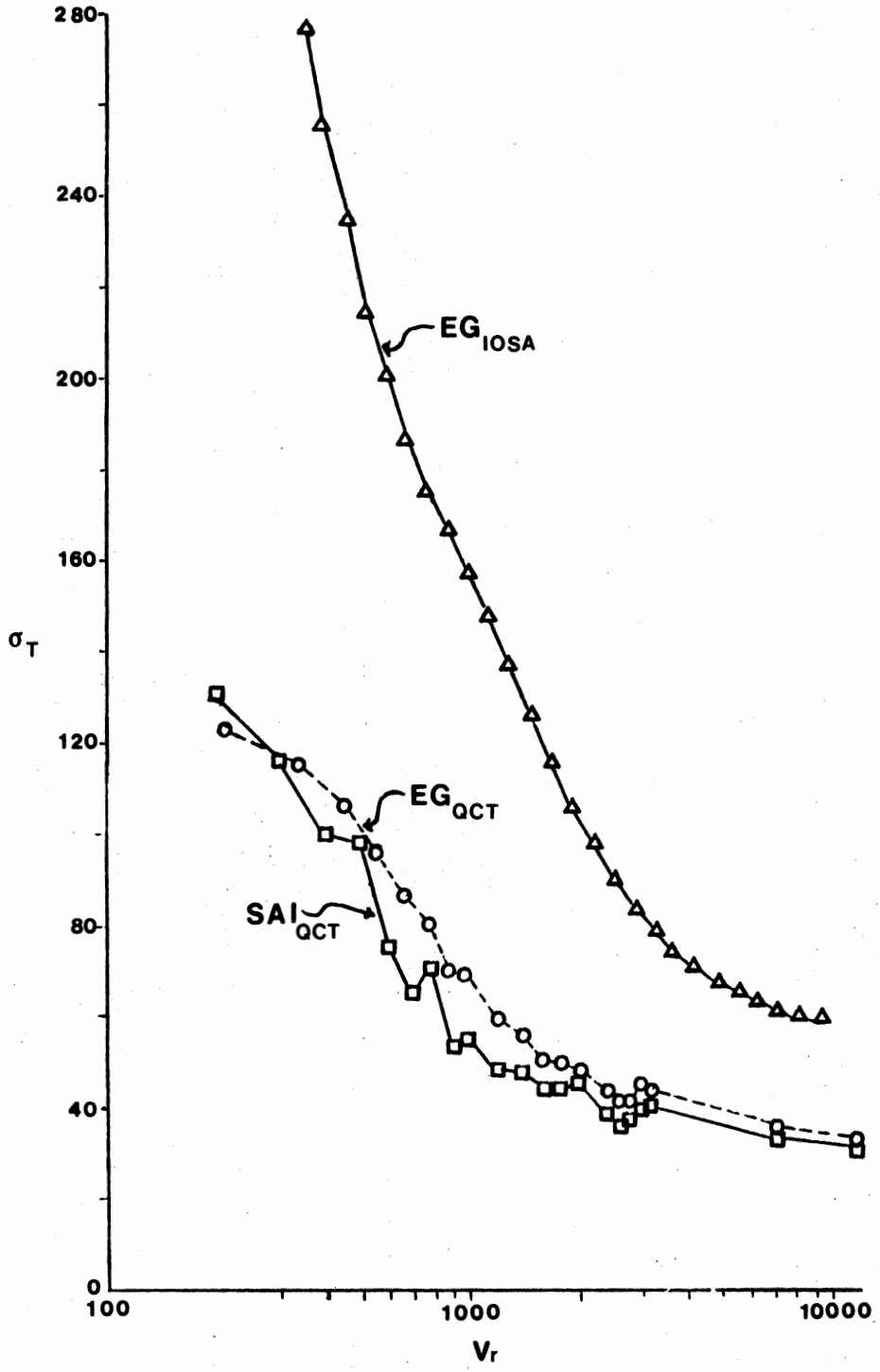

Figure 26. Total Cross Sections for the He - CO_2 System. Squares represent the SAI values, circles the EG values from the QCT calculation, and triangles the EG values from the IOSA calculation. Units are the same as in Figure 24

velocity. These facts indicate that the attractive well of the EG surface is the feature which is favoring the larger amount of rotational energy transfer on this surface.

Figure 25 shows the elastic cross sections calculated quasiclassically. The cross sections calculated from the EG surface are seen to be larger than those calculated from the SAI surface. The large difference between the EG and SAI cross sections once again appears to be due to a feature present on the EG surface but absent on the SAI surface: the long-range attraction provided by the Van der Waal's tail. To confirm this hypothesis, the contribution to the EG elastic cross section from impact parameters in the range 5 - 12 Å was calculated, weighted, and added to the SAI elastic cross section. This step should exclude the effects of the attractive well, which is centered at 3.02 Å at 90° and 4.66 Å at 0°. The result of this calculation is also shown in Figure 25. Except at small relative velocities--less than 500 m/s--the elastic cross sections calculated from the two surfaces now are in good agreement, showing the importance of including the long-range potential on the potential-energy surface when elastic cross sections are calculated.

Parker and Pack (16b) have computed total integral cross sections from the EG surface using a quantum mechanical method known as the infinite order sudden approximation (IOSA). This method allows a simple, quick calculation of total integral and differential cross sections which depends only on the relative kinetic energy for the system. In Figure 26 are shown the total (elastic plus inelastic) cross sections for the He - CO_2 rigid rotor system computed quasiclassically from the

SAI and EG surfaces, and quantum mechanically from the EG surface (16b). The graph clearly shows a discrepancy between the IOSA and quasiclassically calculated total cross sections. In fact, the QCT cross sections are almost uniformly a factor of two less than the IOSA cross sections. This difference arises from the nature of the QCT calculation of elastic cross sections. The total integral cross section, quantum mechanical or quasiclassical, is given by

$$\sigma_T = 1/2 \int_0^{\pi} I(\Omega)\sin\Omega d\Omega,$$

where I is the total differential cross section and Ω is the center of mass scattering angle. A graph of $I(\Omega)\sin\Omega$ vs. Ω should show a spike centered at small Ω which arises from the large number of mainly elastic collisions which cause only a slight deflection of the incoming particle. However, it is not possible to perform the number of trajectories necessary to include accurately the effects of trajectories deflected by angles of 5° - 10° or less. Thus the spike is truncated in a QCT calculation and, therefore, a QCT calculation will badly underestimate the elastic cross section. However, the QCT method does give accurate results for inelastic cross sections because there will be no infinitely large spike at small scattering angles for the inelastic differential cross section.

No comparison was made between the QCT results and the experimentally determined total cross sections of Butz et al (51d) for the reasons just discussed. However, Keil, Parker, and Kuppermann (51c) have also performed molecular beam experiments on the He - CO_2 system and have fitted a potential to their experimentally determined total differential cross sections. This potential-energy surface consists of three

separate potential forms: the EG potential at energies greater than 0.030 eV, an experimentally determined Morse-type potential for energies less than 0.01 eV and $R < 4.4$ Å, and a Van der Waal's tail for $R > 4.4$ Å and energies greater than -0.0004 eV. The areas between the regions are connected with splines to provide a continuous surface. The resulting potential-energy surface is shown in Figure 27. The details of the computation of the surface and its derivatives are given in Appendix C.

The Keil-Parker-Kuppermann (KPK) surface is very similar to the EG surface pictured in Figure 9b. The KPK surface has a shallow attractive well close to the oxygen atoms--at ($R = 4.77$ Å, $\theta = 0°$, 180°), $V = -0.0011$ eV--which becomes deeper as the angle between helium and the CO_2 bond axis approaches 90°. The deepest point of the well occurs at $R = 3.31$ Å, $\theta = 90°$ and is 0.0393 eV in depth. The KPK and EG surfaces also share the same contours for energies greater than 0.030 eV, and both contain an attractive Van der Waal's tail. However, the surfaces do differ significantly. The well on the EG surface penetrates closer to the CO_2 molecule and is twice as deep (0.00824 eV) as the KPK well. This results in a more repulsive potential on the EG surface than on the KPK surface at energies less than 0.030 eV, a difference which is largest at $\theta = 90°$.

The other major difference between the two surfaces is an artificial one caused by the manner in which the KPK surface was calculated. At the boundary of the EG/Morse-type potential, and also at the junction of the Morse-type/Van der Waal's potential, the potential energy is not continuous. Use of cubic splines in these regions forces energy continuity, but a near-discontinuity at each boundary region still exists.

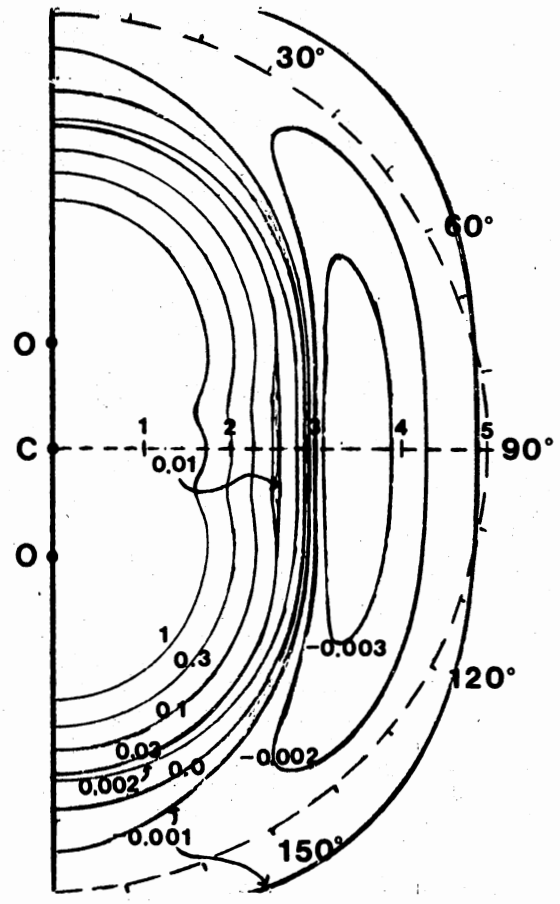

Figure 27. Contour Plot of the KPK Surface for the He - CO_2 System. The positions of the carbon and oxygen atoms are shown. Contours are in eV and distances are in Å

The main effect of these near-discontinuities is to disrupt energy conservation slightly, with the discrepancy usually appearing as excess translational energy. This problem is not significant unless the trajectory passes over both boundary regions, an event which is circumvented by starting the bulk of the trajectories inside the Morse-type/Van der-Waals's boundary.

QCT's were performed on the KPK surface using the relative velocities and rotational temperature already given for the SAI and EG trajectories. No elastic cross sections were computed for the reasons already discussed. At each relative velocity one batch of 250 trajectories was computed with b = 0 - 4 Å and R_s = 5 Å, while a second batch of trajectories was computed for b = 4 - 5 Å and R_s = 6 Å. This split greatly reduced the number of trajectories which encountered both surface discontinuities, as well as increasing the statistical accuracy of the cross sections for $V_r \gtrsim 1200$ m/s, which showed a negligible amount of rotationally inelastic scattering at impact parameters larger than 4 Å. The inelastic cross sections were computed in the same fashion as those calculated from the EG and SAI surfaces and are shown in Figure 24 and in Table XVII.

The inelastic cross sections from the KPK surface are larger than either EG or SAI inelastic cross sections for low relative velocities but, within the calculational uncertainty, are in good agreement with the SAI and EG inelastic cross sections at large velocities. The behavior of the KPK inelastic cross sections at velocities less than 700 m/s is difficult to understand if rotational energy transfer depends only on the attractive well, which is shallower on this surface and which would thus be expected to yield slightly smaller inelastic cross

TABLE XVII

INELASTIC CROSS SECTIONS CALCULATED FROM THE SAI, EG, AND KPK SURFACES. VELOCITIES ARE IN M/S AND CROSS SECTIONS ARE IN A^2

V_r	σ_{inel}(SAI)	V_r	σ_{inel}(EG)	σ_{inel}(KPK)
200	10.6 ± 1.9[a]			
		210	40.3 ± 3.2	52.6 ± 3.0
300	12.4 ± 2.1			
		338	34.4 ± 3.0	45.8 ± 2.9
400	20.5 ± 2.6			
		452	38.9 ± 3.1	43.3 ± 3.0
500	21.8 ± 2.6			
		561	37.4 ± 3.1	46.0 ± 3.1
600	24.1 ± 2.7			
		666	36.2 ± 3.1	---
700	24.4 ± 2.7			
		771	38.8 ± 3.1	35.6 ± 2.9
800	25.7 ± 2.8			
		874	37.3 ± 3.1	---
900	27.8 ± 2.9			
		977	39.9 ± 3.2	34.8 ± 3.0
1000	31.2 ± 3.0			
		1181	37.1 ± 3.1	30.2 ± 3.0
1200	30.4 ± 2.9			
1400	32.6 ± 3.0	1384	37.6 ± 3.1	40.7 ± 3.2
1600	33.5 ± 3.0	1586	37.4 ± 3.1	33.9 ± 3.2
1800	34.3 ± 3.1	1787	39.0 ± 3.2	32.7 ± 3.2
2000	35.0 ± 2.4	1988	39.2 ± 3.2	36.0 ± 3.2
2400	32.3 ± 3.0	2390	35.4 ± 3.1	30.1 ± 3.0
2614	32.2 ± 2.4	2605	35.1 ± 3.1	---
2800	31.4 ± 3.0	2792	34.7 ± 3.1	31.4 ± 3.1
3000	33.7 ± 2.4	2992	39.8 ± 3.2	---
3200	35.7 ± 3.1	3193	38.9 ± 3.2	31.7 ± 3.2
7252	32.5 ± 3.1	7249	34.1 ± 3.2	29.4 ± 3.0
11466	29.7 ± 3.0	11464	32.2 ± 3.1	26.7 ± 3.0

[a]These values represent the statistical (Monte Carlo) uncertainty in the calculated inelastic cross sections.

sections than the EG surface. However, it has been found for the HCl - He and HCl - Ar systems that the rotational energy transfer is also sensitive to the short-range potential (62).

As noted in the comparison of the EG and KPK surfaces, the KPK surface is less repulsive than the EG surface in the region extending from the 0.030 eV contour to the bottom of the attractive well. Since trajectories in the velocity range less than 700 m/s cannot penetrate contours larger than 0.010 eV, it is possible that it is the less repulsive nature of the short- to medium-range potential on the KPK surface which is enhancing the rotational energy transfer in this velocity range. As the relative velocities increase and the trajectories penetrate into the 0.030 eV and larger contours, the trajectories on the KPK surface should behave more like those on the EG surface, and this is indeed what occurs.

The inelastic cross sections calculated from the EG surface have been shown to be in good agreement with those found from the experimentally determined potential at most velocities larger than 700 m/s. Most theoretical studies of rotational energy transfer, however, focus on individual rotational transitions. Thus, it is important that the potential-energy surface give accurate state-to-state as well as total inelastic cross sections. Shown in Figure 28 are state-to-state cross sections calculated on each of the three surfaces at relative velocities of 1800 and 3200 m/s. The three curves behave almost identically, and show that small ΔJ transitions are not the only transitions which can occur in the He - CO_2 system, although $\Delta J = \pm 2$ transitions do predominate. Transitions involving ΔJ as large as 26 are seen to occur with significant cross section.

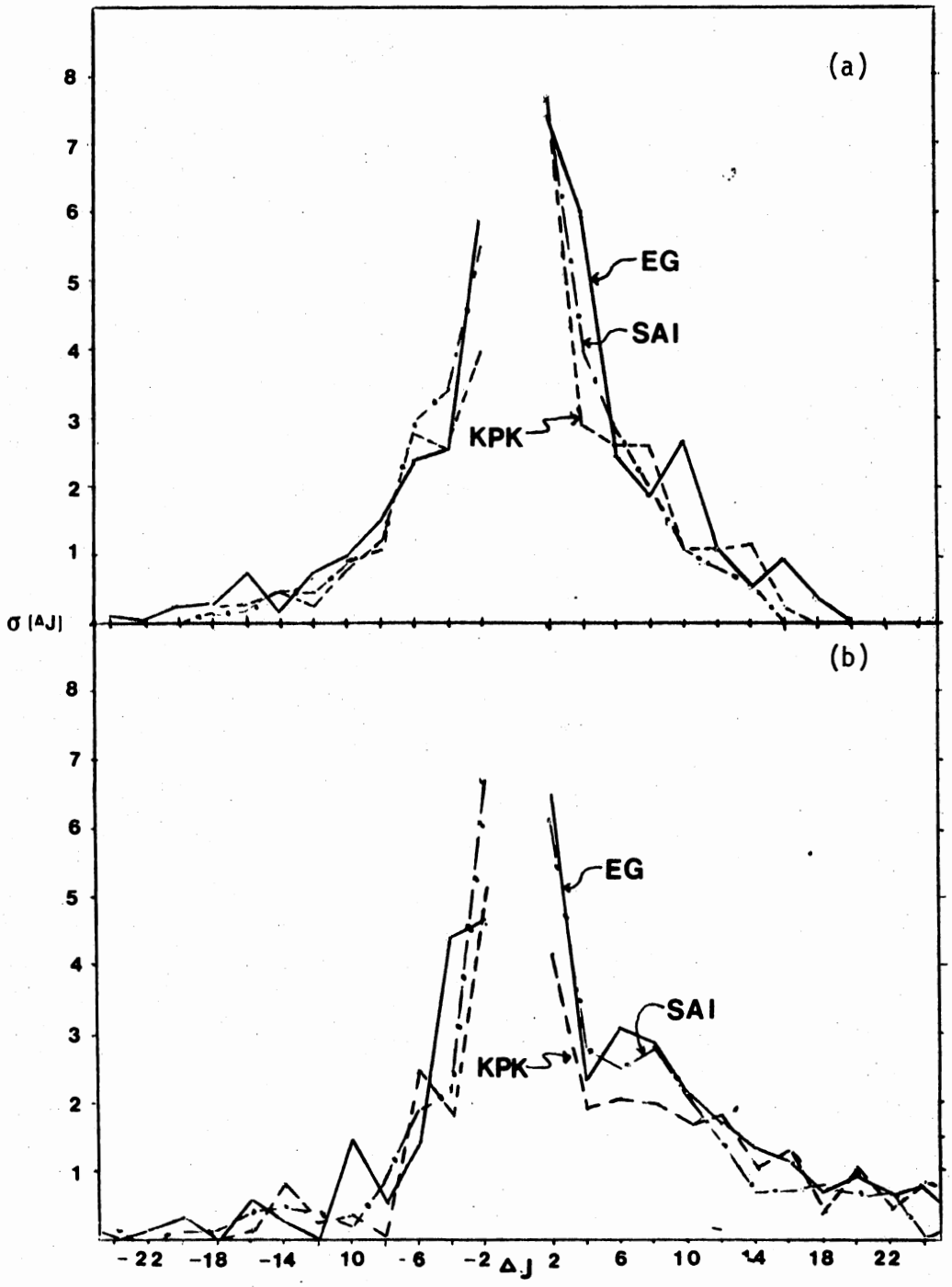

Figure 28. State-to-State Cross Sections for the He - CO_2 System at (a) 1800 and (b) 3200 m/s. Cross Sections are in $Å^2$

Conclusions

The study of the rotationally inelastic scattering in the He - CO_2 rigid rotor system has revealed several facts. First, the QCT method does not yield accurate elastic and total (elastic plus inelastic) cross sections for the He - CO_2 system. Inelastic cross sections, however, may be calculated from a QCT study and appear to be enhanced by the presence of an attractive well on the potential-energy surface, and possibly by a less repulsive short- to medium-range potential as well. Within the statistical uncertainty, inelastic cross sections calculated from all three potential-energy surfaces for relative velocities greater than 1000 m/s show good agreement. Furthermore, individual inelastic cross sections calculated from the SAI, EG, and KPK surfaces in this velocity range agree well, indicating that both the EG and SAI surfaces may be used for studies of rotationally inelastic scattering in this range. At velocities less than 1000 m/s, the presence of an attractive well on the potential-energy surface is required if reliable inelastic cross sections are to be calculated. Thus, the ab initio surface should not be used to calculate inelastic cross sections in this velocity range. Although there was also some discrepancy between the results obtained on the EG and KPK surfaces in the low velocity range, the EG surface yields more realistic values for the inelastic cross sections than does the SAI surface. However, the discrepancy with the KPK result indicates that the EG surface should be used with caution in this region. The possible dependence of the difference between the EG and KPK inelastic cross sections on the short- to medium-range repulsion merits further study.

Finally, the QCT investigation revealed the possible involvement

of several features of the potential-energy surface in affecting the outcome of rotationally inelastic collisions. It is important that the effects of the structure and mass of the rotor and its collision partner on rotationally inelastic collisions be studied. An ideal starting point would be a comparison between He - CO_2 and H_2 - CO_2 rotationally inelastic cross sections calculated from the respective ab initio surfaces. These studies are currently being performed and the results will be reported shortly.

BIBLIOGRAPHY

(1) a) D. M. Rank, C. H. Townes, and W. J. Welch, Science 174, 1083 (1971); b) S. Drapatz and K. W. Michel, Astron. and Astrophys. 36, 211 (1974).

(2) W. L. Fite, Can. J. Chem, 47, 1797 (1969).

(3) For a listing of the systems which have received the most thorough treatments, both ab initio and semiempirical, in recent years and for an excellent review of theoretical and experimental work on inelastic scattering, see J. P. Toennies, "The Calculation and Measurement of Cross Sections for Rotational and Vibrational Excitation," Ann. Rev. Phys. Chem. 27, 225 (1976).

(4) For example, see: a) M. D. Gordon and D. Secrest, J. Chem. Phys. 52, 120 (1970); b) ibid. 53, 4408 (1970); c) R. A. White and E. F. Hayes, J. Chem. Phys. 57, 2985 (1972).

(5) a) M. H. Alexander and E. V. Berard, J. Chem. Phys. 60, 3950 (1974); b) D. Secrest, J. Chem. Phys. 61, 3867 (1974); c) M. H. Alexander, J. Chem. Phys. 61, 3868 (1974).

(6) a) J. R. Walsh, J. H. Ahlberg, and E. N. Nilson, J. Math. & Mech. 11, 225 (1962); b) T. L. Jordan, Report LA-3137, Los Alamos Scientific Laboratories (1965).

(7) D. R. McLaughlin and D. L. Thompson, J. Chem. Phys. 59, 4393 (1973).

(8) N. Sathyamurthy, G. E. Kellerhals, and L. M. Raff, J. Chem. Phys. 64, 2259 (1976).

(9) N. Sathyamurthy and L. M. Raff, J. Chem. Phys. 63, 464 (1975).

(10) For a review which covers semiempirical formulations for hydrogen-halogen systems, see: a) C. A. Parr and D. G. Truhlar, J. Chem. Phys. 75, 1844 (1971); for a review which describes the quasiclassical scattering calculations that have been done and the types of surfaces that have been employed in them, see: b) R. N. Porter, "Molecular Trajectory Calculations", Ann. Rev. Phys. Chem. 25, 317 (1974).

(11) a) S. Sato, Bull, Chem. Soc. Japan 28, 450 (1955); b) S. Sato, J. Chem. Phys. 23, 592 (1955); other systems described by

the LEPS formalism or some modification are: c) H_2I_2: L. M. Raff, L. Stivers, R. N. Porter, D. L. Thompson, and L. B. Sims, J. Chem. Phys. 52, 3449 (1970); d) FH_2: J. C. Polanyi and J. L. Schreiber, Chem. Phys. Lett. 29, 319 (1974); e) ClH_2: A. Persky, J. Chem. Phys. 66, 2932 (1977).

(12) E. A. McCullough, Jr. and R. E. Wyatt, J. Chem. Phys. 54, 3578 (1971).

(13) a) M. Karplus, R. N. Porter, and R. D. Sharma, J. Chem. Phys. 43, 3259 (1965); for an excellent, detailed description of classical and quasiclassical methods, see: b) R. N. Porter and L. M. Raff, "Classical Trajectory Studies of Molecular Collisions," Dynamics of Molecular Collisions, Part B: University of California, Berkeley (1976), Chapter 1.

(14) R. D. Levine and R. B. Bernstein, Acc. Chem. Res. 7, 393 (1974).

(15) E. F. Hayes, A. K. Q. Siu, F. M. Chapman, Jr., and R. L. Matcha, J. Chem. Phys. 65, 1901 (1976).

(16) The surface is calculated in a) G. A. Parker, R. L. Snow, and R. T. Pack, J. Chem. Phys. 64, 1668 (1976); a contour plot of the surface is in b) G. A. Parker and R. T. Pack, J. Chem. Phys. 68, 1585 (1978).

(17) a) R. G. Gordon and Y. S. Kim, J. Chem. Phys. 56, 3122 (1972); b) Y. S. Kim and R. G. Gordon, J. Chem. Phys. 60, 1842 (1974); c) Y. S. Kim and R. G. Gordon, J. Chem. Phys. 61, 1 (1974).

(18) J. C. Polanyi and W. H. Wong, J. Chem. Phys. 51, 1439 (1969).

(19) M. H. Mok and J. C. Polanyi, J. Chem. Phys. 51, 1451 (1969).

(20) N. H. Hijazi and K. J. Laidler, J. Chem. Phys. 58, 349 (1973).

(21) For an excellent treatment of the effect of barrier position on reaction dynamics in realistic systems as well as a discussion of momentum transfer effects, see R. N. Porter, L. B. Sims, D. L. Thompson, and L. M. Raff, J. Chem. Phys. 58, 2855 (1973).

(22) a) W. A. Chupka, M. E. Russell, and K. Refaey, J. Chem. Phys. 48, 1518 (1968); b) W. A. Chupka and M. E. Russell, J. Chem. Phys. 49, 5426 (1968); c) W. A. Chupka, J. Berkowitz, and M. E. Russell, VI International Conference on the Physics of Electronic and Atomic Collisions: M.I.T., Cambridge, Massachusetts (1969), p. 71.

(23) a) K. G. Anlauf, P. J. Kuntz, D. H. Maylotte, P. D. Pacey, and J. C. Polanyi, Disc. Far. Soc. 44, 183 (1967); b) K. G.

Anlauf, D. H. Maylotte, J. C. Polanyi, and R. B. Bernstein, J. Chem. Phys. 51, 5716 (1969); c) J. C. Polanyi and D. C. Tardy, J. Chem. Phys. 51, 5717 (1969).

(24) L. Friedman, Advan. Chem. Ser. 58, 87 (1966).

(25) a) J. A. Rutherford and D. A. Vroom, J. Chem. Phys. 58, 4076 (1973); b) R. H. Neynaber and G. D. Magnuson, J. Chem. Phys. 59, 825 (1973).

(26) P. J. Brown and E. F. Hayes, J. Chem. Phys. 55, 922 (1971).

(27) P. J. Kuntz, Chem. Phys. Lett. 16, 581 (1972).

(28) a) P. J. Kuntz and W. N. Whitton, Chem. Phys. Lett. 34, 340 (1975); b) W. N. Whitton and P. J. Kuntz, J. Chem. Phys. 64, 3624 (1976).

(29) a) D. J. Kouri and M. Baer, Chem. Phys. Lett. 24, 37 (1974); b) J. T. Adams, Chem. Phys. Lett. 33, 275 (1975); c) Ch. Zuhrt, F. Schneider, and L. Zülicke, Chem. Phys. Lett. 43, 571 (1976).

(30) N. Sathyamurthy, R. Rangarajan, and L. M. Raff, J. Chem. Phys. 64, 4606 (1976).

(31) N. Sathyamurthy, J. W. Duff, C. Stroud, and L. M. Raff, J. Chem. Phys. 67, 3563 (1977).

(32) a) D. Secrest and B. R. Johnson, J. Chem. Phys. 45, 4556 (1966); b) D. Rapp and T. Kassal, Chem. Rev. 69, 61 (1969); c) W. A. Lester, Jr. and J. Schaefer, J. Chem. Phys. 59, 3676 (1973); d) R. LeBudde and R. B. Bernstein, J. Chem. Phys. 59, 3687 (1973).

(33) Examples of the most recent work are: a) L. M. Raff, J. Chem. Phys. 60, 2220 (1974); b) T. Valencich and D. L. Bunker, J. Chem. Phys. 61, 21 (1974).

(34) For reviews covering several of the experimental techniques mentioned, see: a) T. L. Cottrell and J. C. McCoubrey, Molecular Energy Transfer in Gases: Butterworths, London (1961); b) R. G. Gordon, W. Klemperer, and J. I. Steinfeld, "Vibrational and Rotational Relaxation," Ann. Rev. Phys. Chem. 19, 215 (1968); c) J. M. Farrar and Y. T. Lee, "Chemical Dynamics," Ann. Rev. Phys. Chem. 25, 357 (1974).

(35) a) J. Ross, Molecular Beams: John Wiley & Sons, New York (1966); b) G. A. Fisk and F. F. Crim, Acc. Chem. Res. 10, 73 (1977).

(36) a) C. B. Moore, "Lasers in Chemistry," Ann. Rev. Phys. Chem. 22, 387 (1971); b) E. Weitz and G. Flynn, "Laser Studies

of Vibrational and Rotational Relaxation in Small Molecules," Ann. Rev. Phys. Chem. 25, 275 (1974).

(37) a) W. A. Rosser, Jr., A. D. Wood, and E. T. Gerry, J. Chem. Phys. 50, 4996 (1969); b) D. F. Heller and C. B. Moore, J. Chem. Phys. 52, 1005 (1970); c) R. S. Chang, R. A. McFarlane, and G. J. Wolga, J. Chem. Phys. 56, 667 (1972).

(38) a) C. B. Moore, R. E. Wood, B. L. Hu, and J. T. Yardley, J. Chem. Phys. 46, 4222 (1967); b) W. A. Rosser, Jr. and E. T. Gerry, J. Chem. Phys. 51, 2286 (1969).

(39) a) J. T. Yardley and C. B. Moore, J. Chem. Phys. 46, 4491 (1967); b) J. C. Stephenson, R. E. Wood, and C. B. Moore, J. Chem. Phys. 54, 3097 (1971).

(40) For an excellent review of theoretical as well as experimental treatments of vibrational energy transfer, see S. Ormonde, Rev. Mod. Phys. 47, 193 (1975).

(41) R. L. Thommarson, G. C. Berend, and S. W. Benson, J. Chem. Phys., 54, 1313 (1971).

(42) J. N. Bass, J. Chem. Phys. 60, 2913 (1974).

(43) a) H. H. Suzukawa, Jr., Ph.D. Thesis: University of California, Irvine (1974); b) H. H. Suzukawa, Jr., M. Wolfsberg, D. L. Thompson, J. Chem. Phys. 68, 455 (1978).

(44) N. Sathyamurthy and L. M. Raff, J. Chem. Phys. 66, 2191 (1977).

(45) E. Guha and S. Saha, J. Chem. Phys. 66, 1707 (1977).

(46) L. M. Raff and N. Sathyamurthy, private communication.

(47) R. K. Preston and R. T. Pack, J. Chem. Phys. 66, 2480 (1977).

(48) a) J. M. Farrar, J. M. Parsons, and Y. T. Lee, Proceedings of the 4th International Conference on Molecular Beams: Cannes, France (1973); b) H. J. Loesch, Chem. Phys. 18, 431 (1976).

(49) Y. Shimoni and D. J. Kouri, Chem. Phys. Lett. 42, 28 (1976).

(50) R. Goldflam, D. J. Kouri, R. K. Preston, and R. T. Pack, J. Chem. Phys. 66, 2574 (1977).

(51) a) T. W. Meyer and C. K. Rhodes, Phys. Rev. Lett. 32, 637 (1974); b) T. W. Meyer, W. K. Bischel, and C. K. Rhodes, Phys. Rev. A 10, 1433 (1974); c) M. Keil, G. A. Parker, and A. Kuppermann, Chem. Phys. Lett. (accepted for publication); d) H. P. Butz, R. Feltgen, H. Pauly, and H. Vehmeyer, Z. Physik 247, 70 (1971).

(52) W. J. Hehre, W. A. Lathan, R. Ditchfield, M. D. Newton, and J. A. Pople, Gaussian-70: Program 236, Quantum Chemistry Program Exchange, Indiana University (1974).

(53) S. Huzinaga, J. Chem. Phys. 42, 1293 (1965).

(54) G. E. Kellerhals, N. Sathyamurthy, and L. M. Raff, J. Chem. Phys. 64, 818 (1976).

(55) M. Baer, private communications.

(56) J. W. Duff and D. G. Truhlar, J. Chem. Phys. 62, 2477 (1975).

(57) C. Stroud, N. Sathyamurthy, R. Rangarajan, and L. M. Raff, Chem. Phys. Lett. 48, 350 (1977).

(58) Several authors have discussed this point. For example, see Chapter 6 of Reference 34a.

(59) D. L. Bunker, Meth. Comput. Phys. 10, 287 (1971).

(60) H. Goldstein, Classical Mechanics: Addison-Wesley Publishing Co., Reading, Massachusetts (1950), p. 42.

(61) G. Herzberg, Molecular Spectra and Molecular Structure, Volume II: Van Nostrand Reinhold Co., New York (1945).

(62) J. C. Polanyi and N. Sathyamurthy, Chem. Phys. 29, 9 (1978).

APPENDIX A

THE ELECTRON GAS POTENTIAL AND ITS DERIVATIVES FOR THE He - CO_2 RIGID ROTOR SYSTEM

The electron gas potential is given as the sum of a Hartree-Fock potential and a scaled correlation term

$$V_{EG}(R,\theta) = V^{HF}(R,\theta) + aV^{COR}(R,\theta),$$

where the individual potentials are approximated by an expansion of Legendre polynomials

$$V^{i}(R,\theta) = \sum_{n=0,2,\ldots}^{8} v_n^i(R)\, P_n(\cos\theta) \qquad i=HF,\ COR$$

to give a continuous potential in θ. The $v_n^i(R)$ are given by

$$v_n^{HF}(R) = A_{n1}\exp(A_{n2}R + A_{n3}R^2)$$

$$v_n^{COR}(R) = \begin{cases} -B_{n1}\exp(B_{n2}R + B_{n3}R^2) & R \le R_n \\ \dfrac{-C_6(n)}{R^6} - \dfrac{C_8(n)}{R^8} & R \ge R_n, \end{cases}$$

where the coefficients A and B have been determined by a least squares fit of $|\ln v_n|$ and where the coefficients B_{n1} have been scaled to make v_n^{COR} continuous at R_n. All parameters are given in Table XVIII.

The derivatives of the EG potential are

$$\partial V_{EG}/\partial R = \sum_{\substack{n=0 \\ n\ \text{even}}}^{8} P_n(\cos\theta)\left[(A_{n2} + 2A_{n3}R)\, v_n^{HF}(R) - \begin{matrix}(B_{n2} + 2B_{n3}R)\, v_n^{COR}(R) \\ \left(\dfrac{-6C_6(n)}{R^7} - \dfrac{8C_8(n)}{R^9}\right)\end{matrix}\right]$$

where the last term is the top term for $R \le R_n$ and the bottom for $R \ge R_n$, and

$$\partial V/\partial\theta = \sum_{\substack{n=0 \\ n\ \text{even}}}^{8} [v_n^{HF}(R) + v_n^{COR}(R)]\partial P_n(\cos\theta)/\partial\theta.$$

The Legendre polynomials and their derivatives are

$$P_0(\cos\theta) = 1$$

$$\partial P_0/\partial\theta = 0$$

$$P_2(\cos\theta) = (3\cos^2\theta - 1)/2$$

$$\partial P_2/\partial\theta = -3\cos\theta \sin\theta$$

$$P_4(\cos\theta) = (35\cos^4\theta - 30\cos^2\theta + 3)/8$$

$$\partial P_4/\partial\theta = -(140\cos^3\theta - 60\cos\theta)(\sin\theta)/8$$

$$P_6(\cos\theta) = (231\cos^6\theta - 315\cos^4\theta + 105\cos^2\theta - 5)/16$$

$$\partial P_6\partial\theta = -(1386\cos^5\theta - 1260\cos^3\theta + 210\cos\theta)(\sin\theta)/16$$

$$P_8(\cos\theta) = (12870\cos^8\theta - 24024\cos^6\theta + 13860\cos^4\theta - 2520\cos^2\theta + 70)/256$$

$$\partial P_8/\partial\theta = -(102960\cos^7\theta - 144144\cos^5\theta + 55440\cos^3\theta - 5040\cos\theta)(\sin\theta)/256.$$

TABLE XVIII

PARAMETERS USED IN THE GENERATION OF THE ELECTRON GAS SURFACE FOR THE He - CO_2 RIGID ROTOR SYSTEM[a]

n =	0	2	4	6	8
A_{n1}	17.2995	65.5752	105.137	178.531	314.919
A_{n2}	-0.982289	-1.12538	-1.44877	-1.90354	-2.40207
A_{n3}	-0.0917494	-0.0766468	-0.0522417	-0.0239120	0.0
B_{n1}	0.122126	0.0569431	0.0252919	0.0162599	0.0636620
B_{n2}	-0.628088	-0.663263	-0.976097	-1.16525	-1.88254
B_{n3}	-0.0470607	-0.0399192	-0.0215588	-0.0280915	0.0
R_n	5.72050	6.27735	6.39141	∞	∞
$C_6(n)$	16.75	3.88	0.0	0.0	0.0
$C_8(n)$	278.	290.	57.	0.0	0.0

[a]Reference 16, Table XI

[b]All values are in Hartree atomic units

APPENDIX B

ON THE ORIGIN OF THE DYNAMICAL DIFFERENCES ON THE DIATOMICS-IN-MOLECULES AND SPLINE-FITTED *AB INITIO* SURFACES FOR THE $He + H_2^+$ REACTION

On the origin of the dynamical differences on the diatomics-in-molecules and spline-fitted *ab initio* surfaces for the $He+H_2^+$ reaction[a)]

N. Sathyamurthy and J. W. Duff

Department of Chemistry, University of Toronto, Toronto, Canada M5S 1A1

C. Stroud[b)] and L. M. Raff

Department of Chemistry, Oklahoma State University, Stillwater, Oklahoma 74074
(Received 8 April 1977)

The dynamic behavior of the $He—H_2^+—HeH^+ + H$ reaction has been examined on a DIM and a cubic spline fit to the *ab initio* surface values of Brown and Hayes. Examination of the total integrated reaction probability and the variation of vibration–translation energy transfer as a function of initial H_2^+ vibration phase on these two surfaces, as well as on two composite spline-fitted surfaces, indicates that the origin of the dynamical differences on the DIM and SAI surfaces for the $He+H_2^+$ reaction resides primarily in differences in shape of the inner repulsive wall. For this reaction, this region is shown to be the most important topological feature of the surface. Vibrational excitation probabilities on the two surfaces at energies below reaction threshold are also presented and compared with the results of Chapman and Hayes on the DIM surface. In spite of the influence of a well, the trajectories are, on the average, direct and short-lived on the SAI surface. In contrast, they are indirect and long-lived on the DIM surface.

INTRODUCTION

Significant progress has been made in recent years[1,2] in relating the topological features of potential-energy surfaces, such as height and location of the barrier, curvature of the minimum energy path, etc., to dynamical outcome. Such correlations have provided valuable assistance in interpreting experimental data in terms of the potential-energy surface features. In addition, they provide useful guidelines in the computation and interpolation of *ab initio* surfaces in that they indicate the topological features that must be obtained with greatest accuracy.

The endothermic reaction

$$He + H_2^+ \rightarrow HeH^+ + H \qquad (R1)$$

is a particularly important example of a three-body process because it is the simplest possible nonthermoneutral ion–molecule reaction. As such, it is a leading candidate for "benchmark" calculations designed to serve as a testing ground for more approximate theoretical studies. The experimental observations of Chupka, Berkowitz, and Russell[3] indicate that the reaction cross section for (R1) increases whenever the available energy is partitioned into vibration. This suggests[1] that the crest of the barrier is located in the exit channel. *Ab initio* calculations[4] of the potential-energy surface for collinear (R1) support such an expectation. However, as has been observed before for $He+H_2$ inelastic collisions,[5] two different interpolations of the *ab initio* surface for (R1) are found to lead to drastically different dynamical results.[6] Quantum mechanical[7] and quasiclassical[8] calculations using the diatomics-in-molecules (DIM) functional fit[8] to the *ab initio* surface show that there is no vibrational enhancement of the reaction probability whereas similar studies on the spline-fitted[9] *ab initio* (SAI) surface[6,7] show vibrational enhancement. Yet potential-energy contours of the two surfaces are almost superimposable and both surfaces are nearly identical in properties such as the height and location of the barrier, minimum energy path, and its curvature. The origin of the dynamical difference on the DIM and SAI surfaces has remained a puzzle.

In the present paper we provide additional insight into the interrelationship of surface topology and dynamics. By examination of (a) the variation of final vibrational energy with initial vibrational phase of the reactant molecule; (b) collinear trajectories on the scaled and skewed potential-energy surfaces; and (c) reaction probabilities on composite spline-fitted surfaces, we show that differences in the topology of the inner repulsive wall between the SAI and DIM surfaces is primarily responsible for the computed variations in dynamic behavior on the two surfaces.

RESULTS AND DISCUSSION

The computational procedure and a description of the potential-energy surfaces may be found elsewhere.[6,8]

Previously reported calculations,[6] given in Table I, have shown that the reaction probability at a given total energy on the SAI surface is significantly different than

TABLE I. Reaction probabilities[a] on the two surfaces at two different total energies.

E_{tot}	v	DIM	SAI
1.1 eV	0	0.31	0.02
	1	0.24	0.17
1.2 eV	0	0.33	0.03
	1	0.215	0.210

[a]Reference 6.

[a)]Supported, in part, by NSF Grant MPS75-18967.
[b)]CONOCO Fellow.

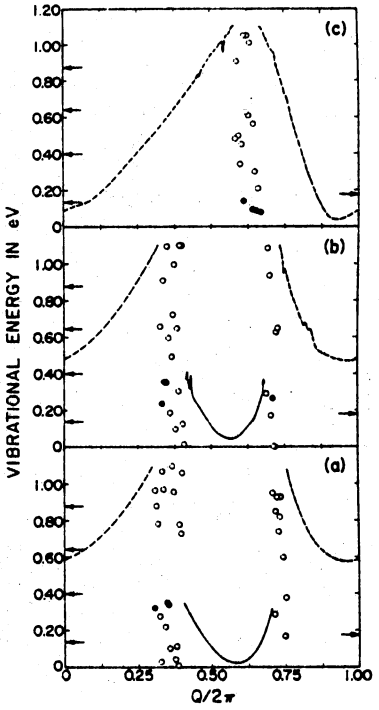

FIG. 1. Final vibrational energy in eV as a function of initial vibrational phase for $v = 0$ of H_2^+ on three different surfaces at a total energy of 1.1 eV. (a) DIM, (b) SDIM, and (c) SAI. —— reactive region, - - - nonreactive region, ● reactive trajectories, and ○ nonreactive trajectories. — on the left axis indicates the vibrational energies of the $v = 0$, 1, 2, 3 of H_2^+. — on the right axis indicates the $v = 0$ of HeH$^+$.

that for the DIM surface. This difference is found to be maximum for the $v = 0$ vibrational state of H_2^+. For the $v = 1$ and higher states, the differences are greatly reduced. More detailed investigation has shown that the two surfaces also predict a very different partitioning of the available energy into the vibrational degree of freedom of the final diatomic molecule. This is illustrated in Figs. 1(a) and 1(c) where the final vibrational energy of the product/reactant molecule on the DIM and SAI surfaces, respectively, is plotted as a function of the initial vibrational phase of H_2^+ in the $v = 0$ state. In going from the DIM to the SAI surface, a significant portion of the reactive region has become nonreactive, and the final vibrational energy for the nonreactive trajectories has decreased sharply. The corresponding plots for the $v = 1$ state of H_2^+, shown in Figs. 2(a) and 2(c), show a smaller difference in all respects. Most of the reactive region is retained, and the reaction probability is 0.24 on the DIM surface compared to 0.17 on the SAI surface. It is apparent that as the initial H_2^+ vibrational energy decreases, the computed differences in the dynamic results on the two surfaces increases. In the limit of zero vibrational energy, the differences should be maximum. Calculations with no zero-point energy included for the $v = 0$ state indicate this to be the case.

It should be noted that the differences discussed above are not an artifact of the spline-fitting procedure itself.[10] This may be verified by repeating all computations on the spline-fitted DIM surface (SDIM).[6] The results obtained on the SDIM surface are given in Figs. 1(b) and 2(b). Comparison of Figs. 1(a) with 1(b) and 2(a) with 2(b) shows that the results on the DIM and SDIM surfaces are almost identical. Root trajectories[11] on the two surfaces are also almost identical as illustrated in Figs. 3(a) and 3(b).

The variation of vibrational energy transfer between the SAI and DIM/SDIM surfaces suggests that the inner repulsive wall of the surface may be an important topological feature since it is known that vibrational energy transfer depends primarily upon the short-range repulsive part of the intermolecular potential.[12]

Examination of vibrationless collinear trajectories, each with identical initial conditions, on the two surfaces also suggests that the inner repulsive wall may be the primary source of the above differences. Such trajectories at a total energy of 1.1 eV are shown in Figs. 4(a) and 4(b). Both trajectories exhibit nearly identical be-

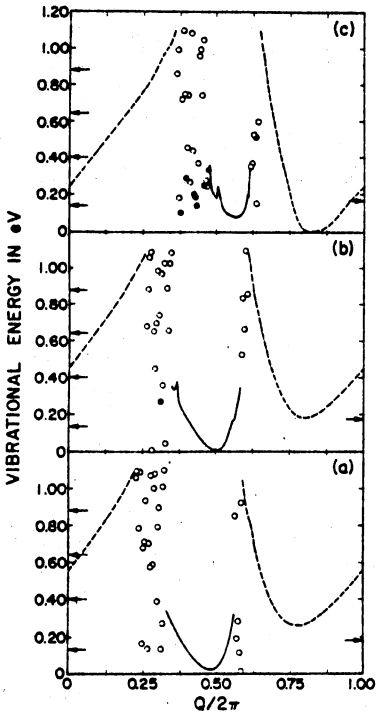

FIG. 2. Same as Fig. 1 for $v = 1$ of H_2^+.

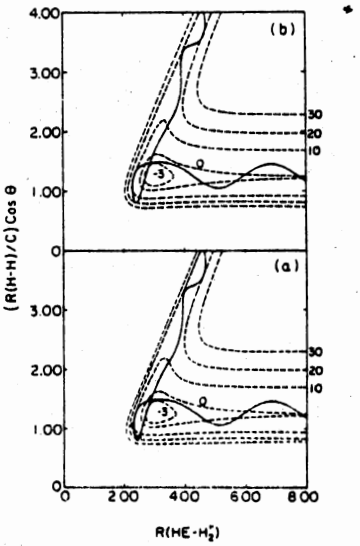

FIG. 3. Root trajectories on the (a) DIM and (b) SDIM surfaces at a total energy of 1.1 eV for $v=0$ of H_2^+. —— trajectory; - - - potential-energy contours in kcal/mole; distances are in a.u. c is the scaling factor and θ is the skewing angle. For definition, refer to S. Glasstone, K. J. Laidler, and H. Eyring, *The Theory of Rate Processes* (McGraw-Hill, New York, 1941), p. 102.

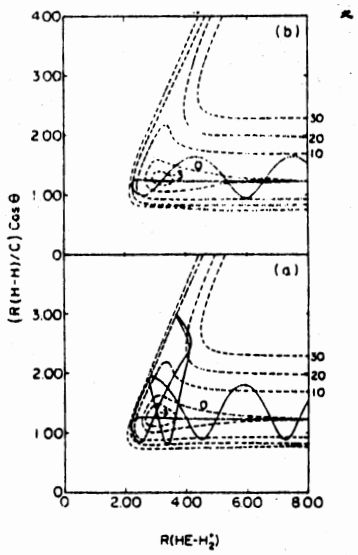

FIG. 4. Vibrationless trajectories on the (a) DIM and (b) SAI surfaces at a total energy of 1.1 eV. —— trajectory; - - - potential-energy contours in kcal/mole; distances in a.u.

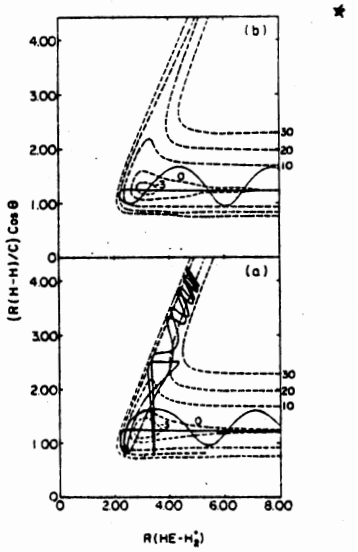

FIG. 5. Same as Fig. 4, at 1.2 eV.

havior as they traverse the entrance valley and the attractive well. However, once the repulsive inner wall is encountered the two trajectories diverge sharply. The trajectory on the scaled and skewed SAI surface, given in Fig. 4(b), shows a simple behavior as the trajectory is reflected from the inner repulsive wall. On the DIM surface [see Fig. 4(a)], on the other hand, the same trajectory experiences a differently shaped inner wall and suffers a larger angle of reflection resulting in subsequent reflection into the product valley. The trajectory becomes nearly reactive. However, all the available energy becomes product vibration, and the products are unable to separate. The system therefore falls back into the reactant valley resulting in high vibrational excitation of H_2^+. This type of behavior accounts for the fact that the nonreactive part of Fig. 1(a) for the DIM surface has larger vibrational energy than its SAI counterpart. At 1.2 eV, the behavior is similar (see Fig. 5). The trajectory on the SAI surface is simply nonreactive while the DIM trajectory becomes almost reactive.

The above results indicate that the inner repulsive wall plays a significant role in deciding the dynamical outcome of a collision. This has been previously noted by Schreiber.[13] A succinct description of collinear collision chemistry using potential surfaces constructed assuming hard sphere and/or square well pairwise interactions has also been presented by Mahan.[14]

It is possible that the shapes of the entrance channel and attractive well are also important topological features of the surface.[15] These features could alter the vibrational phase of the diatom at the instant the repulsive wall is encountered and thereby change the collisional outcome. Hence it becomes necessary to sepa-

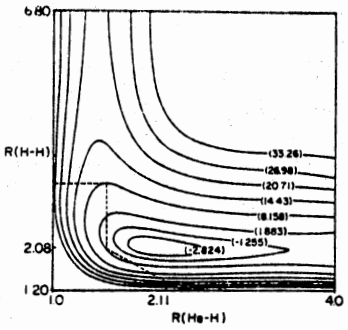

FIG. 6. Composite surface CPS1 showing the contour lines for the collinear SAI surface with the region to the lower left of the dashed line to be replaced with the corresponding potential-energy values from the SDIM surface. Distances are in a.u. Energies are in kcal/mole relative to the He + H_3^+ asymptotic limit.

rate the effect of the short-range repulsive forces from those of the entrance channel and the attractive well.

The above separation has been accomplished by investigation of the dynamics on composite spline-fitted surfaces. The two surfaces employed for this purpose are illustrated in Figs. 6 and 7. Figure 6 shows the contour map for the collinear SAI surface while Fig. 7 gives the position of the same contour lines for the SDIM surface. The composite surfaces are generated by replacing the inner repulsive regions (indicated by the areas to the lower left of the dashed lines in Figs. 6 and 7) with the corresponding potential-energy values from the opposite surface. Thus, the composite surface given in Fig. 6 has the entrance channel and attractive well of the SAI surface but the inner repulsive wall of the SDIM surface. The composite of Fig. 7 has the SDIM entrance channel and attractive well with the SAI repulsive inner wall. We designate these two composite surfaces CPS1 and CPS2, respectively.

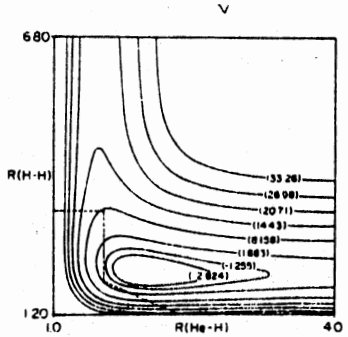

FIG. 7. Composite surface CPS2 showing the contour lines for the collinear SDIM surface with the region to the lower left of the dashed line to be replaced with the corresponding potential-energy values from the SAI surface. Distances are in a.u. Energies are in kcal/mole relative to the He + H_3^+ asymptotic limit.

TABLE II. Comparison of reaction probabilities on the SAI, SDIM, CPS1, and CPS2 surfaces at a total energy of 1.1 eV with H_3^+ initially in the $v=0$ vibrational state.

Surface	Computed reaction probability
SAI	0.018
SDIM	0.30
CPS1	0.368
CPS2	0.008

The reaction probability for (R1) at a total energy of 1.1 eV with H_3^+ initially in the $v=0$ vibrational state has been computed on the SAI, SDIM, CPS1, and CPS2 surfaces. In each case the same 500 trajectories were examined. The results are given in Table II. As can be seen, surfaces with the SAI inner repulsive wall have very low reaction probability regardless of the nature of the entrance channel and attractive well, while surfaces with the SDIM inner wall have a much larger reaction probability for both the SDIM and SAI entrance channel and attractive well. The entrance channel and attractive well do exert some influence on the reaction probability as can be seen by noting the difference of 0.068 for the results on the SDIM and CPS1 surfaces. This difference is outside the range of expected statistical error and must therefore be due to phasing differences produced by the entrance channel and attractive well. However, the topological feature of greatest importance is clearly the short-range repulsive wall.

Examination of the variation of final vibrational energy as a function of initial H_3^+ vibrational phase on surfaces CPS1 and CPS2 leads to the same qualitative conclusions. These results are shown in Figs. 8 and 9 for surfaces CPS1 and CPS2, respectively. Comparison of Figs. 8 and 1(b) shows that the results on SDIM and CPS1 are nearly identical. A similar conclusion may be drawn with respect to the SAI and CPS2 surfaces by comparison of Fig. 9 with Fig. 1(c). Thus, translation–vibration energy transfer, as well as the total integrated reaction probability, depends predominantly upon the inner repulsive wall of the surface.

The above conclusions are probably not restricted to the HeH_3^+ system alone. For instance, the difference in the shape of the repulsive wall has been identified[2] as a source of the dynamical difference on the different surfaces for the reaction

$$H_2 + I \rightarrow HI + H, \qquad \text{(R2)}$$

along with the difference in the position of maximum curvature of the minimum energy path with respect to the repulsive energy release along the reaction coordinate. Polanyi and Sathyamurthy[16] have also recently found that large differences in dynamical behavior among a variety of endothermic reactions could be explained in

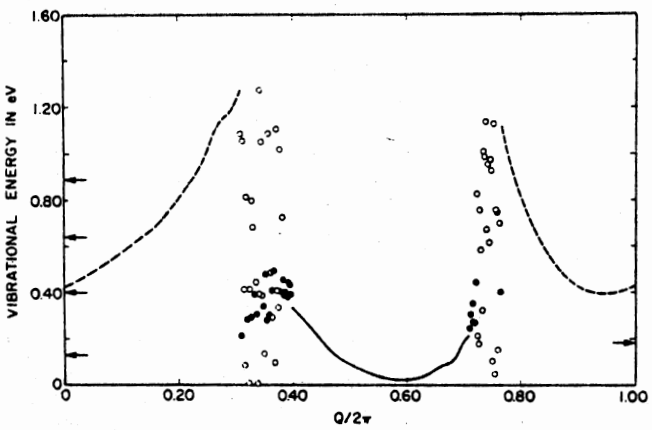

FIG. 8. Final vibrational energy in eV as a function of initial vibrational phase for $v=0$ state of H_2^+ on the CPS1 composite surface. E_{tot} = 1.1 eV, —— reactive region, - - - nonreactive region, • reactive trajectories, ○ nonreactive trajectories.

terms of the shape of the inner repulsive wall of the potential-energy surface.

Hayes *et al.*[17] have recently published an *ab initio* surface for the reaction

$$Ne + H_2^+ - NeH^+ + H. \qquad (R3)$$

They have fitted their results to a DIM function, and the resulting surface is very similar to that for (R1). A vibrationless collinear trajectory at 1.1 eV for (R3) is also found to be reactive suggesting that there may not be vibrational enhancement for (R3) on the DIM surface. Several thousand trajectories for the $v=0$, 1, and 2 vibrational states of H_2^+ at energies varying between 0.94 and 1.4 eV confirm this.[18,19] Hence, it appears that a DIM functional fit has a bias in its description of the shape of the inner repulsive wall and alternate procedures, such as spline interpolation, may be needed in order to reproduce the *ab initio* data with sufficient accuracy. Studies in this direction are in progress.[19]

We have also examined collinear vibrational inelastic scattering at energies below the reaction threshold for the He + H_2^+ collisions. Chapman and Hayes[20] have computed the vibrational excitation probabilities $P_{0\to1}$ by quantum mechanical procedures as a function of the total energy of the system and have observed large oscillations. They explained these oscillations in terms of open- and closed-channel resonances. This provides a further opportunity to compare quasiclassical trajectory (QCT) methods to quantum mechanical methods and to compare the two surfaces.

Batches of 100 trajectories were computed on the DIM surface at total energies of 0.48, 0.51, and 0.537 eV with the H_2^+ in its $v=0$ state. The $P_{0\to1}$ values are reported in Table III along with the quantal results. Not

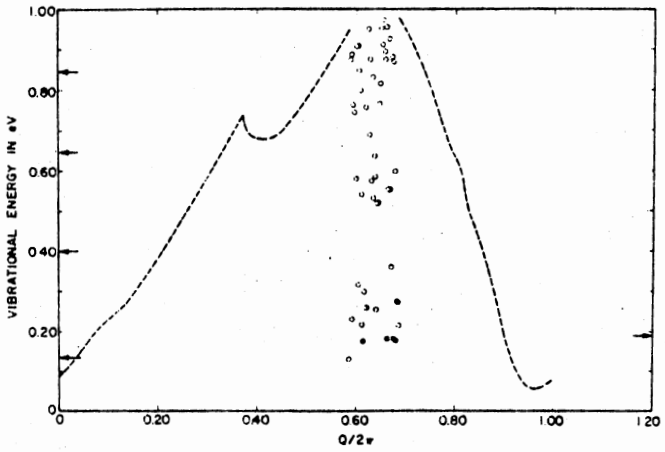

FIG. 9. Final vibration energy in eV as a function of initial vibrational phase for $v=0$ state of H_2^+ on the CPS2 composite surface. E_{tot} = 1.1 eV, —— reactive region, - - - nonreactive region, • reactive trajectory, ○ nonreactive trajectory.

TABLE III. Vibrational excitation probabilities $P_{0\to1}$ on the two surfaces.

E_{tot}	DIM			SAI	
in eV	QM[a]	QCT	INDECENT	QCT	INDECENT
0.48	0.95	0.456	0.253	···	0.241
0.50	0.47	···	0.361	···	0.261
0.51	0.05	0.534	0.271	···	0.269
0.52	0.24	···	0.003	···	0.275
0.537	0.80	0.621	0.368	0.495	0.284

[a]Reference 20.

surprisingly, the QCT results vary smoothly from 0.456 to 0.534 to 0.621 while the quantal results vary rapidly from 0.95 to 0.05 to 0.80. A plot of the final vibrational energy of H_3^+ as a function of its initial vibrational phase at a total energy of 0.537 eV in Figure 10(a) shows large oscillations suggesting that a classical S matrix[11,21] study might be able to reproduce the quantum oscillations. For comparison, corresponding INDECENT[22] trajectories were computed and their results, presented in Table III, show purely statistical behavior. As one would expect, the trajectories are very complex and long lived, an example of which is shown in Fig. 11(a).

Results on the SAI surface are distinctly different. There are no violent oscillations in the vibrational energy vs vibrational phase plot at 0.537 eV, shown in Fig.

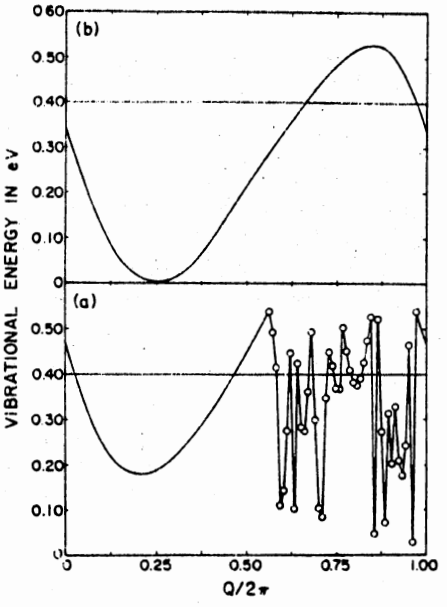

FIG. 10. Final vibrational energy as a function of initial vibrational phase for $v=0$ of H_3^+ at a total energy of 0.537 eV for (a) DIM and (b) SAI surfaces. The horizontal line indicates the $v=1$ state of H_3^+.

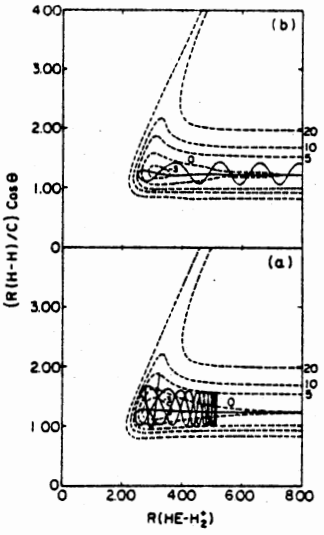

FIG. 11. INDECENT trajectories at 0.2437 eV for (a) DIM and (b) SAI surfaces. —— trajectory; - - - potential-energy contours in kcal/mole; distances in a.u.

10(b), suggesting that large resonances may not be observed in this energy range on the SAI surface but are rather an artifact of the DIM fit. Also, similar to the behavior at energies above reaction threshold, the SAI surface is less efficient in converting translational energy into vibrational energy than is the DIM surface. Vibrational excitation probabilities from INDECENT calculations show a smooth behavior and the trajectories are also direct and short-lived as shown in Fig. 11(b).

Chapman and Hayes[20] estimate the lifetimes in the resonance region as 3×10^{-14}–1×10^{-13} sec. The increased lifetime for an average trajectory on the DIM surface when compared to an average trajectory on the SAI surface is estimated to be 0.9×10^{-13} sec. This suggests that quantum mechanical resonance is reflected in classical calculations in the form of "snarled" trajectories of comparable lifetime.

CONCLUSIONS

For Reaction (R1), the inner repulsive wall is the most crucial topological feature of the potential-energy surface. This is particularly true for the lower initial H_3^+ vibrational states. The difference in shape of the repulsive wall seems to be the origin of the dynamical difference on the DIM and SAI surfaces for the He + H_3^+ reaction. The DIM analytic function probably has a bias in its description of the inner repulsive wall region even though it reproduces other features of the *ab initio* surface correctly. Hence, in fitting *ab initio* data, alternate interpolation procedures must be considered and care must be taken to fit accurately the inner repulsive wall region as well as other topological features. Plots

of vibrationless trajectories, final vibrational energy (v') as a function of initial vibrational phase (q), and the use of spline-fitted composite surfaces can serve as valuable diagnostic tools.

The DIM and SAI surfaces predict significantly different vibrational excitation probabilities below reaction threshold with the DIM surface being more efficient in converting translational energy into vibrational motion. The DIM surface exhibits a large "chattering region" in its v' vs vibrational phase plots, which is probably indicative of the resonance behavior observed by Chapman and Hayes[20] for this surface. Interestingly, despite the 3.5 kcal/mole well on the SAI surface, it does not exhibit any "chattering region" and hence possibly no resonance.

ACKNOWLEDGMENTS

It is a pleasure to thank Professor D. G. Truhlar for inspiring this study. N. S. would like to thank Drs. J. L. Schreiber and R. B. Davidson for valuable discussions and Professor J. C. Polanyi for his kind hospitality and support. J. W. D. is grateful to Professor P. Brumer for support during this work. We also extend our thanks to the National Science Foundation for financial support on grant MPS75-18967.

[1] J. C. Polanyi, Acc. Chem. Res. 5, 161 (1972).
[2] J. W. Duff and D. G. Truhlar, J. Chem. Phys. 62, 2477 (1975).
[3] W. A. Chupka, J. Berkowitz, and M. E. Russell, VI International Conference on the Physics of Electronic and Atomic Collisions (M.I.T., Cambridge, Massachusetts, 1969), p. 71.
[4] P. J. Brown and E. F. Hayes, J. Chem. Phys. 55, 922 (1971).
[5] M. H. Alexander and E. V. Berard, J. Chem. Phys. 60, 3950 (1974).
[6] N. Sathyamurthy, R. Rangarajan, and L. M. Raff, J. Chem. Phys. 64, 4606 (1976).
[7] (a) D. J. Kouri and M. Baer, Chem. Phys. Lett. 24, 37 (1974). (b) C. Stroud, N. Sathyamurthy, R. Rangarajan, and L. M. Raff, Chem. Phys. Lett. 48, 350 (1977).
[8] P. J. Kuntz, Chem. Phys. Lett. 16, 581 (1972).
[9] (a) D. R. McLaughlin and D. L. Thompson, J. Chem. Phys. 59, 4393 (1973). (b) N. Sathyamurthy and L. M. Raff, J. Chem. Phys. 63, 464 (1975). (c) N. Sathyamurthy and L. M. Raff, "Spline Packages," Program 322, Quantum Chemistry Program Exchange, Indiana University, 1976.
[10] N. Sathyamurthy, G. E. Kellerhals, and L. M. Raff, J. Chem. Phys. 64, 2259 (1976).
[11] W. H. Miller, Adv. Chem. Phys. 25, 69 (1974).
[12] This point has been discussed by several authors. For example, see T. L. Cottrell and J. C. McCoubrey, *Molecular Energy Transfer in Gases* (Butterworths, London, 1961), Chap. 6.
[13] J. L. Schreiber, Ph.D. thesis, University of Toronto, Toronto, Canada, 1973.
[14] B. H. Mahan, J. Chem. Educ. 51, 308, 377 (1974).
[15] The authors are indebted to the referee for discussions related to this point.
[16] J. C. Polanyi and N. Sathyamurthy (to be published).
[17] E. F. Hayes, A. K. Q. Siu, F. M. Chapman, Jr., and R. L. Matcha, J. Chem. Phys. 65, 1901 (1976).
[18] N. Sathyamurthy (unpublished).
[19] C. Stroud and L. M. Raff (unpublished).
[20] F. M. Chapman, Jr. and E. F. Hayes, J. Chem. Phys. 62, 4400 (1975); 65, 1032 (1976).
[21] J. R. Stine and R. A. Marcus, Chem. Phys. Lett. 29, 575 (1974).
[22] C. F. Giese and W. R. Gentry, J. Chem. Phys. 63, 3144 (1975).

APPENDIX C

CALCULATION OF THE KPK POTENTIAL-ENERGY SURFACE AND ITS DERIVATIVES

The potential-energy surface determined experimentally by Keil, Parker, and Kuppermann (51c) has the following form

EG potential	$V_{EG} \geq 0.030$ eV
V = Morse-type potential	$V_{Morse} < 0.010$ eV and $R \leq 4.4$ Å
Van der Waal's tail	$V_{VdW} \geq -0.0004$ eV and $R \geq 4.4$ Å

The form of the EG potential is given in Appendix A. The form of the Morse-type potential is

$$V_{Morse} = [\varepsilon_0+\varepsilon_2 P_2(\cos\theta)][\exp(2\beta(1-R/R_m(\theta))) - 2\exp(\beta(1-R/R_m(\theta)))] ;$$

$$R_m(\theta) = R_{m_\perp}\left[\frac{1+r_q\sin^2\theta}{1+r_q}\right]^{1/2} ,$$

where ε_0, ε_2, β, $R_{m_\perp}$, and r_q are constants fitted to the experimentally determined differential cross sections and are given in Table XIX. The Van der Waal's tail has the form

$$V_{VdW} = \sum_{\substack{n=0 \\ n \text{ even}}}^{8} -\left(\frac{C_6(n)}{R^6} + \frac{C_8(n)}{R^8}\right) P_n(\cos\theta)$$

where $C_6(n)$, $C_8(n)$, and $P_n(\cos\theta)$ are the same quantities as those used in the calculation of the EG surface. In the expression for V_{VdW}, R must be in atomic units and the resulting potential is in hartrees.

The EG and Morse-type potentials are joined by cubic splines, which ensures continuity of the potential energy across the junction. Splines are also used to connect the Morse-type potential to the Van der Waal's tail in the region $R > 4.4$ Å, $V_{Morse} > -0.0006$ eV, and $V_{VdW} < -0.0004$ eV. In the course of a trajectory the system may sample parts of four different potentials.

The derivatives for these regions must be calculated carefully.

The EG and spline derivatives have already been given. The derivatives for the Morse-type potential are

$$\partial V/\partial R = [\varepsilon_0+\varepsilon_2 P_2(\cos\theta)][\exp(2\beta(1-R/R_m)) - \exp(\beta(1-R/R_m))]\ (-2\beta/R_m)$$

$$\partial V/\partial\theta = -3\ \varepsilon_2 \sin\theta\cos\theta[\exp(2\beta(1-R/R_m)) - 2\exp(\beta(1-R/R_m))] +$$

$$(2\beta R/R_m^{\,2})(R_{m_\perp} r_q/(1+r_q))[(1+r_q\sin^2\theta)/(1+r_q)]^{-1/2}(\varepsilon_0+\varepsilon_2 P_2(\cos\theta))$$

$$[\exp(2\beta(1-R/R_m)) - \exp(\beta(1-R/R_m))]\sin\theta\cos\theta\ ,$$

where the units are eV/Å for $\partial V/\partial R$ and eV/radian for $\partial V/\partial\theta$. The derivatives for the Van der Waal's tail are

$$\partial V/\partial R = \sum_{\substack{n=0 \\ n\ \text{even}}}^{8} \frac{6C_6(n)}{R^7} + \frac{8C_8(n)}{R^9}\ P_n(\cos\theta)$$

$$\partial V/\partial\theta = \sum_{\substack{n=0 \\ n\ \text{even}}}^{8} -\left[\frac{C_6(n)}{R^6} + \frac{C_8(n)}{R^8}\right] (\partial P_n(\cos\theta)/\partial\theta)$$

where the units are hartree/bohr for $\partial V/\partial R$ and hartree/radian for $\partial V/\partial\theta$. The derivatives of $P_n(\cos\theta)$ are given in Appendix A.

TABLE XIX

EXPERIMENTALLY DETERMINED MORSE PARAMETERS FOR THE He - CO_2 SYSTEM[a]

ε_0	= 0.00298 eV
ε_2	= -0.00191 eV
β	= 4.59
$R_{m_\perp}$	= 3.31 Å
r_q	= -0.52

[a]Reference 51c

VITA 2

Courtney Lynn Stroud

Candidate for the Degree of

Doctor of Philosophy

Thesis: I. INVESTIGATION OF THE EFFECTS OF SURFACE TOPOLOGY UPON COLLISION DYNAMICS IN THE HeH_2^+ AND NeH_2^+ SYSTEMS
II. AN *AB INITIO* STUDY OF ROTATIONALLY INELASTIC SCATTERING IN THE He - CO_2 SYSTEM

Major Field: Chemistry

Biographical:

Personal Data: Born in Oklahoma City, Oklahoma, on April 20, 1954.

Education: Graduated from Casady High School in June, 1972; received the Bachelor of Science degree in biochemistry from Oklahoma State University in May, 1975; completed requirements for the Doctor of Philosophy degree at Oklahoma State University, December, 1978.

Professional Experience: Graduate Teaching Assistant, Oklahoma State University, 1975-1976; National Science Foundation Research Assistant, Oklahoma State University, 1976-1978; CONOCO Fellow, Oklahoma State University, spring 1977.

Membership in Honorary and Professional Societies: Member of the Honor Society of Phi Kappa Phi; member of Phi Lambda Upsilon, Honorary Chemical Society; member of Sigma Xi, Research Society; associate member of the American Chemical Society.